BIOFUNCTIONALIZATION ON HYDROGEN-TERMINATED SILICON(111) SURFACES

A Thesis Presented to

the Faculty of the Department of Chemistry

University of Houston

In Partial Fulfillment

of the Requirement for the Degree

Master of Science

By

Kai Liu

August 2012

BIOFUNCTIONALIZATION ON HYDROGEN-TERMINATED SILICON(111) SURFACES

Kai Liu

APPROVED:

Dr. Chengzhi Cai, Chairman

Dr. T. Randall Lee

Dr. Olafs Daugulis

Dr. Shoujun Xu

Dr. Dean Muirhead

Dr. Mark A. Smith, Dean College of Natural Sciences and Mathematics

ACKNOWLEDGMENTS

First, I would like thank all the people who have helped me and believed in me during different times; and who have brought smiles on my face whenever I think about them.

I would like to express my gratitude to my supervisor, Dr. Chengzhi Cai, whose expertise, understanding, and patience, added considerably to my graduate experience. I appreciate his vast knowledge and skill in many areas (e.g., vision, aging, ethics, interaction with participants), and his assistance in writing reports (i.e., grant proposals and this thesis).

I would like to thank all other members of my committee, Dr. T. Randall Lee, Dr. Olafs Daugulis, and Dr. Shoujun Xu, the assistance they have provided at all levels of this research project.

I would like to thank Dr. Dean Muirhead as external committee member.

I would like to thank Dr. Carl Zhang from the Faculty of Chemistry Program at University of Houston-Clear Lake for taking time out of his busy schedule to provide insightful recommendations.

Finally, I would like to thank my parents for providing support during my study at University of Houston.

BIOFUNCTIONALIZATION ON HYDROGEN-TERMINATED SILICON(111) SURFACES

An Abstract of Thesis

Presented to

the Faculty of the Department of Chemistry

University of Houston

In Partial Fulfillment

of the Requirements for the Degree

Master of Science

By

Kai Liu

August 2012

ABSTRACT

This thesis describes our attempt to develop a versatile bioelectrical platform based on our understanding of both surface chemical and physical processes. We envisioned the fine tuning of such platform through modification strategies such as “Click” chemistry, which allows us to control its electrochemical property. Such an endeavor would greatly benefit the study of neurological disorder diseases by providing an ideal neural culture platform, which currently presents a great challenge in interfering with neural system in vivo. Several major tasks involved in our research were: 1) improvement of organic film passivation apparatus for high quality film formation to prevent oxidation of underlying bulk silicon; 2) development of easily reproducible acetylenylated base layer on silicon surfaces for convenient introduction of organic moieties; and 3) development of novel redox biomolecule which allows attachment to acetylenylated monolayer via *step-wise* procedure, as well as direct electron transfer between the redox biomolecule and underlying silicon substrate.

To realize our vision, we built a film passivation apparatus that provides near ideal ultra-high vacuum (UHV) condition for adsorbate grafting. The hypothesis is that by removing reactive oxygen species, a densely packed monolayer can be formed, which protects underlying bulk silicon from oxidation in both aqueous and organic electrolytes. We demonstrated monolayers presenting

oligo(ethylene glycol) (OEG) prepared using this apparatus remained resistant to model protein fibrinogen after 56 days in phosphate buffer saline (PBS).

In order to incorporate new moieties to our platform, we optimized the design of trimethylgermanyl protected acetylenylated self-assembling molecule (SAM). Subsequently, we grafted OEG onto acetylenylated base layer via a *step-wise* strategy to incorporate the ability to block nonspecific bindings. The anti-biofouling property of the grafted film was tested to be similar to that of the OEG-presenting film formed by *pre-assembled* strategy.

To develop a versatile method to tune the electrochemical property of the films, we immobilized electrochemical active ferrocene moiety onto the acetylenylated silicon substrates. Cyclic voltammetry was employed to study the electrochemical property of the ferrocene grafted films. By optimizing the design of the biocompatible acetylenylated base layer, we established a simple modular approach to produce SAMs to study the electrochemical behavior of a well-studied model redox molecule.

TABLE OF CONTENTS

LIST OF FIGURES

LIST OF TABLES

TABLE OF SCHEMES

LIST OF ABBREVIATIONS

Å	Angstrom
AFM	Atomic force microscope or atomic force microscopy
CV	Cyclic voltammetry
DFT	Density functional theory
DMFS	Dimethyl(4,4,4-trfluorobutil)silyl
EG	Ethylene glycol
EPS	Extracellular polymeric substances
MEPs	Minimum energy pathways
NMR	Nuclear magnetic resonance
OEG	Oligo(ethylene glycol)
PBS	Phosphate-buffered saline
PEG	Poly(ethylene glycol)
SAM	Self-assembled monolayer
Si(100)	Silicon(100)
Si(111)	Silicon(111)
TMG	Trimethylgermanyl
TMS	Trimethysilyl
UHV	Ultrahigh vacuum
UV	Ultraviolet
XPS	X-ray photoelectron spectrometer

CHAPTER 1. GENERAL INFORMATION

I.1. Overview

Analogous to computers, brains rely on a network of billions of basic operating units called neurons to function, and both use electrical signals to transmit information.[1] Neurodegeneration occurs when the neurons lose their function. Many neurological disorder diseases such as Alzheimer's and Parkinson's are the result of such a process.[2,3] Despite the fact that neurological disorder diseases affect millions of people in the world, the choice of effective treatment remains limited. To overcome this problem, many researchers have contributed to enhance the accessibility of the neural systems using nanoparticles as drug transport and delivery systems.[4-6] The more challenging task is to regulate and monitor the drug transport and delivery process on the neural system, which relies on neural interfacing.[7] Yet little progress has been made on this issue due to obstacles to interpret and interfere with neural systems in vivo. To tackle these issues, researchers have been trying to develop practical methodologies for the development of bio-electronic hybrid systems.[8,9] Such endeavors will benefit from in vitro studies of the interface between organic neurons and inorganic electronics on neural culture platforms. Silicon surfaces are suitable platform candidates to interface to both organic and inorganic surrounding environment, because surface modification via organic molecules enables a controllable method to tune both

chemical and physical properties of the surface.[10,11] In this thesis, we will use "Click" chemistry to modify both surface chemical and physical properties. Furthermore we will demonstrate the possibility of creating 3D scaffold for neuron interaction using cyclic voltammetry. Spectroscopic techniques such as X-ray photoelectron spectroscopy and ellipsometry are employed to analyze surface properties. Three major research areas covered in this thesis are outlined here.

I.2. Self-assembled monolayers

Self-assembled monolayers (SAMs) are molecular assemblies with well-defined packing density formed by chemisorption of molecules.[12] The first case of SAMs formation by adsorption of self-assembling molecules on surface was reported in 1980, where Sagiv reported the formation of SAMs from chloro- and alkoxy-silanes with hydroxyl-terminated surfaces.[13]

SAMs on Si substrates enable surface modification at the molecular level, and one of the advantages is to create multi-functional surfaces by which are of particular interest in the fields of molecular electronics.

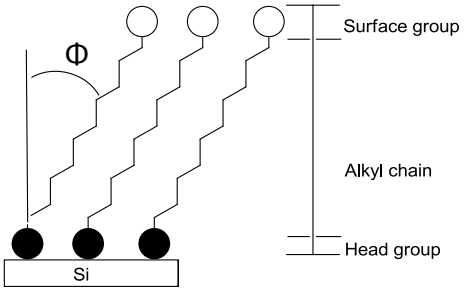

Figure I.1 Schematic diagram depicting the components of a self-assembed

monolayer assembled on a Si substrate via chemisorption. The self-assembling molecule is titled from the surface normal at Φ degrees.

The structure of SAMs on Si substrate is illustrated in **Figure I.1**. In general, self-assembling molecules include three parts: (i) head group that has high binding affinity with the surface, (ii) alkyl chain or aromatic rings that contribute to packing of the monolayers on the surface via inter-chain van der Waals interactions and electrostatic interactions, (iii) end group, which defines the chemical property of the monolayer.

Two of the most commonly employed SAMs on Si substrate are organosiloxane on silicon oxide, and hydrosilylation of alkyne and alkene on hydrogen-terminated silicon surfaces.

Organosiloxane-based monolayers gained wide interest due to modification of silanized glass and optical devices.[14] The properties of organosiloxane films, i.e. chemical composition, thickness, orientation and lateral order of the alkyl chains have been studied in detail.[15] The formation of organosiloxane SAMs on Si substrate involves five steps.[16,17] The first step involves the formation of hydroxylated surface. This is commonly done by treating silicon surface in a bath of hydroxychloric acid and hydrogen peroxide. Alternatively, dry etching by oxygen plasma has also been used to generate hydroxylate Si surfaces.[18] The mechanism of SAMs attachment onto hydroxylate silicon surfaces via chemisorption has been well studied[19] and key steps are depicted in **Figure I.2**. Approximately 10^{15} –OH groups/cm^2 can be generated on treated Si surface, which enables chemisorption

of organic molecules on the Si substrate. The second step is the physisorption of silane molecules on hydroxylated surface. The general procedure includes dipping freshly prepared hydroxylated surface into silane solution, in which silane molecules are physisorped onto the hydroxylated surface. In the third step, the silane head groups formed trihydroxysilane $–Si(OH)_3$ in the presence of water via hydrolysis. These highly polar $–Si(OH)_3$ subsequently forms covalent bonds with the hydroxyl groups on the Si substrate. In the end polycondenstation occurs between adjacent silanol groups forming polysiloxane networks, as the result, surface coverage increase over the time and a well-ordered monolayer is obtained.

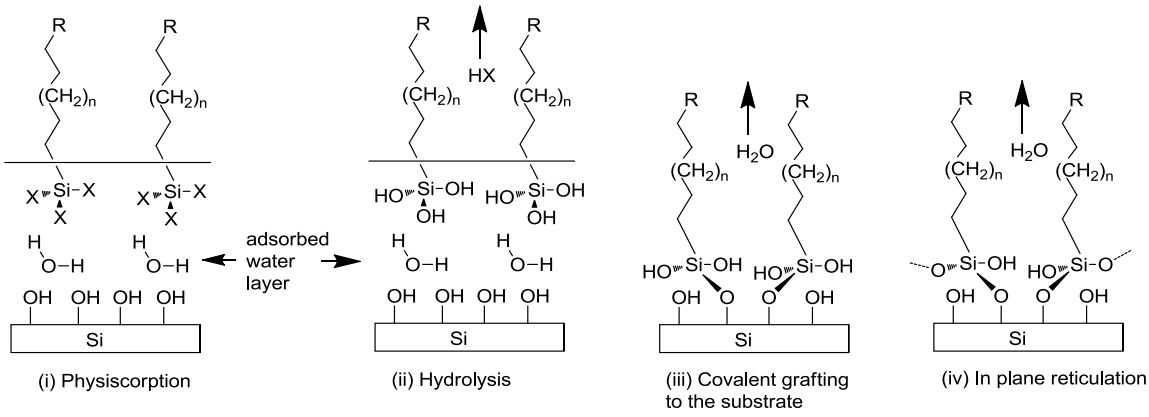

Figure I.2 Major steps in SAMs formation on hydroxylate silicon surfaces. Reproduced from ref **19**.

The major advantage of organosiloxane SAMs on SiO_2 substrate lays on simplicity of its formation. However, this methodology suffers from both reproducibility [20] and the vulnerability of Si-O bond to hydrolysis under basic condition.[21]

In order to form a stable base layer by which modification can be conducted at molecular level, hydrosilylation of 1-alkenes and 1-alkynes on hydrogen-terminated Si surfaces provides a suitable alternative to the organosiloxane system. This strategy was first reported by Linford *et al.* on Si surface platform.[22] The key advantage of the monolayer formed hydrosilylation over organosiloxane SAMs is the formation of a nonpolar Si-C bond between the alkyne or alkene head group and the silicon substrate. The Si-C bond formation avoids the possibility of multilayer formation which was common in organosiloxane SAMs. Furthermore, it is stable under both acidic and basic conditions; thus, SAMs formed by hydrosilylation are not subject to hydrolysis. The hydrosilylation reaction on surface can be roughly classified into radical initiation,[3] thermally induced hydrosilylation,[3,23] and UV irradiation.[24-26] Radical initiation mechanism was proposed for all cases. For photochemical hydrosilylation, the Si-H bond undergoes homolytic cleavage at temperatures over 150 °C, which yields a silicon radical at the surface that can react with the self-assembling molecules with head groups of alkenes or alkynes.

There are two major disadvantages of the hydrosilylation strategy. One of the disadvantages of this system is only limited functional group can be used as end groups. Many useful functional groups such as –OH,[27] –C(O)H,[27] –NH_2,[28] –Br,[29] –C(O)Cl,[30] and –SH[31] have been found to be highly reactive toward the hydrogen-terminated surfaces. Therefore, protection and subsequent deprotection is necessary to achieve diverse functionalized silicon surfaces, rendering

hydrosilylation strategy tedious.

Secondly, it is difficult to produce high quality SAMs without the formation of silicon oxide via hydrosilylation.[32] The resultant silicon oxide would compromise the electronic property of the SAMs and accelerate its degradation, therefore promoting the use of vacuum atmosphere during the hydrosilylation modification process.

I.3. Anti-biofouling monolayers

Biofouling is a succession of events that lead to the attachment of microorganisms (**Figure I.3**). It occurs in a wide range of medical and industrial applications; all of them share one characteristic, which is a microbial biofilm.[33] This vague term is often used to describe the phenomenon of microcolonies aggregating on surfaces. Because biofouling is a universal problem presenting in virtually every industrial and life-science-related fields, there is a continuous interest in developing novel anti-biofouling materials.

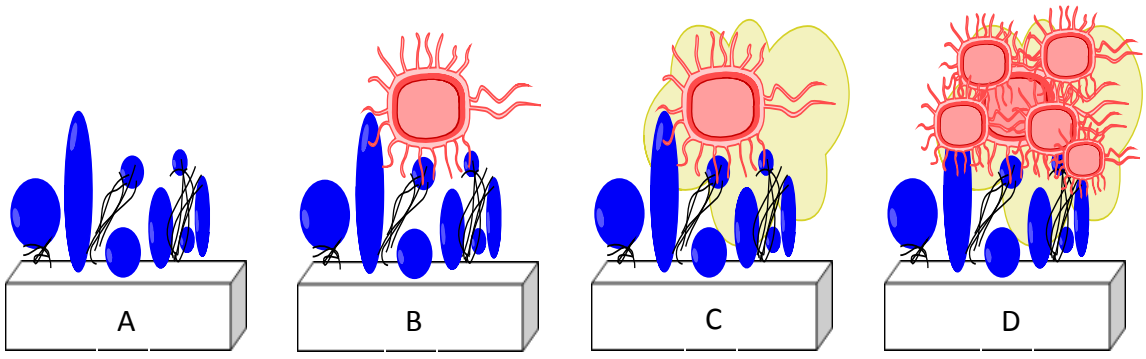

Figure I.3. Simplified schematic representation of major steps of biofouling caused

by prokaryote biofilm formation. (A) Adsorption: adsorption of organic and inorganic molecules on the film; (B) Immobilization: bacteria are immobilized on the film; (C) Consolidation: Bacteria produced extra-cellular polymer, which consolidates its attachment; (D) Colonization: multicellular species form a microbial film on the film. Reproduced from ref. **33**.

Biofilms are one of the most ancient life forms dating 3.5 billion years old, evidently by the fact that they can exist under an array of harsh environments including the bottom of the ocean.[34] Biofilms share one feature; they are held onto the surface by extracellular polymeric substances (EPS).[35] All three domains, including archaea, bacteria, and eukaryote, excrete EPS. In fact, it can be grown on most of the hydrophilic surfaces; regardless of nutrient condition.[36] Traditionally the major component of EPS is believed to be composed of extracellular polysaccharides or exopolysaccharides. However, recent studies have shown that an array of polymers, including polysaccharides, proteins, glycoproteins, nucleic acids, phospholipids, and humic acids could also be present.[37] It is known that the determine factor for biofilm formation is the initial bacterial adhesion.[38] Pedry studied the bacterial adhesion to both hydrophoblic and hydrophilic substrate using contact angle measurements.[39] He described the bacterial adhesion as an equilibrium process, and hydrophobicity generally reduces such equilibrium.

Several strategies have been developed for anti-biofouling purposes. One of the most commonly employed strategies is the use of strongly hydrophilic polymers that establish a steric barrier between biological organisms and coated substrates.

Natural products exhibiting anti-adhesive properties such as chitosan have been well documented.[40,41] In addition, Cao *et al.* reported that alginic acid, hyaluronic acid, and pectic acid have shown anti-adhesive property towards proteins and marine organisms.[42] Protein adsorption resistivity has also been reported for zwitterionic molecules such as sulfobetaine and phosphorylcholine.[43,44]

Among reported hydrophilic polymers, organic molecules such as polyethylene glycols (PEGs) are often considered as the gold standard in anti-biofouling materials.[45] Many publications have been trying to explain the protein adsorption resistance mechanism of PEGs based on steric repulsion, which has osmotic and elastic components.[46-48] Osmotic component comes from the solvation of PEG chains, and elastic component is based on conformational entropy of PEG chains. De Gennes attempted to rationalize the protein resistant property of PEG,[49,50] he suggested that the ethylene oxide units are miscible with water owing to the hydrogen bonding of the O atom. Therefore the -CH_2- groups are trapped inside water networks. When proteins reach the interphase with PEGs via diffusion, PEGs are compressed and water molecules associated with hydrogen-bonding are released due to compression which is energetically unfavorable, therefore the protein adsorption is minimized. Indeed Jeon has found that the protein adsorption is dependent of both thickness and the surface coverage of the PEG chains, which is associated with hydrophilicity of the PEG film.[50] But such explanation cannot be used to rationalize the protein-resistant property of the OEG film ($n<6$). Prime and Whitesides found both hydroxyl- and methoxy-terminated OEG alkanethiolate

SAMs adopting helical conformation on Au substrate exhibit protein resistance, even with surface coverage as low as 35%;[51] thereby demonstrating that protein adsorption on OEG films is insensitive to surface density comparing to PEG films but rather the SAMs conformation, which Szleifer et al. proposed as the anti-biofouling mechanism based upon single-chain mean theory.[52] In short, during protein approach, the change in conformational entropy of the OEG chain is unfavored, providing repulsion against protein adhesion. Although the exact mechanism for anti-biofouling is unclear and requires much additional research, to design novel anti-biofouling materials, one has to understand the factors influencing the interaction, which will be discussed in the following chapter.

I.4. Functionalizing Si(111) for electrochemical interface

There has been an explosion of research in the field of molecular electronics since Aviram and Ratner suggested that molecules are capable of performing the functions of semiconductor electronics.[53] The basic components of a molecule behaving as electrochemical interface include a redox-active surface group, an alkyl chain that finely tunes the electrochemical property, and a tethered head group that can undergo facile attachment to the substrate. For organic monolayers formed by these molecules, several charge-transport mechanisms have been proposed to achieve electron transfer across molecular junctions: (1) electron tunneling through the molecular monolayer barrier;[54] (2) direct charge transport via redox active surface group through holes (defects) on the

monolayer;[54,55] and (3) recombination of electrons between redox active surface groups when the monolayer is electroactive.[56]

I.5. References

(1) Donoghue, P. J. *Nat. Neurosci.* **2002**, *5*, 1085.

(2) Martin, L. J.; Al-Abdulla, N. A.; Brambrinl, A. M.; Kirsch, J. R.; Sieber, F. E.; Portera-Cailliau, C. *Brain Res. Bull*. **1998**, *46*, 281.

(3) Sriram, K.; Matheson, J.M.; Benkovic, S.A.; Miller, D.B.; Luster, M.I.; O'Callaghan, J.P. *FASEB J.* **2002**, *16*, 1474.

(4) Basarkar, A.; Singh J. *Int. J. Nanomedicine.* **2007**, *2*, 353.

(5) Maysinger, D.; Morinville, A. *Trends Biotechnol.* **1997***, 15*, 410-418.

(6) Bodor, N; Prokai, L.; Wu, W. M.; Farag, H.; Jonalagadda, S.; Kawamura, M.; Simpkins, J. *Science* **1992***, 257*, 1698.

(7) Jain, K. K. *Neurodegener. Dis.* **2007***, 4*, 287.

(8) Katz, E.; Willner, I. *Angew. Chem., Int. Ed.* **2004**, *43*, 6042.

(9) Liu, Q.; Cai, H.; Xu, Y.; Li, Y.; Li, R.; Wang, P. *Biosens. Bioelectron*. **2006**, *22*, 318.

(10) Kobayashi, S.; Nishikawa, T.; Takenobu, T.; Mori, S.; Shimoda, T.; Mitani, T.; Shimotani, H.; Yoshimoto, N.; Ogawa, S.; Iwasa, Y. *Nat. Mater.* **2004**, *3*, 317.

(11) Laine, R. M.; Zhang, C.; Sellinger, A.; Viculis, L. *Appl. Organometall. Chem.* **1998**, *12*, 715.

(12) Ulman, A. *Chem. Rev.* **1996**, *96*, 1533.

(13) Sagiv, J. *J. Am. Chem. Soc*. **1980**, *102*, 92.

(14) Roscoe, S. B.; Kakkar, A. K.; Marks, T. J.; Malik, A.; Durbin, M. K.; Lin, W.;

Wong, G. K.; Dutta P. *Langmuir*, **1996**, *12*, 4218.

(15) Tillman, N.; Ulman, A.; Schildkraut, J. S.; Penner, T. L. *J. Am. Chem. Soc*. **1988**, *110*, 6136

(16) Wasserman, S. R.; Tao, Y. T.; Whitesides G.M. *Langmuir* **1989**, *5*, 1074.

(17) Tillman, N.; Ulman, A.; Schildkraut, J.S.; Penner, T.L. *J. Am. Chem. Soc.* **1988**, *110*, 6136.

(18) Petitdidier, S.; Bertagna, V.; Rochat, N.; Rouchon, D.; P. Besson, R. Erre, M. Chemla, *Thin Solid Films* **2005**, *476*, 51.

(19) Aswal, D.K. *Anal. Chim. Acta* **2006**, *568*, 84.

(20) Le Grange, J. D.; Markham J. L. and Kurkjian, C. R. Langmuir, 1993, 9, 1749.

(21) CalistriYeh, M.; Kramer, E. J.; Sharma, R.; Zhao, W.; Rafailovich, M. H.; Sokolov, J.; Brock, J.D. *Langmuir* **1996**, *12*, 2747.

(22) Linford, M.R.; Chidsey, C.E.D. *J. Am. Chem. Soc.* **1993**, *115*, 12631.

(23) Sung, M.M.; Kluth, J.; Yauw, O.W.; Maboudian, R. *Langmuir* **1997**, 13, 6164.

(24) Terry, J.; Linford, M.R.; Wigren, C.; Cao, R.; Pianetta, P.; Chidsey, C.E.D. *Appl. Phys. Lett.* **1997**, *71*, 1056.

(25) Cicero, R.L.; Linford, M.R.; Chidsey, C.E.D. *Langmuir* **2000**, *16*, 5688.

(26) Gotz, G.; Bidlingmaier, B.; Wezstein, M. *Angew. Chem., Int. Ed.* **1998**, *37*, 2462.

(27) Boukherroub, R.; Morin, S.; Sharpe, P.; Wayner, D.D.M.; Allongue, P. *Langmuir* **2000**, *16*, 7429.

(28) Strother, T.; Hamers, R.J.; Smith, L. M. *Nucleic Acids Res.* **2000**, *28*, 3535.

(29) Jin, H.; Kinser, C. R.; Bertin, P.A.; Kramer, D.E.; Libera, J. A.; Hersam, M. C.; Nguyen, S. T.; Bedzyk, M. J. *Langmuir* **2004**, *20*, 6252.

(30) Linford, M. R.; Chidsey, C.E.D. *J. Am. Chem. Soc.* **1993**, *115*, 12631.

(32) Cai Y. and Roberts, B. P. *Tetrahedron Lett.* **2001**, *42*, 4581.

(31) Kilian, K. A.; Bo, T.; Cking, K.; Gaus, M.; Gooding, J. *J. Biomaterials*, **2007**, *28*, 3055.

(32) Linford, M. R.; Fenter, P.; Eisenberger, P. M.; Chidsey, C. E. D. *J. Am. Chem. Soc.* 1995, 117, 3145.

(36) Staudt, C. ; Horn, H.; Hempel, D. C.; Neu, T. R. *Biotechnol. Bioeng.* **2004***, 88*, 585.

(37) McSwain, B. S.; Irvine, R. L.; Hausner, M.; Wilderer, P. A. *Appl. Environ. Microbiol.* **2005**, *71*, 1051.

(38) Brusscher, H. J.; Bos, R.; van der Mei, H.C. *FEMS Microbiol. Lett.* **1999**, *128*, 5229.

(39) Pedry, L. Ph.D. Thesis, Stanford University, 2005. (Interaction of Bacteria with Hydrophobic and Hydrophilic Interfaces)

(40) No, H. K.; Park, N. Y.; Lee, S. H.; Meyers, S. P. *Int. J. Food Microbiol*. **2002**, *74*, 65.

(41) Roller, S.; Covill, N. *Int. J. Food Microbiol*. **1999**, *47*, 67.

(42) Cao, X.; Pettit, M. E.; Conlan, S. L.; Wagner, W.; Ho, A. D.; Clare, A. S.; Callow, J. A.; Callow, M. E.; Grunze, M.; Rosenhahn, A. *Biomacromolecules* **2009**, *10*, 907.

(43) Zhang, Z.; Chao, T.; Chen, S.; Jiang, S. *Langmuir* **2006**, *22*, 10072.

(44) Chen, S.; Zheng, J.; Li, L.; Jiang, S. *J. Am. Chem. Soc.,* **2005**, *127*, 14473.

(45) Gölander, C-G.; Jönsson, S-E.; Vladkova, T.; Stenius, P.; Eriksson, J-C. *Coll. Surf.* **1986**, *21*, 149.

(46) de Gennes, P. G. *Ann. Chim.* **1987**, *77*, 389.

(47) Taunton, H.J.; Toprakcioglu, C.; Fetters, L.J.; Klein, J. *Nature* **1988**, *332*, 712-714.

(48) Jeon, S.I.; Lee, J.H.; Andrade, J.D.; de Gennes, P.G. *J. Coll. Int. Sci.* **1991**, *142*, 149.

(49) Jeon, S. I.; Andrade, J. D. *Ibid.* **1991**, *142*, 159.

(50) De Gennes, P. G. *Adv. Coll. Int. Sci.* **1987**, *27*, 189.

(51) Prime, K. L.; Whitesides, G. M. *J. Am. Chem. Soc*. **1993**, *115*, 10714.

(52) Szleifer, I. *Physica A: Statistical and Theoretical Physics* **1997**, *244*, 370.

(53) Aviram, A.; Ratner, M. A. *Chem. Phys. Lett.* **1974**, *29*, 277.

(54) Yaffe, O.; Scheres, L.; Puniredd, S. R.; Stein, N.; Biller, A.R.; Lavan, H.; Shpaisman, H.; Zuilhof, H.; Haick, H.; Cahen, D.; Vilan, A. *Nano Lett.* **2009**, *9*, 2390.

(55) Ulgut, B.; Abrua, H. D. *Chem. Rev.* **2008**, *108*, 2721.

(56) Zigah, D.; Herrier, C.; Scheres, L.; Giesbers, M.; Fabre, B.; Hapiot, P.; Zuilhof, H. *Angew. Chem., Int. Ed.* **2010**, *49*, 3157.

CHAPTER II. OLIGO(ETHYLENE GLYCOL) FUNCTIONALIZATION OF Si(111) SUBSTRATE

II.1 Introduction

II.1.1. Assembly of organic molecules on Si(111) surfaces via Si-C bonds for biological applications

Building a device to study the interaction between ultrathin organic films and biological targets requires modifying the surface at molecular scale. High packing density of a single type of molecule is often desired for such modification. The most widely employed strategy to achieve this modification is SAMs, first reported by Zisman *et al.* in 1946.[1] Among commonly encountered self-assembly systems for Si(111) substrate, hydrosilylation offers the unique advantage of anchoring alkyl chains onto the substrate via Si-C non-polar covalent bonds. The resultant SAMs, therefore, are prone to hydrolysis. Linford *et al.* first demonstrated the reaction of alkenes on hydrogen-terminated silicon via radical chain mechanism,[2,3] by which alkenes were inserted into Si-H presenting substrate using diacyl peroxide radical initiator. The resulting film was demonstrated to have both acidic and basic resistivity, thus revealing its potential applications in the biological applications.

The recent developments of drug carriers, medical implants, and biosensors have generated a significant demanding of anti-biofouling materials,

in order for these novel devices to be functioned properly in-situ. Traditionally, poly (ethylene glycol) (PEG)-based polymers were extensively used for this purposes.[4] However, the high strains of the PEG chain fold leads to the free radical oxidative degradation, as the activation energy of hydrogen abstraction is lowered.[5] The oxidative degradation of PEG compromises the ability of the PEG film to resist nonspecific protein absorption over the time, thus and a novel anti-biofouling material with higher stability is needed.[6]

Since proteins are polyampholytes (protein surfaces are both positively and negatively charged), they can adhere to charged surfaces.[7] Indeed, most of the reported anti-biofouling materials bear balanced overall charge, and can be classified into one of the two major classes including hydrophilic and zwitterionic materials.[8] To search for the suitable functional groups in order to design novel biomolecule that is protein resistant, Chapman *et al*. surveyed a variety of functional groups and determined that anti-biofouling functional groups share some common structural characteristics: polar functional groups, hydrogen bond-accepting groups, there is no hydrogen bond-donating groups, and there is no net charge.[9] Commonly encountered hydrophilic anti-biofouling materials including PEG, polysaccharides, and polyamides have been found to share the above criteria.[10] Currently SAMs that present oligo(ethylene glycol) groups (OEG) are still the most effective protein-resistant surfaces available.[11,12]

II.1.2. Alkyne vs. alkene

Since Chidsey *et al.* first reported the preparation of organic SAMs on oxide free silicon,[3] several methods to produce SAMs from 1-alkene and 1-alkyne have been published. Generally, the passivations can be classified according to reaction conditions including UV irradiation,[2,13] radical initiation, and thermally induced hydrosilylation.[14] Such harsh conditions usually yield densely packed monolayers,[15] but they are not compatible with many bioactive materials that readily degrade under these conditions. To overcome this problem, Sun *et al.* developed a mild reaction condition that allows 1-alkene to be attached to Si(100) surface under visible light.[16] Liu *et al.* went a step further and developed a passivation strategy that does not require external activation. They found activated 1-alkynes such as propiolate esters can be attached onto Si(111) at room temperature in the dark.[17] Such a strategy, however, suffers from drawbacks including up to 40 h reaction time as well as low coverage.

It has been widely accepted that most monolayer formations that require external activation undergo different types of radical chain mechanisms. A general mechanism has proposed for hydrosilylation is illustrated in **Figure II.1**. Since radical initiation and UV irradiation offer considerably strong energy to homolytically cleave the strong Si-H bond, which is insufficient in terms of thermal activation and milder conditions, one can imply that they would adopt different initiation mechanisms. Sun *et al.* proposed that under mild conditions, photoexcited electron hole pairs would form near silicon surface. Si-C bond is

formed and β carbon radical is generated via nucleophilic attack of 1-alkyne or 1-alkene at this photoexcited electron hole pairs.[18]

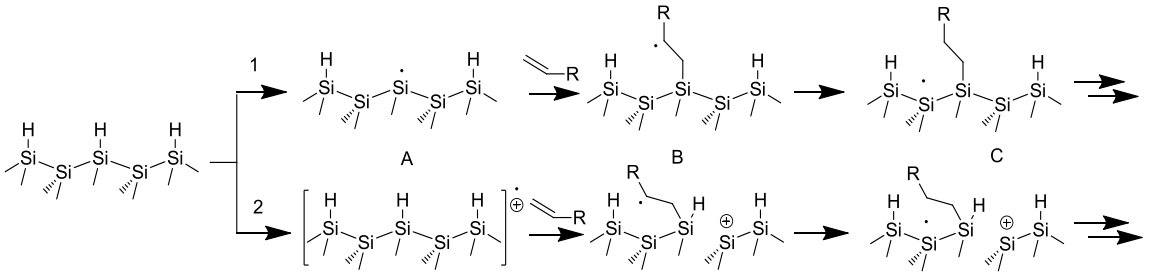

Figure II.1. Proposed mechanism for hydrosilylation of 1-alkene on hydrogen-terminated silicon surface (1) under UV irradiation, or radical initiation and (2) under thermally induced or visible light-initiated hydrosilylation. Reproduced from ref **19**.

While both 1-alkyne and 1-alkene undergo similar initiation mechanism (**Figure II. 2**), the surface coverage varies as the 1-alkyne modified are up to 30% more densely packed comparing to 1-alkene modified surface.[20,21] Such an experimental difference implies reactivity difference between 1-alkyne and 1-alkene, therefore it is important to utilize this effect in terms of optimizing the design of novel unsaturated adsorbates. Takeuchi *et al.* used periodic density functional theory (DFT) calculations to study the difference between 1-alkyne and 1-alkene in the initiation steps.[22] Based on calculated minimum energy pathways (MEPs), Takeuchi concluded that 1-alkene is lesser reactive because the stabilization energy for radical intermediate is small, and the activation barrier for subsequent H-abstraction is large. Therefore 1-alkene is likely to desorb

comparing to 1-alkyne.

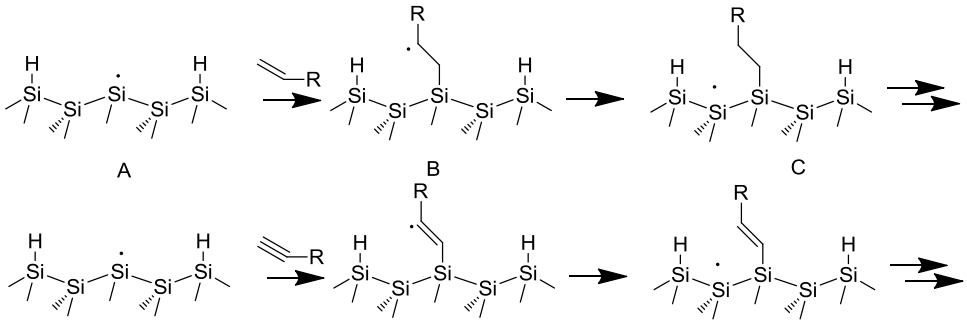

Figure II.2. Proposed mechanism for hydrosilylation of 1-alkene (top) and 1-alkyne (bottom) on hydrogen-terminated silicon surface under UV irradiation or radical initiation.

The advantage of 1-alkyne over 1-alkene self-assembling molecules also extends to the stability of the film. Puniredd *et al.* has shown that Si-CH=CH-CH_3 surface is stable toward oxidation after two months exposure in the air.[23]

II.1.3. Preparation of ethynyl-presenting oligo(ethylene glycol) monolayers

Previously, we have developed a practical method to introduce handles on the SAMs for tethering molecular probes,[24] which was based on Huisgen's 1,3-dopolar cycloaddition reaction between terminal alkyne and azide catalyzed by Cu(I) catalyst. The unique bio-orthogonal property of the "Click" reaction allows it to be carried out in both *in vitro* and *in vivo* applications.[25,26] In order to incorporate 1-alkene self-assembling molecules that contains ethynyl group as a handle, the ethynyl group must be protected because the ethynyl group exhibits much higher reactivity comparing to alkenyl group.[27] Former group

member Dr. Guoting Qing has screened different bulk protecting groups including trimethysilyl (TMS), trimethylgermanyl (TMG), and fluorinated alkylsilyl (DMFS) protecting groups. TMG protecting group was selected based on its ability to be removed from terminal alkynes at very mild and neutral conditions.[28-30]

In search of a mild passivation condition to attach 1-alkene onto hydrogen-terminated silicon, our group has found that UV irradiation is robust enough to form high quality and protein resistant OEG monolayers.[24] Initially, a setup shown in **Figure II.3** was built for fulfilling this purpose. A piece of freshly prepared hydrogen-terminated silicon was placed on top of a vacuum manipulator inside a vacuum apparatus. A drop of self-assembling molecule was placed on the bottom of quartz glass facing towards the silicon surface to be passivated. To reduce contamination from air, both hydrogen-terminated silicon and self-assembling molecule were degassed by vacuum equivalent to 10^{-3} torr for 15 min. This would remove some moisture and organic contaminants with relatively low boiling temperature. Afterwards, the hydrogen-terminated silicon surface was elevated by the vacuum manipulator to bring to contact with the self-assembling molecules, allowing self-assembling molecules to cover the silicon surface uniformly. The surface hydrosilylation was then initiated by exposure to 254 nm UV irradiation generated by a handheld UV lamp for 2h.

With this apparatus, we were able to perform surface hydrosilyalation with ease. But numerous problems associated with this apparatus prevent it from being used to generate large batch of films functionalized with different

molecules. First of all, the size of the film was limited to 1 inch^2, which greatly limited the amount of duplicate samples to be prepared. Secondly, the vacuum generated by the mechanical vacuum pump was insufficient to remove reactive impurities such as H_2O and O_2. Thirdly, vapors of self-assembling molecules with high molecular weight could accumulate inside the vacuum apparatus; the residual self-assembling molecules would contaminate silicon substrate over the time.

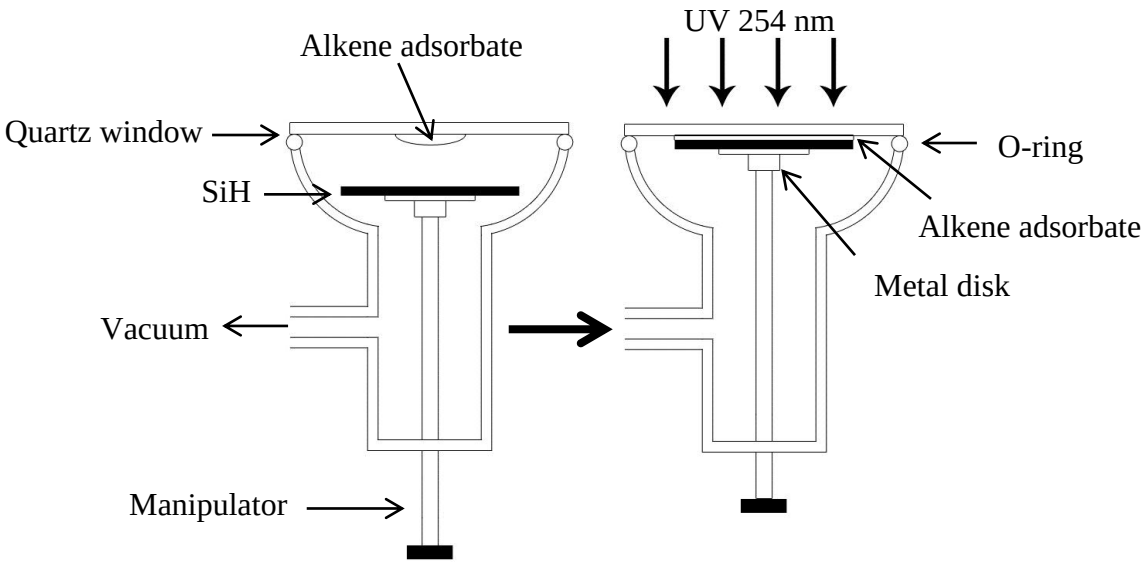

Figure II.3. Apparatus used for UV-initiated hydrosilylation on hydrogen-terminated silicon surface.

To address the limitations of our first-generation film deposition apparatus, we built a second film deposition apparatus. The new film deposition apparatus features several improvements over the old one. The chamber used for film passivation is mounted underneath a vacuum glove box, which can be purged

with ultra-high purity nitrogen and maintained at pressure equivalent to 2 inches water column if necessary. Such design allowed the freshly prepared hydrogen-terminated silicon substrate to be stored for prolonged period of time without significant degradation. Secondly, the film passivation chamber is maintained by a turbomolecular pump using ultra-high vacuum (UHV) (1×10^{9} torr). The UHV allows better removal of reactive impurities such as H_2O and O_2 as well as the residual gas from the instrument itself. Thirdly, the deposition chamber is attached to multiple thermal pads that are capable of heating up to 90 °C. The heating feature can be used to remove high boiling point self-assembling compound accumulated inside the deposition chamber experiments.

In the present work, we will demonstrate the use of a convenient strategy to produce trimethyl germanyl (TMG) protected ethynyl-presenting SAMs on Si(111) substrate, and modify it with OEG via Cu(I) catalyzed one-pot deprotection and Huisgen 1,3-dipolar cycloaddition. The resulting films were characterized by water contact angle measurements, X-ray photoelectron spectrometer (XPS), atomic force microscope (AFM), and ellipsometer.

II.2. Results and discussion

II.2.1. Improvements in film preparation

Improved apparatus for surface hydrosilylation. Although our first-generation film deposition apparatus enabled us to prepare films via UV initiated surface hydrosilylation conveniently, drawbacks such as film size (< 1 inch^2)

and defects produced from the reactive impurities such as H_2O and O_2 significantly limits its application. Furthermore, the mechanical vacuum pump is incapable of removing residuals of high boiling temperature self-assembling compounds, which build up inside the deposition chamber after each experiment. This generates a source of contamination when different self-assembling compounds are used. We came to realize that the exerting control over radical-initiated surface hydrosilylation can only be achieved under ideal condition such as the one under ultra-high vacuum (UHV). Therefore a second-generation film-deposition apparatus was built (**Figure II.4, II.5**) to meet the UHV condition. In the new apparatus, silicon wafer up to 5 inches diameter can be passivated. A vacuum glovebox is built on top of a UHV chamber; it serves as a temporary storage for the freshly prepared hydrogen-terminated silicon, thereby reduces the surface contamination across the substrate surface. Inside the glovebox, the silicon substrate is attached to the lower end of an UHV manipulator via the carbon conductive tape, which does not generate gas under UHV. Several droplets of the self-assembling molecules are deposited on top of a quartz window. Both silicon substrate and the quartz window are lowered into the UHV chamber, which is sealed by a Viton O-ring. To establish UHV condition, the UHV chamber is pumped with mechanical pump to the intermediate vacuum (10^{-3} torr) before engaged with the turbomolecular pump, which generates UHV (10^{-9} torr) inside the UHV chamber. Once most of the reactive impurities such as H_2O and O_2 species are removed by the UHV, the silicon substrate is lowered by the UHV

manipulator and is brought to contact with the droplets of self-assembling molecule on the quartz window. The droplets of the self-assembling molecule form a thin layer, which is sandwiched between the silicon substrate and the quartz window. To afford a uniform coverage of UV irradiation over the film, we used a transilluminator with UV (254 nm) as the irradiation source. The surface hydrosilylation is usually close to completion in 2h.

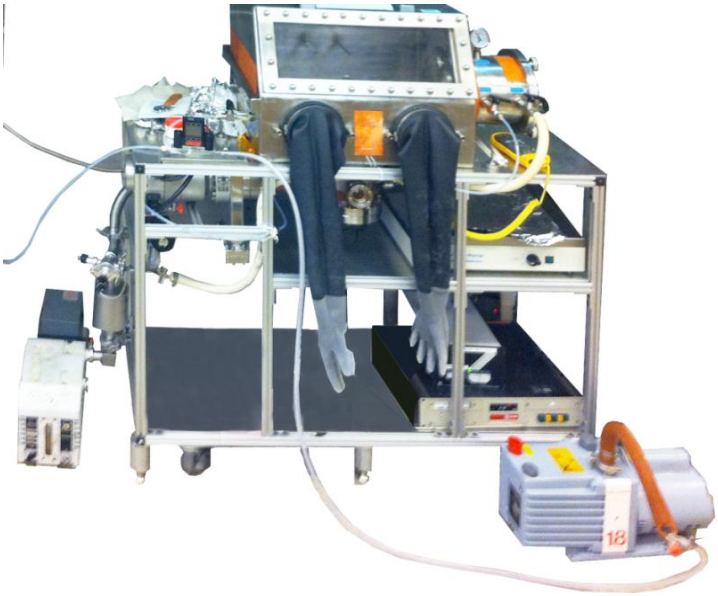

Figure II.4. The second-generation film-deposition apparatus.

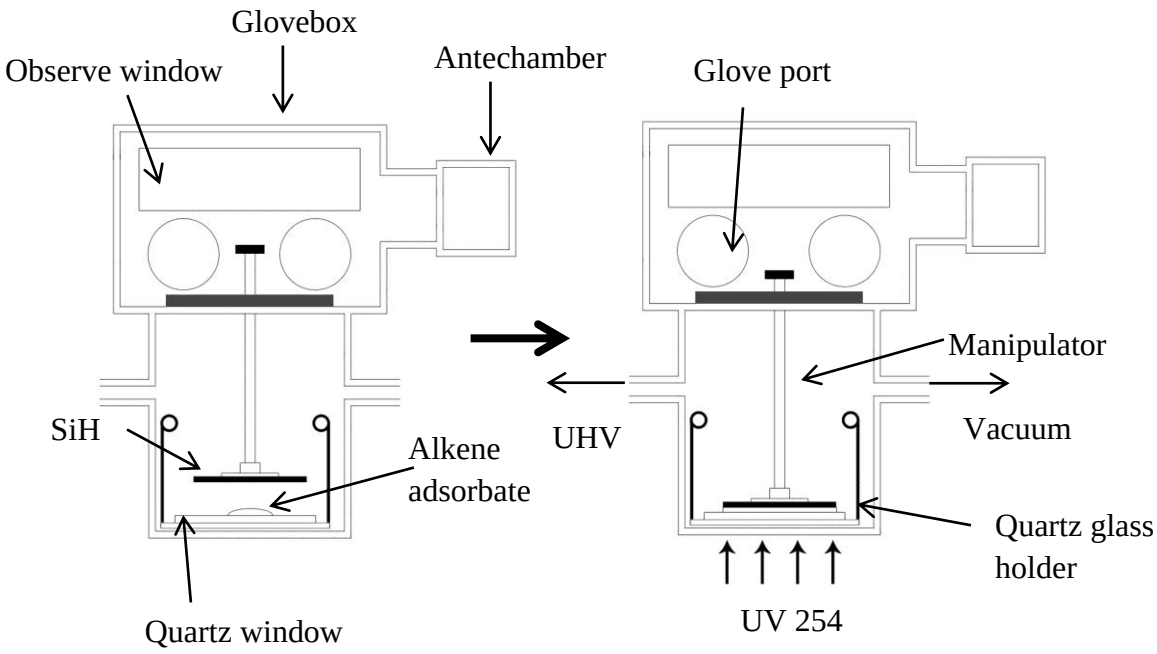

Figure II.5. Schematic diagram of the second-generation film-deposition apparatus for passivating hydrogen-terminated Si(111) substrate.

The new generation of film-deposition apparatus presents numerous improvements. First, the introduction of UHV by the turbomolecular pump can effectively remove the reactive impurities such as H_2O and O_2 species. Secondly, it is convenient to maintain the UHV chamber. It can be cleaned with organic solvent such as the 200 proof ethanol. Water, ethanol, and residual self-assembling molecules trapped inside the chamber can be easily removed by baking the UHV chamber at 100 °C under UHV. As the result, this apparatus is very efficient to screen different self-assembling molecules without contaminations. Together with these advantages, this UHV apparatus is able to provide substantial improvement over the SAMs quality as demonstrated by the

long-term stability against non-specific adsorption of proteins.

II.2.2. Oligo(ethylene glycols) monolayers on Si(111)

Characterization. 2,5,8,11,14,17,20,23-Octaoxatritriacont-32-ene was grafted onto the hydrogen-terminated Si(111) using the UHV apparatus via UV initiated surface hydrosilylation (**Scheme II.1**). The film was characterized by ellipsometer, AFM, XPS, as well as contact angle.

The survey scan of XPS reveals the progression of the hydrosilylation on the silicon substrate. For a freshly prepared hydrogen-terminated silicon substrate, both Si2s and Si2p signals were detected at 150 and 100 eV respectively. No other elements were detected indicating that physisorption did not occur at a significant scale. The narrow scan of XPS in the region of Si2p revealed the absence of SiO_2 signal; this indicates the native silicon oxide layer was completely removed by the anisotropic etchant, ammonium fluoride. After the hydrosilylation of the hydrogen-terminated silicon substrate under UV exposure for 2 h, the resulting SAM was characterized by XPS. The XPS survey scan shows two new elements including both C and O, thus verifies the silicon substrate has been modified.

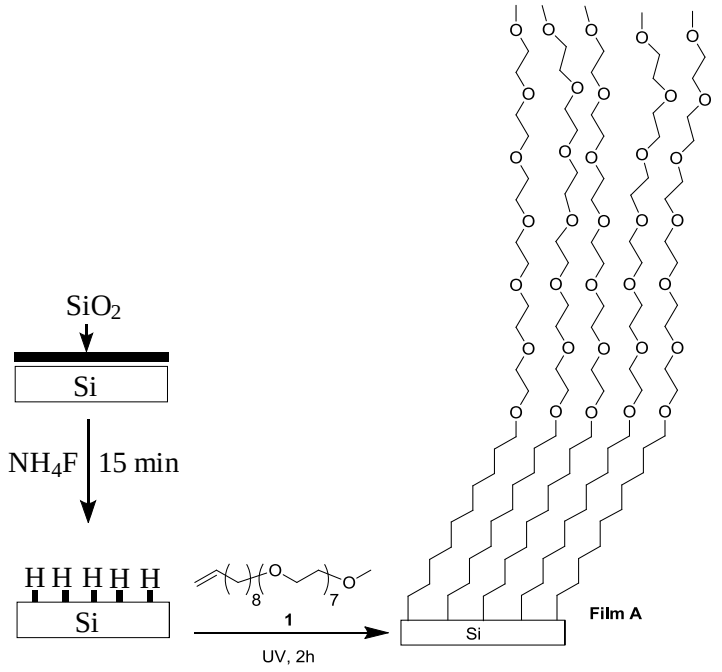

Scheme II.1. Preparation of EG7-OMe Presenting Film **(A)** Promoted by Hydrosilylation on Hydrogen-terminated Si(111).

High-resolution XPS measurements were obtained to quantify the EG7 modified substrate (**Figure II.6**). The C1s spectrum was obtained and peaks are found to be at 285.1 eV and 286.7 eV after deconvolution, corresponding to alkyl (C-C) and etheric (C-O) signals respectively. The area ratio of alkyl (C-C) peak over etheric (C-O) peak was calculated to be 0.53, which is close to the theoretical value (0.56). The atomic concentration ratio of C over O in the surveyed area is 2.71, which is also close to the theoretical value (3.125). The narrow scans over Si2p region revealed no SiO_2 formation on the SAMs.

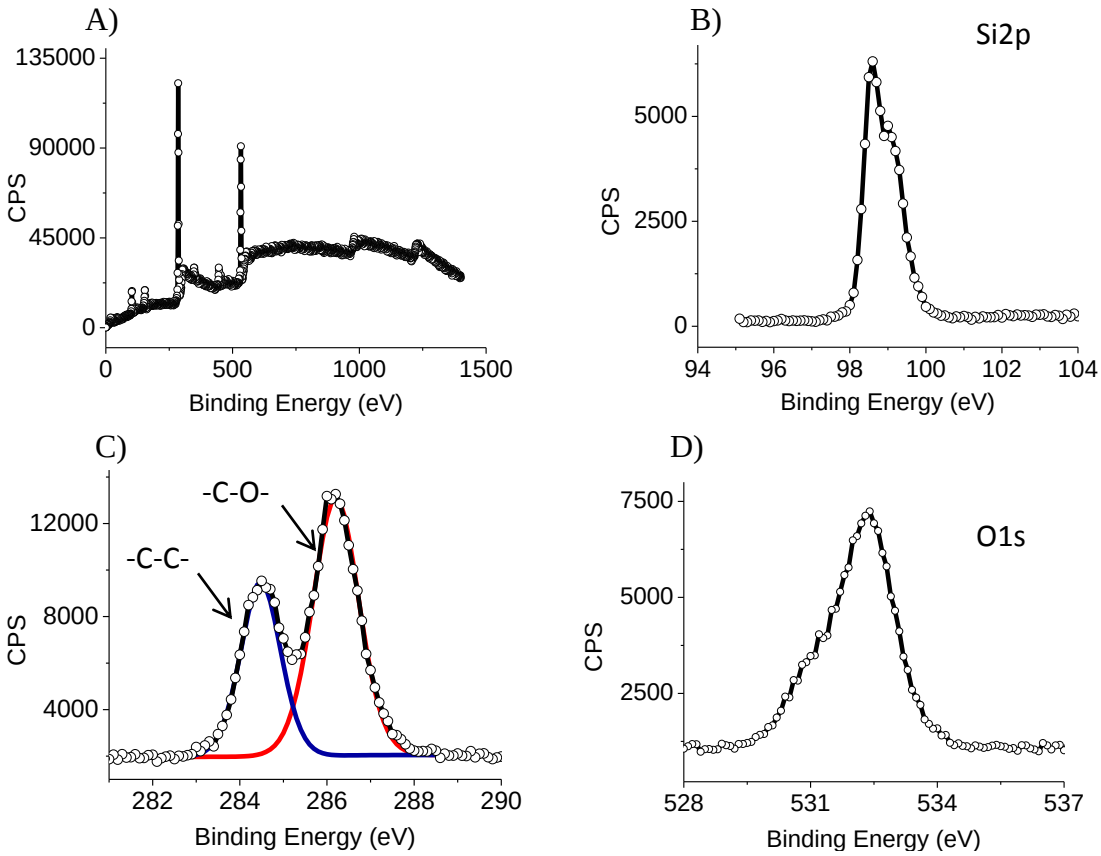

Figure II.6. High-resolution XPS spectra of EG7-OMe film. (A) Survey spectrum; (B) Narrow scan of the Si2p region, showing absence of oxide growth during surface hydrosilylation; (C) Narrow scan of C1s region, the ratio of C-C/C-O peaks is characteristic to EG7-OMe film; (D) Narrow scan of O1s region, which arises after surface hydrosilylation.

The contact angle measurement was obtained to be 51±1°, which coincides with the literature values (51±1).[43]

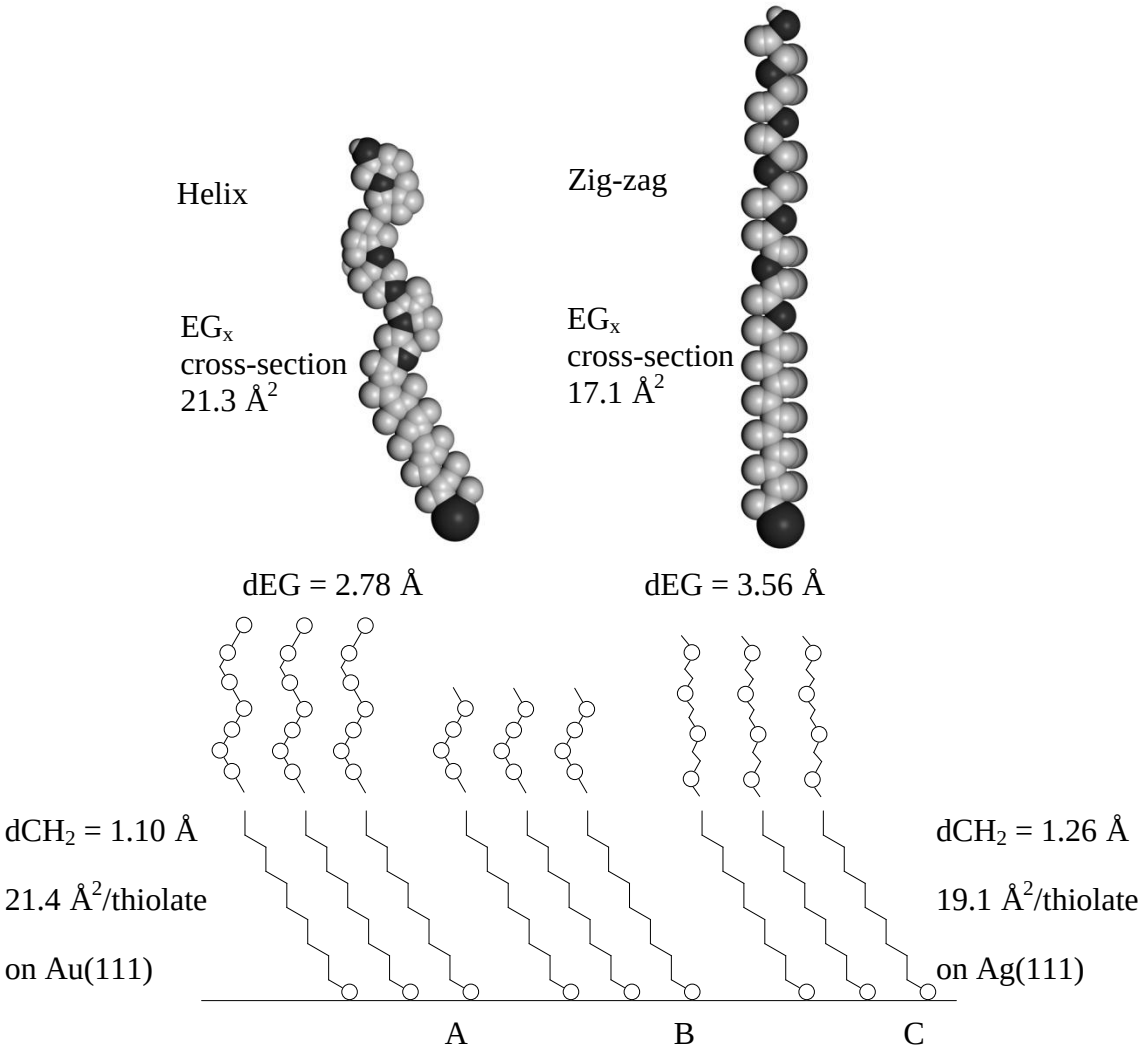

Scheme II.2. Molecular Cross-section and Incremental Thickness of Each Methylene and Ethylene Glycol Unit for (A) EG6-OH on Au with Perpendicular Orientation of the EG6 Helix, and Alkyl Chain Tilted 30° to the Normal Plane; (B) EG6-OH on Au with Perpendicular Orientation of the EG3 Helix, and Alkyl Chain Tilted 30° to the Normal Plane, (C) EG3-OMe on Ag with Zigzag Conformation of the EG3 Unit and Perpendicular Orientation of the Alkyl Chain. Reproduced from ref **31.**

The ellipsometric measurement of the EG7 film was 41±1 Å, which is consistent with the theoretical length of a single EG7 molecule calculated by MM2 using ChemDraw. This result suggests that the adsorbed EG7 molecules on the substrate adopted a perpendicular conformation for the alkyl chain and a zig-zag conformation for the EG7 units. The ordered conformation of EG7 molecules could be the result of the lateral constraints from the dense packing.

The morphology of EG7 film was characterized using the AFM using the contact mode, and the results are summarized in **Figure II.7.**

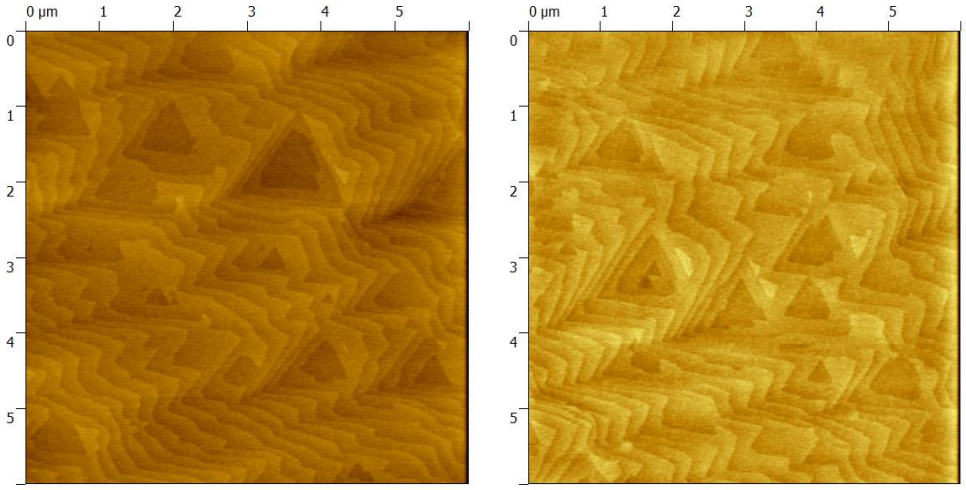

Figure II.7. Contact mode AFM image (6 × 6 μm^2) of bare silicon hydride substrate (left), after grafted with EG7-OMe using hydrosilylation under UV (254 nm). The *z* scale (contrast) is 8 nm.

To verify the densely packed conformation of the EG7 film, we used the following equation to calculate the film coverage. This method was developed by Cicero *et al.* to determine the ratio of the self-assembling molecules to the

surface silicon atoms.[45] Former group member Dr. Guoting Qing has adopted this method and first applied it to the EG7 films.

$$\frac{N_{chains}}{N_{surf,\,Si}} = \left(\frac{S_{ML}^{C}}{S_{Si}^{Si}}\right)\left(\frac{d_{ML}}{L_{carbon}}\right)\left(\frac{\sigma_{Si}\,\lambda_{Si}^{Si}\,\rho_{Si}^{Si}}{\sigma_{C}\,\lambda_{ML}^{C}\,N_{surf,\,Si}}\right)\frac{e^{(-d_{ML}/\lambda_{ML}^{Si}\sin\theta)}}{1-e^{(-d_{ML}/\lambda_{ML}^{C}\sin\theta)}} \quad (1)$$

by which N_{chains} is the number of hydrocarbon chains per unit area; $N_{surf,\,Si}$ (7.8×10^{14} atoms/cm^2) is the density of silicon atoms in atoms cm^{-2}; S_{ML}^{C} is the integration area of XPS peak of C1s signal; S_{Si}^{Si} is the integration area of XPS peak of Si2p signal; d_{ML} is the ellipsometry measurement of the monolayer thickness; L_{carbon} is the number of the carbon atoms in the hydrocarbon chain; σ_{Si} and σ_C are atomic sensitivity factors for silicon (0.368) and carbon (0.314) respectively; ρ_{Si}^{Si} is the density of Si atoms in the bulk silicon (5.0×10^{22} atoms/cm^3); λ_{ML}^{C} and λ_{ML}^{Si} are attenuation lengths for C1s (35.4 Å) and Si2p (39.5 Å) signals respectively; and θ (45°) is the takeoff angle of the XPS analyzer. The surface density of the EG7 monolayer is calculated to be 4.92×10^{14} molecules/cm^2 by substituting corresponding values into Eq 1.

The unit surface area per grafted EF7 molecule (A_m) is estimated by the ellipsometric measurement of the film thickness using the following equation derived by Sofia *et al.*:[46]

$$A_m = \frac{MW}{\rho T_h N_A} \quad (2)$$

where ρ is the constant of the density of the EG7 molecule on the substrate, which we substituted with the reported value of PEG (1 g/cm^3); T_h is the

ellipsometric measurement of EG 7 film thickness, which is 41 Å; N_A is the Avogadro's number, which is 6.02 × 10^{23} molecules/mole; and *MW* is the molecular weight of EG7 molecule, which is 478.7 g/mol. We calculated the unit surface area per grafted EG7 molecule (A_m) on Si (111) substrate to be 1.94 $Å^2$/molecule. Considering the molecular cross-section of PEG in the all-trans, zigzag form is 17.1 $Å^2$,[47] the EG7 molecules occupies much smaller space and thus is able to afford much higher packing density.

The EG7 film density can be estimated by simply inverting the above equation to the following form:

$$D_m = \frac{\rho T_N N_A}{MW} \quad (3)$$

where D_m is the EG7 film density, which we calculated to be 5.15 × 10^{14} molecules/cm^2. This result is comparable to the D_m calculated from the small film prepared by former group member Dr. Guoting Qing (4.8 × 10^{14} molecules/cm^2) using old generation film apparatus. The value is also consistent with the packing density of OEG thiolate monolayer on Au surface (4.7 × 10^{14} molecules/cm^2) reported by Harder *et al.*[48]

Since the newly prepared EG7 film exhibits higher % OEG coverage, we expect it has good long-term stability in ambient environment.

Long-term stability and anti-biofouling property. The methodology for testing organic thin films against the non-specific protein adsorption has been previously reported by us.[37] The fibrinogen is abundant in the plasma, and is

responsible for the coagulation cascade.[49] A major obstacle in the surgical implant is the blood clotting on the surface of the implant, thus disabling the function of the implant. Therefore it is suitable to choose the fibrinogen in the PBS buffer as a model protein for the adsorption experiments. To match the isotonic condition in the human body, we dissolved the fibrinogen in 1 × PBS buffer. The anti-biofouling property of the EG7 film was tested by complete immersion of the EG7 film in the fibrinogen (1 mg/mL) dissolved in 1 × PBS buffer. The incubation was conducted inside an incubator at 37 °C for 1 h. The film was washed with the Milipore water for 30 sec prior XPS characterization. The percentage protein absorption is calculated based on the following formula:

$$\mathrm{Abs}_{\mathrm{protein}}\,\% = \frac{S_{ML}{}^{N}}{S_{SiH}{}^{N}} \times 100\% \quad (4)$$

which $S_{ML}{}^{N}$ is the integration area of the XPS N1s signal of the EG7 monolayer; and $S_{SiH}{}^{N}$ is the integration area of XPS N1s signal of the freshly prepared hydrogen-terminated silicon.

High-resolution XPS spectrums in the N1s region were used to quantify the amount of the fibrinogen protein adsorbed onto the EG7 film surface. The N1s region has shown that the freshly prepared EG7 films are completely resistant to the non-specific adsorption of the fibrinogen protein; and no significant N1s peak can be observed (**Figure II.8**). Using Eq 4, the protein absorption is calculated to be 0.5%, which is expected. It is known that the OEG film is prone to degradation due to the internal hydroperoxide,[50] and the remaining silicon oxide would

compromise the anti-biofouling property of the SAMs and accelerate its degradation. Therefore we further analyzed both conformation and hydrocarbon composition of the EG7 film after incubation in the fibrinogen solution. Ellipsometric measurement of the EG7 film after incubation was 41 ± 1 Å, which is consistent with the measurement of a freshly prepared EG7 film. This result suggests that the EG7 molecules adsorbed onto the Si(111) substrate retained a perpendicular conformation that is normal to the substrate surface. C1s region was analyzed using the high-resolution XPS and peaks are found to be at 285.1 eV and 286.7 eV, corresponding to alkyl (C-C) and etheric (C-O) signals respectively. The area ratio of alkyl (C-C) peak over etheric (C-O) peak was calculated to be 0.53. Narrow scans over the Si2p region revealed no SiO_2 formation on the film. Calculated ratio of alkyl (C-C) peak over etheric (C-O) peak was consistent with the calculation of a freshly prepared EG7 film, indicating degradation does not occur on the EG7 film with high packing density (5.15×10^{14} molecules/cm^2) after exposing to the fibrinogen solution (1 mg/mL in 1 × PBS) for 1 h.

Encouraged by the absence of EG7 film degradation after 1h incubation in the fibrinogen solution (1 mg/mL in 1 × PBS), we evaluated the long-term stability of the EG7 film. We took the advantage of the new UHV hydrosilylation apparatus, which conveniently allows us to passivate a 4” Si(111) wafer that was further cleaved into 21 small films. The EG7 films were incubated in 1 × PBS solution to mimic the isotonic condition of the human body, and a set of

triplicates were taken out each week to incubate inside the fibrinogen solution (1 mg/mL in 1 × PBS) for 1h. The incubated EG7 films were analyzed by both ellipsometer and high-resolution XPS. The results showed that even after 56 days incubation in 1 × PBS solution, the EG7 films showed little degradation and remained protein resistant (**Figure II.9** and **II 10**).

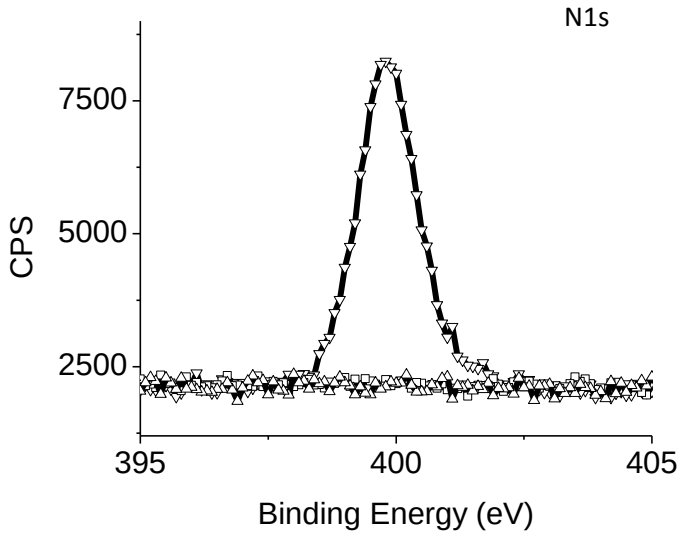

Figure II.8. High-resolution N1s spectra of films after 1 h incubation in fibrinogen solution (1 mg/mL) in 0.01M PBS buffer at room temperature for hydrogen-terminated silicon (∇), for freshly prepared EG7-OMe film (∆).

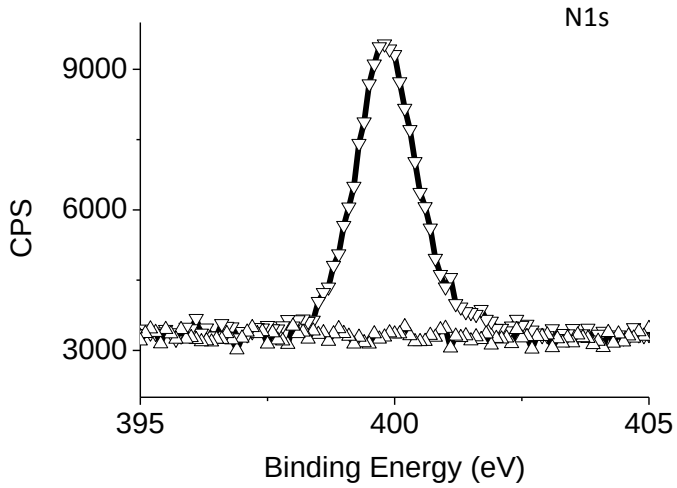

Figure II.9. High-resolution N1s spectra of EG7-OMe film after 1 h incubation in fibrinogen solution (1 mg/mL) in 0.01M PBS buffer at room temperature for hydrogen- terminated silicon (∇), for EG7-OMe film (Δ) after 56 days incubation in 1 × PBS solution.

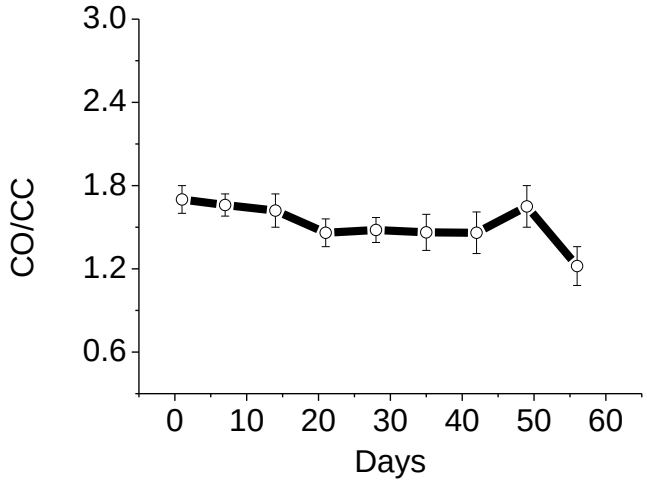

Figure II.10. C-C/C-O ratio calculated from the high-resolution C1s spectra of EG7-OMe films after 1 h incubation in fibrinogen solution (1 mg/mL) in 0.01M

PBS buffer at room temperature. The C-C/C-O ratio shows little variation over 8 weeks incubation in 1 × PBS solution.

II.3. Conclusion

Passivation of Si(111) substrate with 2,5,8,11,14,17,20,23-Octaoxatritriacont-32-ene (EG7) was carried out under near-ideal condition inside an UHV apparatus to afford an anti-biofouling film. The Si(111) substrate surface was nearly 100% passivated and the coverage has greatly improved comparing to our previous attempts. No visible silicon oxide was detected in the narrow scans of the Si2p region using high-resolution XPS; this demonstrates the ability of UHV of removing reactive oxygen and water radicals to near completion. In separate experiments, the long-term stability of the EG7 film was tested in 1 × PBS solution, and degradation occurred slowly over the course of eight weeks, evidently from the slow declining of the C-C/C-O signal ratio calculated from the deconvoluted C1s signal via high-resolution XPS. The UHV approach provides a general platform to prepare functionalized silicon surface from the high boiling temperature self-assembling molecules with very little oxidation. We also demonstrated that the OEG film degrades slowly when storing in 1 × PBS solution, which is of both scientific and commercial values. Atomic force microscope (AFM), X-ray photoelectron spectroscope (XPS), ellipsometer, and contact angle were used to characterize and quantitate all films used in these

experiments. The combination of these analytical tools proves film analysis to be accurate and repeatable.

II.4. Experimental procedures

Materials. Air sensitive reactions were performed under the nitrogen environment using the Schlenk technique. All reagents were purchased from Sigma-Aldrich and Quanta Biodesign, and were used without further purification. Flash chromatography was carried out on silica gel using 230-400 mesh silica gel from SiliCycle. Thin layer chromatography was performed using TLC Aluminum foils precoated with silica gel purchased from Fluka.

All 1H- and 13C-NMR spectrum were recorded on 400 MHz 1H and 500 MHz 1H spectrometers in deuterochloroform with chloroform as an internal reference unless otherwise stated. Chemical shifts are reported in ppm (δ). Coupling constants, J, are reported in Hz.

Surface hydrosilylation of alkene adsorbates under 10^{-4} torr vacuum. Commercial 1 × 1 $inch^2$ Si(111) wafer (n-type, 1-12 Ωcm, < 0.5° mis-cut) was cleaned according to simplified RCA process, which was first developed by RCA laboratories. First, the silicon wafer was rinsed thoroughly with both mili-Q water and ethanol to remove residual particles and inorganic contaminants. Removal of the organic contaminates was accomplished by immersing the silicon wafer inside the Piranha solution (H_2SO_4:H_2O_2 3:1) for 20 min at 80 °C. This industry

standard cleaning removes organic contaminates from the silicon wafer surface by oxidizing them (Caution: the Piranha solution generates extreme heat). Piranha solution was removed from the silicon surface by rinsing thoroughly with the mili-Q water and dried in the stream of an ultra-high purity argon gas. Oxide removal was achieved by immersing the freshly cleaned silicon wafer in NH_4F solution for 15 min followed by a rapid rinse using degassed mili-Q water. Finally the hydrogen-terminated silicon substrate was dried with a stream of ultra-high purify argon gas. The freshly prepared hydrogen-terminated silicon substrate was immediately placed onto the sample holder inside a home-made vacuum chamber. The home-made vacuum chamber generated intermediate vacuum (10^{-4} torr), which removed moisture from the hydrogen-terminated silicon substrate. The hydrogen-terminated silicon substrate was brought into contact with about 0.5 mg of the liquid adsorbates **1**, which uniformly covered the top layer of hydrogen-terminated silicon substrate. Hydrosilylation on hydrogen-terminated silicon substrate was achieved by illuminating with UV (254 nm) for 2 h. Upon successful hydrosilylation, the substrates modified with adsorbates **1** are washed with both 200 proof ethanol and mili-Q water, and is finished by drying with a stream of ultra-high purity argon gas.

Surface hydrosilylation of alkene adsorbates under 10^{-8} torr vacuum. In order to remove residual gas and moisture effectively, we built a home-made ultra-high vacuum chamber capable of generating 1×10^{-8} torr vacuum. We were able to passive 4” silicon wafer using this apparatus. The surface

hydrosilylation procedure is same as described above, the same surface hydrosilylation procedure was used to prepare hydrosilylation on the hydrogen-terminated silicon substrate using adsorbates **1**.

Preparation of 1 mg/mL fibrinogen in 0.08 M PBS buffer. Fibrinogen solution (1 mg/mL) in the PBS solution (pH 6.7, ionic strength 0.08 M) was prepared as follows. 0.16 M PBS solution with high ionic strength was prepared (pH 6.7) and the adequate amount of fibrinogen was added. The fibrinogen stock solution was shaken at 80 rpm at room temperature and is completely dissolved in 15 min. In order to obtain working fibrinogen solution (1 mg/mL) in PBS solution at pH 6.7, the fibrinogen stock solution was diluted 2 times. The fibrinogen working solution (1 mg/mL) was settled for 1 hour at room temperature before use.

Protein resistance. Films **A** and hydrogen-terminated silicon surface were freshly prepared, and XPS N1s signal intensity was measured. All above films were immersed in the fibrinogen solution (1 mg/mL in 0.01 PBS buffer) at pH 7.4. The films were gently shaken by an orbital shaker and incubated for 1 h. The films were washed with mili-Q water thoroughly to wash away any non-binding fibrinogen and dried under a steam of ultra-high purity argon gas. After incubation, the elliposometer showed the thickness of hydrogen-terminated silicon surface is 61 Å, which roughly corresponded to a monolayer of fibrinogen. Therefore, the incubated hydrogen-terminated silicon surface was considered to have absorbed 100 % fibrinogen. All incubated films were measured for

XPS N1s signal intensity again. The percentage of fibrinogen absorbance of film **A** was calculated by dividing the increase of the N1s signal by that of the hydrogen-terminated silicon surface.

AFM imaging. AFM imaging of the surfaces was performed using a MultiMode Nanoscope IIIa AFM (Digital Instruments Inc., Santa Barbara, CA). Images were acquired in the contact mode to capture both topological and friction force images simultaneously. All imaging data were obtained as follows, first topological imaging was obtained with scanning angle 0° and a scan rate of 1.39 Hz (tip velocity of 36.1 *í*m/s), then the scanning angle was changed to 90° for lateral force microscopy mode. Silicon nitride cantilever was purchased from MikroMasch, San Jose, CA. with a resonance frequency of 132.9 kHz and a nominal force constant of 1.75 N/m. Freshly cleaved 1 cm^2 mica was placed between films and steel AFM sample stage to avoid undesired Ohmic contact.

X-ray photoelectron spectroscopy (XPS). XPS data was collected on a PHI 5700 X-ray photoelectron spectrometer which is equipped with a monochromatic Al KR X-ray source (1486.7 eV), with takeoff angle (TOA) of 45° from the film surface. High- and low-resolution XPS spectra were recorded with window pass energies of 23.5 and 187.85 eV respectively. Electron-binding energies were calibrated using C1s line as reference at 286.4 eV (C-C). The atomic concentrations were calculated using the PHI Multipak 5.0 software (Physical Electronics).

Estimation of molecular length. The molecular structure of

each compound was exported into the Chem3D program from ChemBio Office Suit 12 by CambridgeSoft. The molecular length of each compound was estimated using the molecular mechanics modeling method with MM2.

Elliposometer. Film thickness measurements were obtained from a Stokes Ellipsometer LSE from the Gaertner Scientific Corporation equipped with 6328 Å laser, and the measuring beam was positioned at a 70° incidence angle. Prior film thickness measurements, a fresh prepared hydrogen-terminated Si(111) substrate was measured by the elliposometer to determine the optical constants of the Si(111) substrate (n_s = 3.8925 ± 0.0006, and k_s = 0.0378 ± 0.0012). The refractive index of 1.46 was used for all films prepared, because 1.46 is the literature value for the SiO_2 reflective index and it is very close to that of the organic monolayers. At least nine measurements were taken at random locations on the film surface, which demonstrated excellent consistency in the monolayer thickness across the surface. Average values and standard deviations of the film thickness were reported.

Contact angle. Contact angles were measured by the Rame-Hart model 100 goniometer in ambient conditions. One drop of mili-Q water was deposited onto the film surface during each measurement. At least three measurements were taken at random locations on all film surfaces.

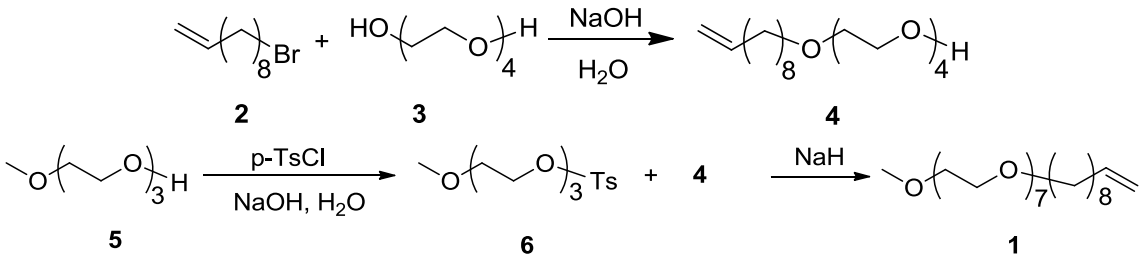

2 **3** **4**

5 **6** **1**

3,6,9,12-tetraoxadocos-21-en-1-ol (4)

To an oven dried 100 mL round bottom flask, tetra ethylene glycol **3** (21.2 mL, 123 mmol, 8.2 equiv) was added to a mixture of NaOH/H_2O (1:1 w/w, 1 equiv). Bromide **2** (3.0 mL, 15.0 mmol) was slowly added into the mixture. The reaction mixture was heated to 70 °C and stirred overnight. The reaction mixture was diluted with both water and hexane, and the aqueous layer was extracted with hexane. The combined organic phase was dried over Na_2SO_4 before concentrated *in vacuo*. The crude was purified by flash chromatography (ethyl acetate) to give **4** as colorless oil. ^{1}H NMR was consistent with previously reported values.[24]

^{1}H-NMR (500 MHz, $CDCl_3$) δ 5.74-5.88 (m, 1H), 4.91-5.02 (m, 2H), 3.56-3.74 (m, 16H), 3.44 (t, *J* = 6.8 Hz, 2H), 2.02-2.07 (m, 2H), 1.56-1.60 (m, 2H), 1.22-1.39 (m, 10H).

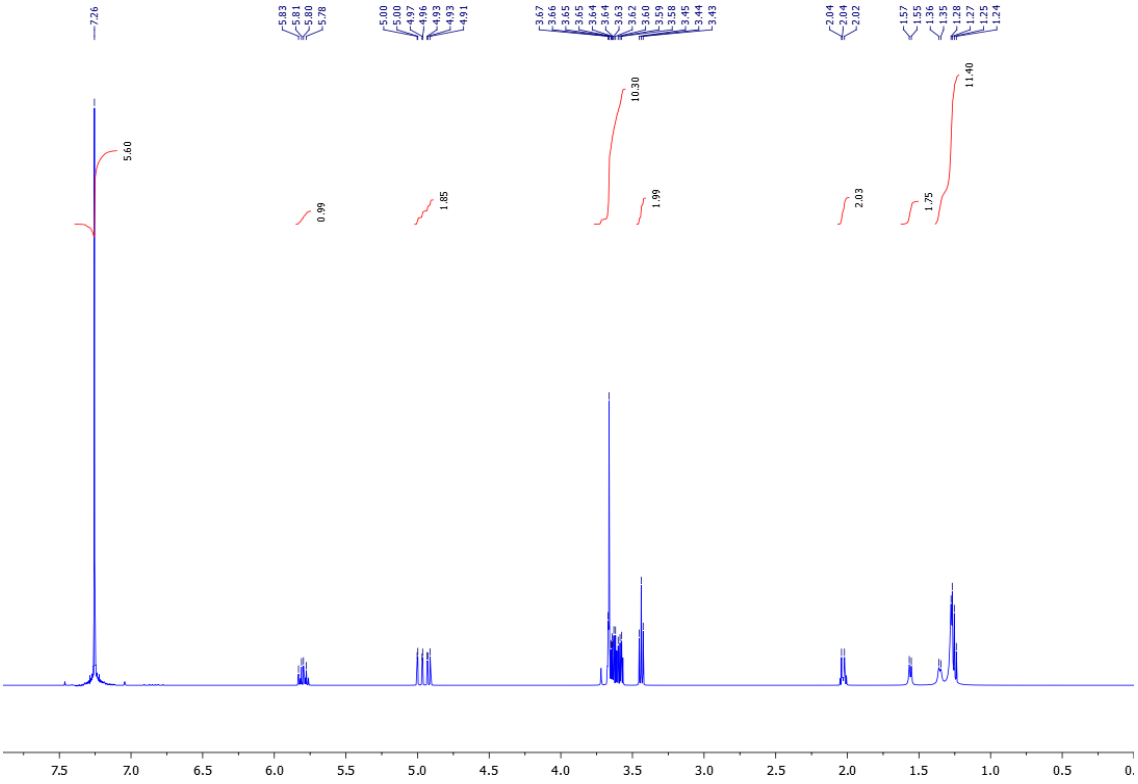

2-(2-(2-methoxyethoxy)ethoxy)ethyl 4-methylbenzenesulfonate (6)

To a solution of triethylene glycol monomethyl **5** (3.8 g, 11.4 mmol) dissolved in a mixture of NaOH/H_2O (1:1 w/w, 1 equiv) was added *p*-toluenesulfonyl chloride (3.3 g, 17 mmol, 1.5 equiv). The reaction mixture was stirred at room temperature overnight. The reaction mixture was diluted with water and hexane, and the aqueous layer was extracted with hexane. The combined organic phase was dried over Na_2SO_4 before concentrated *in vacuo*. The crude was purified by flash chromatography (ethyl acetate) to give **6** as colorless oil (2.32 g, 64 % yield). ^{1}H NMR was consistent with previously reported values.[32]

^{1}H-NMR (500 MHz, $CDCl_3$) δ 7.78 (dd, *J* = 8.0, 6.3 Hz, 2H), 7.48 – 7.28 (m,

2H), 4.15 (t, *J* = 4.8 Hz, 2H), 3.74 – 3.48 (m, 10H), 3.36 (d, *J* = 4.8, 3H), 2.43 (d, *J* = 5.9 Hz, 3H).

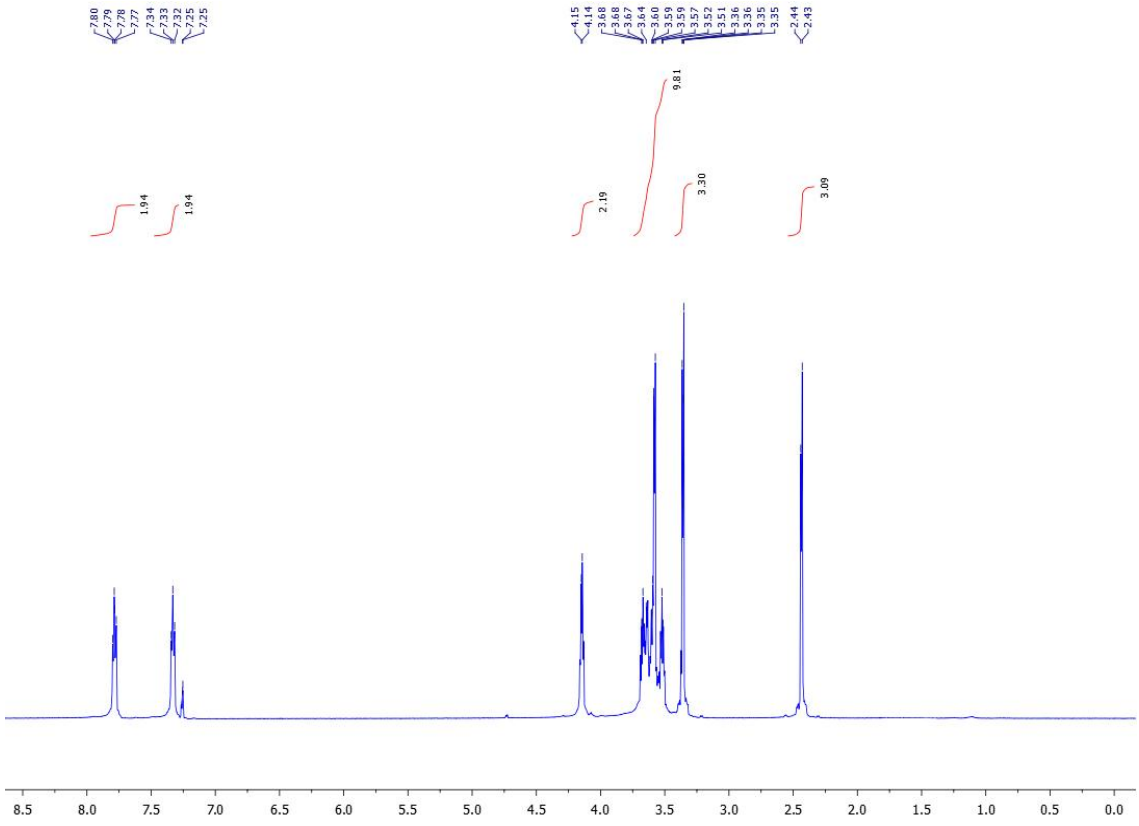

2,5,8,11,14,17,20,23-octaoxatritriacont-32-ene (1)

To a solution of 3,6,9,12-tetraoxadocos-21-en-1-ol **4** (1.0 g, 3.01 mmol) in dry THF (20 mL), NaH (115 mg, 3.01 mmol, 63 % in oil) was slowly added under the nitrogen at 0 °C. The reaction mixture was stirred until no more bubble is generated. The mixture is treated with a solution of **6** in dry THF (10 mL). The reaction mixture was stirred at room temperature overnight before quenched by

diluting with water and hexane. The aqueous layer was extracted with hexane. The combined organic phase was dried over Na_2SO_4 and filtered. The residue was concentrated *in vacuo* and was purified by flash chromatography (ethyl acetate/hexane = 1/1) to give product **1** as colorless oil. ^{1}H NMR was consistent with previously reported values.[24]

^{1}H-NMR (500 MHz, $CDCl_3$) δ 5.88 – 5.72 (m, 1H), 5.02 – 4.86 (m, 2H), 3.71 – 3.50 (m, 28H), 3.43 (m, 2H), 3.37 (s, 3H), 2.07 – 1.99 (m, 2H), 1.61 – 1.52 (m, 2H), 1.36 – 1.24 (m, 11H).

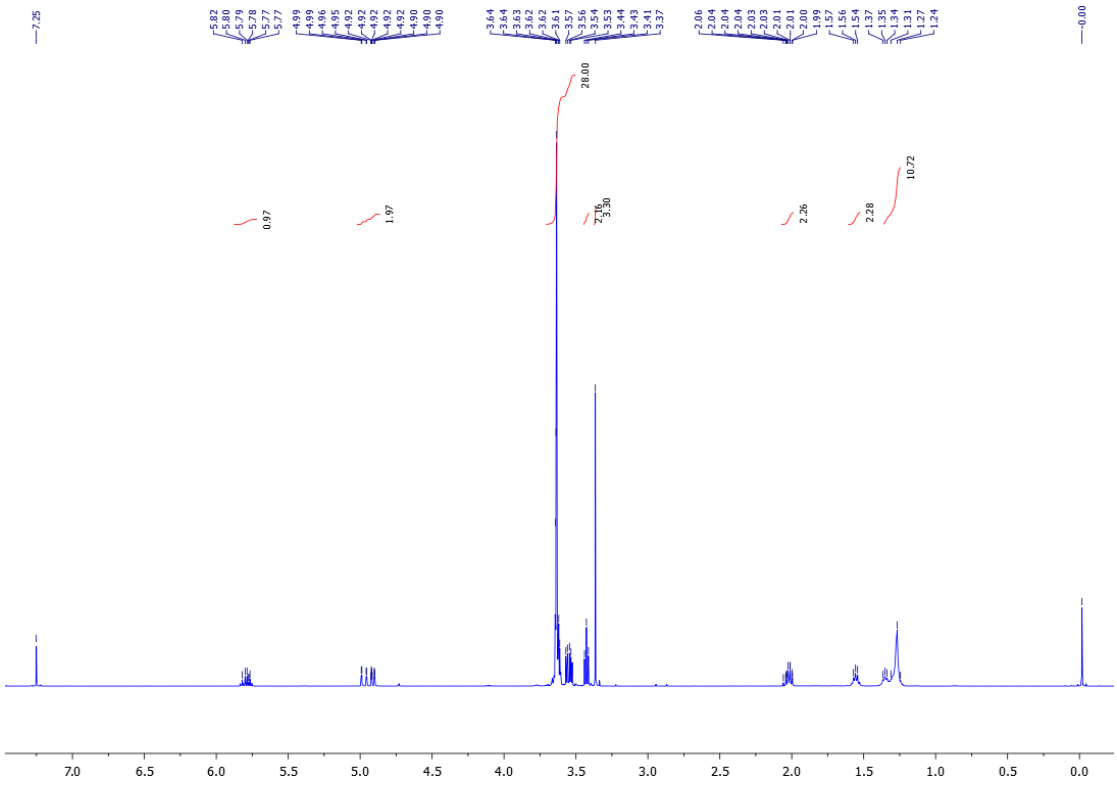

II.5. References

(1) Bigelow, W. C.; Pickett, D. L.; Zisman, W. A. *J. Colloid Sci.* **1946**, *1*, 26.

(2) Linford, M. R.; Chidsey, C. E. D. *J. Am. Chem. Soc.* **1993**, *115*, 12631.

(3) Linford, M. R.; Fenter, P.; Eisenberger, P. M.; Chidsey, C. E. D. *J. Am. Chem. Soc.* **1995**, *117*, 3145.

(4) Lee, S. W.; Laibinis, P. E. *Biomaterials* **1998**, *19*, 1669.

(5) Bigger, S. W.; Scheirs, J.; Delatycki, O.; Billingham, N. C. *Polym. Int.* **1991**, *26*, 181.

(6) Dekeyser, C. M.; Buron, C. C.; Mc Evoy, K.; Dupont-Gillain, C. C.; Marchand-Brynaert, J.; Jonas, A. M.; Rouxhet, P. G. *J. Colloid Interface Sci.* **2008**, *324*, 118.

(7) Chen, Y.; Thayumanavan, S. *Langmuir* **2009**, *25*, 13795.

(8) Chen, S.; Li, L.; Zhao, C.; Zheng, J. *Polymer* **2010**, *51*, 5283.

(9) Chapman, R. G.; Ostuni, E.; Takayama, S.; Holmlin, R. E.; Yan, L.; Whitesides, G. M. *J. Am. Chem. Soc.* **2000**, *122*, 8303.

(10) Ostuni, E.; Chapman, R. G.; Holmlin, R. E.; Takayama, S.; Whitesides, G. M. *Langmuir* **2001**, *17*, 5605.

(11) Herold, D. A.; Keil, K.; Bruns, D. E. *Biochem. Pharmacol.* **1989**, *38*, 73.

(12) Deng, L.; Mrksich, M.; Whitesides, G. M. *J. Am. Chem. Soc.* **1996**, *118*, 5136.

(13) Cai, Y. D.; Roberts, B. P. *Tetrahedron Lett.* **2001**, *42*, 4581.

(14) Kilian, K. A.; Boecking, T.; Gaus, K.; Gal, M.; Gooding, J. J. *Biomaterials*

2007, *28*, 3055.

(15) Sieval, A. B.; van den Hout, B.; Zuilhof, H.; Sudholter, E. J. R. *Langmuir* **2000**, *16*, 2987.

(16) Sun, Q. Y.; de Smet, L.; van Lagen, B.; Wright, A.; Zuilhof, H.; Sudholter, E. J. R. *Angew. Chem. Int. Ed.* **2004**, *43*, 1352.

(17) Liu, Y.; Yamazaki, S.; Yamabe, S.; Nakato, Y. *J. Mater. Chem.* **2005**, *15*, 4906.

(18) Sun, Q. Y.; de Smet, L.; van Lagen, B.; Giesbers, M.; Thune, P. C.; van Engelenburg, J.; de Wolf, F. A.; Zuilhof, H.; Sudholter, E. J. R. *J. Am. Chem. Soc.* **2005**, *127*, 2514.

(19) Scheres, L.; Giesbers, M.; Zuilhof, H. *Langmuir* **2010**, *26*, 10924.

(20) Scheres, L.; Giesbers, M.; Zuilhof, H. *Langmuir* **2010**, *26*, 4790.

(21) Yuan, S. L.; Cai, Z. T.; Jiang, Y. S. *New J. Chem.* **2003**, *27*, 626.

(22) Takeuchi, N.; Kanai, Y.; Selloni, A. *J. Am. Chem. Soc.* **2004**, *126*, 15890.

(23) Puniredd, S. R.; Assad, O.; Haick, H. *J. Am. Chem. Soc.* **2008**, *130*, 9184.

(24) Qin, G.; Cai, C. *Science China-Chemistry* **2010**, *53*, 36.

(25) Parrish, B.; Breitenkamp, R. B.; Emrick, T. *J. Am. Chem. Soc.* **2005**, *127*, 7404.

(26) Baskin, J. M.; Prescher, J. A.; Laughlin, S. T.; Agard, N. J.; Chang, P. V.; Miller, I. A.; Lo, A.; Codelli, J. A.; Bertozzi, C. R. *Proc. Nat. Acad. Sci. USA.* **2007**, *104*, 16793.

(27) Ng, A.; Ciampi, S.; James, M.; Harper, J. B.; Gooding, J. J. *Langmuir* **2009**,

25, 13934.

(28) Ernst, A.; Gobbi, L.; Vasella, A. *Tetrahedron Lett.* **1996**, *37*, 7959.

(29) Ernst, A.; Vasella, A. *Helv. Chim. Acta* **1996**, *79*, 1279.

(30) Cai, C. Z.; Vasella, A. *Helv. Chim. Acta* **1995**, *78*, 732.

(31) Harder, P.; Grunze, M.; Dahint, R.; Whitesides, G. M.; Laibinis, P. E. *J. Phys. Chem. B* **1998**, *102*, 426.

(32) Xue, C.; Sun, R.; Annab, R.; Abadi, D.; Jin, S. *Tetrahedron Lett.* **2009**, *50*, 853.

CHAPTER III. ETHYNYL-PRESENTING MONOLAYERS ON SILICON(111)

III.1. Introduction

Over the past decades nervous system-related health problems such as hearing loss, chronic pain, and diabetes have placed a great demand on producing nanomaterials to interface with the neural tissues.[1-3] Unfortunately such a challenging endeavor remains unsolved by the current technologies. Numerous attempts were conducted to develop neural electrodes as early as 2500BC when ancient Egyptians used an electrical catfish to generate electrical shocks to treat pain.[4] Later when Hodgkin and Huxley first studied the electrical signals from individual neuronal fibers,[5] people realized the importance of reducing the size of electrodes, which greatly benefits the study of neuron signal transduction. Nowadays, treatment of the neural disease greatly relies on the neural electrodes.[6] As the result of increasing applications of the neural implant, an increasing interest has arisen in developing novel bio-compatible nanomaterials that can reduce inflammation while capable to access and stimulate neural tissues.

Si(100) and the Si(111) are two of the most important crystallographic faces of silicon that are employed in the semiconductor industry (Figure III.1).

The orientation is designated by the Miller indices, which are indicated by number in the parentheses. Si(111) substrate modified by the covalent grafting of organic monolayer is of particular interest to the bioelectrochemical interface community because the ease of producing ordered atomically flat film with high surface density.[7-10] Such advantage is often desired because the densely packed organic monolayer effectively masks the underneath silicon surface, which is semi-conductive due to the electrically active defect, thus avoids unnecessary electronic interferences. Si(100), on the other hand, is widely used in the semiconductor industry,[11] but it is lesser preferred in the laboratory because the dihydride surface produced from HF etching is rough, resulting in lesser ordered film with low coverage.[12] Such Si(100) film property would adversely affect the electrical properties of the surface, which is largely influenced by the degree of surface defects.[13]

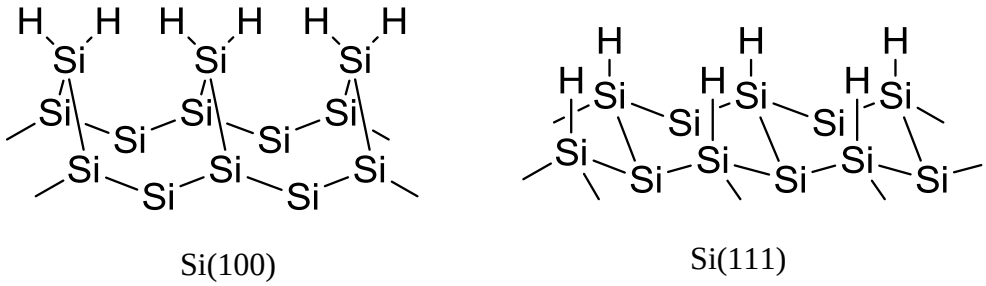

Figure III.1. Structure of hydrogen-terminated silicon based on different silicon crystal orientation. Reproduced from ref **14**.

The previous chapter comprises the modification of the OEG derived monolayers on p-type Si(111) substrate via the “Click” strategy. Film

characterizations indicate such modification strategy is robust and the resulting films exhibit anti-biofouling property. We believe that the electrical behavior of OEG-based monolayers can be precisely tuned via the EG chain length to produce good silicon-interface property. In order to develop a direct detection method to evaluate the electrical property of organic SAMs, electroactive moieties need to be integrated. Ferrocene derivative would be a top choice as it is known as a fast, reversible redox compound, and it has been used as a mediators in the biosensors.[15]

In this chapter, we compared the electrical property between films derived from both 1-alkene and 1-alkyne. Film derived from 1-alkyne is studied because it has been shown that 1-alkyne can form Si-C bond with hydrogen-terminated silicon substrate without any external activations.[16] We have shown that the UV initiated hydrosilylation likely facilitate the cross-linking between germanyl protecting groups on the organic SAMs, which further reduced the yield of the "Click" reaction. By mild hydrosilylation with 1-alkyne derived self-assembling molecules, we would expect lesser extent of polymerization to occur and improvement in the yield of the "Click" reaction.

This chapter focuses on the attachment and subsequent electrochemical characterizations of the ferrocene-modified SAMs. In addition, we highlight that the regioselectivity of the alkyne self-assembling monolayer eliminates the usage of a protecting group, thus simplifies the preparation of SAMs via hydrosilylation. A home-made three-electrode cell was used to characterize the electrochemical

properties of the SAMs, complementary XPS and elliposometric measurements are provided to analyze the film quality.

III.1.1 Click reactions

Sharpless first introduced the concept of “Click” chemistry in 2001.[17] Of the various criteria, he defined “Click” reaction to be of giving consistently high yields, insensitive to reaction environments, and easy work-ups without chromatographic purification.[18] To date, over 937 publications have been presented on this scope. Even though a broad range of reaction would satisfy Sharless’s criteria, such as C=C additions, nucleophilic opening of strained rings, cycloadditions, and “special” carbonyl chemistry, now days “to Click it” has narrowed down to the range of 1,3-dipolar cycloaddition between the terminal alkyne and the azide. Traditionally, the classic Huisgen 1,3-dipolar cycloaddition requires an elevated reaction temperature and the products often involve a mixture of regioisomers, thus disqualifying it to be a true “Click” reaction. In 2001, Tornoe and Meldal introduced the Cu(I) catalyzed 1,3-dipolar cycloaddition, offering both high regioselectivity and enhanced reaction rate.[19] The fact that 1,3-dipolar cycloaddition is quantitative, robust, insensitive, and orthogonal, enabled the possibility of its application in the biomolecular ligation.[20] However, Cu(I) catalyzed 1,3-dipolar cycloaddition falls short for in vivo application due to the cytotoxic effect of the Cu catalyst.[21]

A breakthrough came when researchers found that the strained cycloalkyne and the alkene are highly reactive towards the cycloaddition

reaction. Alder first discovered that the norbornene is more reactive toward the phenyl azide comparing with the acyclic alkenes,[22] by which Huisgen found the reactivity to be greater than 10^2 acceleration.[23] Houk concluded that the enhancement in the reactivity is contributed to the distortion energy of both 1,3-dipoles and dipolarophiles to their transition state geometries is related to the activation energy of 1,3-dipolar cycloaddition, rather than the energy of the reaction,[24,25] ex: cyclooctyne and 3,3-difluorcyclooctyne dipolarphiles are highly reactive.[26] Holk *et al.* reasoned that it is the distortion energy, rather than strain relief, contributes to the fast coupling rate.[25] Bertozzi and co-workers have adopted both ring strain and electron-withdrawing groups into their design of "Click" reagent, demonstrating this biologically inert reaction as an attractive alternative to the Sharpless copper-catalyzed "Click" cycloaddition for use in the living systems.[21,27-32]

III.1.2. Click reactions on silicon surface

The SAMs formation on silicon substrate via hydrosilylation has been proven to be robust;[33] the ability to modify SAMs in both efficient and selective fashion can greatly expand the functional diversity that is limited due to the reactivity towards Si-H. Such strategy can be characterized as a *step-wise* approach to modify the surface. Click reaction is a suitable candidate to satisfy such an endeavor because of its efficiency and modularity. Notably, its bio-orthogonal nature provides a suitable bridge between the biomolecules and the

base monolayer.[34] The CuAACs are an archetypal click reaction, and numerous researches have been focused on the CuACC reaction on the silicon SAMs in the field of surface chemistry recently.[35-37] Much work on the surface CuACC reactions were done on gold and silicon oxide substrates,[38-41] but there has been an explosion of interest on non-oxidized silicon since Lewis *et al.* demonstrated that the covalent attachment of acetylene and methylacetylene onto non-oxidized silicon substrate through a two-step Si chlorination/alkylation process.[42] Inspired by their work, Heath and co-workers reported the first copper-catalyzed Huisgen 1,3-dipolar cycloaddition of azides and terminal alkynes on non-oxidized silicon surface.[37] Since this work, numerous molecules have been "clicked" onto the silicon surfaces, some notable examples include, oligo(ethylene glycol),[33] ferrocene,[43] and peptide.[44]

Previous work by our group has shown that OEG-grafted silicon monolayer via the CuACC reaction is highly resistant to the nonspecific absorption of the fibrinogen, and the mannose-grafted monolayer attracts E. coli strands that are mannose-binding.[33] However such strategy suffers from some major drawbacks that limit its application as the bioelectrochemical interface; the uncontrolled undergrowth of the CuACC-grafted SAMs contributes to the low packing density of the monolayer. It is known that both functional groups and surface packing density determine the anti-biofouling property. The undergrowth is explained by the base layer that consist ten ethylene glycol units, which contribute to the flexibility of the CuACC-grafted SAMs. Although chain flexibility

of the long ethylene glycol unit can also contributes to the enhancement of the anti-biofouling property against the protein adsorption, steric repulsion reduces the packing density of the SAMs. Thus the oxidation of the underlying silicon substrate is facilitated, and the long term anti-biofouling property is affected. Secondly, an ideal bioelectrochemical interface would require tunneling to occur across the SAMs. In our previous design of the base layer, both aliphatic chains and long ethylene glycol are dielectric and contain considerably long ethylene glycol unit, which inhibits tunneling current to pass through. Therefore our previously developed base monolayer is inadequate to be used as a bioelectrochemical interface.

III.1.3. Attachment of ferrocene derivative

Several methods for attaching ferrocene moiety onto non-oxidized Si(111) surface have been reported, they can be classified into pre-synthesized route and step-wise route as first summarized by Gooding and Ciampi.[45] For the pre-synthesized route, several ferrocene derivatives have been successfully attached directly onto the hydrogen-terminated silicon surfaces (Scheme III.1), including vinyl (**1a**)[46,47] and ethynyl (**2**)[48,49] substituted ferrocene. On the other hand, ferrocene derivatives have been attached step-wise via orgaonolithium (**1b**)[50], “click” (**3**)[37], and carbodiimide strategies (**4**)[51].

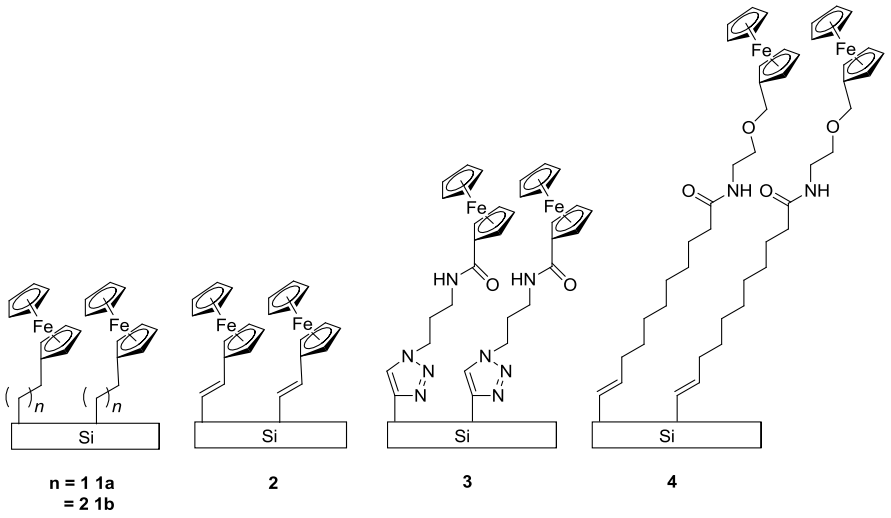

Scheme III.1. Ferrocene-passivated Si-H via Si-C Bond. Reproduced from ref **14**.

An obvious advantage of the pre-synthesized route is the ability to purify the ferrocene derived self-assembling molecules, providing greater certainty over the presenting molecules on the surface. The disadvantage is, however, the resulting films are usually lesser ordered with low coverage, diluting the surface concentration of the ferrocene. Such films usually are unable to provide protection against oxidation of the underlying silicon, and degradation could occur within two days.[50,52] In case of the stepwise approach, the underlying silicon is well protected by the densely packed base SAMs, which protects it from the oxidation, and provides a handle for the attachment of various functional groups. Kilian *et al.* has reported that film prepared via the step-wise approach is stable up to two months.[53]

III.1.4. Cyclic voltammetry

Within the scope of this chapter, we are interested in studying the charge transport at SAMs, which is sandwiched between the electrode and the electrolyte. Cyclic voltammetry (CV) is well suited to evaluate the electrochemical property as well as the surface coverage of the ferrocene-modified SAMs. A typical electrochemical cell for CV measurement includes a working electrode, a counter electrode, and a reference electrode. The cell reaction takes place at the working electrode, and the counter electrode balances the reaction at the working electrode, thus allowing the potential of the working electrode to be measured against the reference electrode. During the CV measurement, the potential is varied at a constant rate while the current are monitored (**Figure III.2**). To allow the efficient study of the thin film CV, we built a customized three electrode cell (**Figure III.3**).

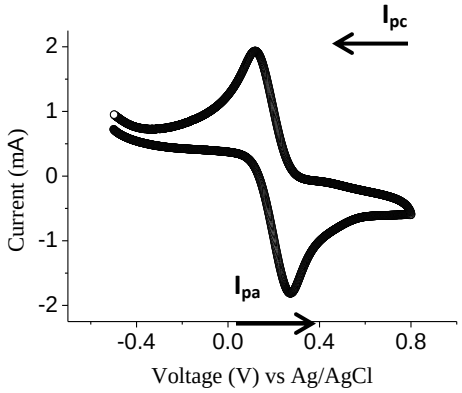

Figure III.2. Cyclic voltammogram showing reversible peak of ferrocene in acetonitrile. I_{pa} is the peak current by which ferrocene oxidizes to ferrocenium,

and I_{pc} is the reduction peak of ferrocenium. Potential scan direction is indicated by the arrow. Cyclic voltammogram was recorded using a DY2100 mini potentiostat by Digi-Ivy Inc. using our home-made Teflon three-electrode cell.

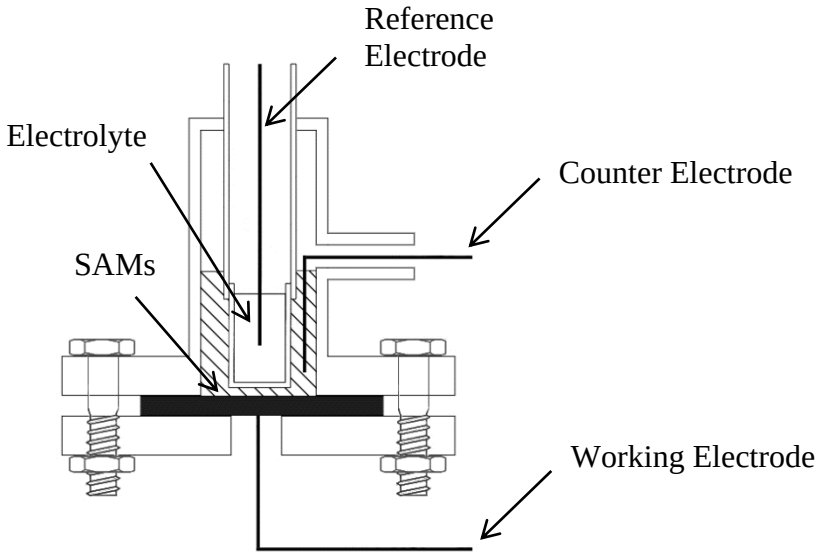

Figure III.3. Main components of the three-electrode teflon cell we designed and built.

III.2. Results and discussion

III.2.1. Ethynyl-presenting monolayer on Si(111)

Previously we have demonstrated the feasibility of using the TMG-protected ethynyl surfaces in the Huisgen's 1,3-dipolar cycloaddition reactions.[33] The TMG group can be conveniently removed by a catalytic amount of Cu(I) in the presence of the protic solvents,[54,55] which enables a one-pot deprotection and click reaction on the Si(111) surface. The model azide molecule **7** "Clicked" onto the surface features a 10 EG unit, thus rendering the resultant film protein resistant. However both synthesis and purification of such azido compound **7**

bearing 10 EG units are tedious (5 steps); it often contains trace amount of impurities including short EG units that are hard to distinguish by the NMR. Furthermore, both alkyl chains and EG chain are dielectric materials, incorporation long EG unit can drastically reduce the possibility for tunneling current to pass through SAMs, and it cannot be used as bioelectrochemical interface to facilitate communication between the target organisms and the molecules using bioelectrochemical or electrophysiological signals. Therefore, we have designed a series of TMG-protected α,*ω*-alkenynes with significantly shorter EG units as adsorbates. These newly proposed α,*ω*-alkenynes have the advantage of the ease of synthesis, as well as the enhanced packing due to the absence of the steric hindrance caused by the flexible long EG chains (**Figure III.4**).

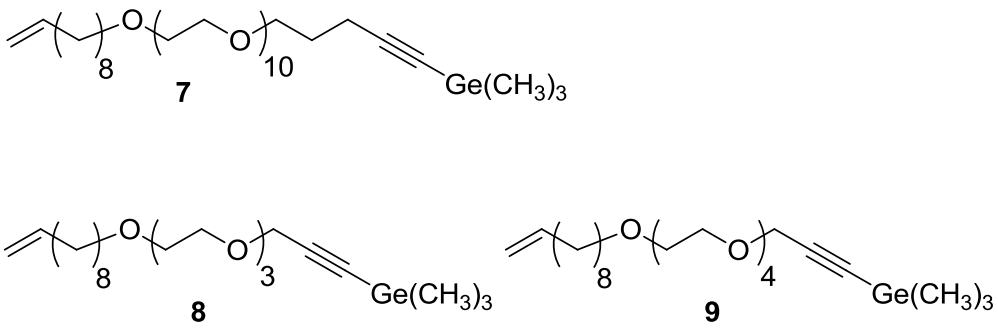

Figure III.4. TMG-protected α,*ω*-alkenynes adsorbates.

The hydrosilylation of both alkene adsorbates **8** and **9** were carried out using the UHV hydrosilylation apparatus under UV (253 nm wavelength) exposure for 2h (**Scheme III.2**).

The high-resolution scan of XPS reveals the alkene **8** and **9** were successfully grafted onto the Si(111) substrate via hydrosilylation (**Figure III.5, 6**), gives rise to two C1s peaks in the narrow scan of XPS in the region of C1s. The C1s peaks can be deconvoluted to two peaks, corresponding to alkyl (C-C) and etheric (C-O) signals respectively. The C-O/C-C ratios derived from peak area are in well agreement with the theoretical values. To demonstrate radical initiated polymerization did not occur, we obtained additional narrow scans of XPS in the region of N1s, O1s, and Ge2p for all films. The C/N/O/Ge composition for films **B** and **C** are consistent with theoretical valuew derived from the molecular formula. The C/O/Ge composition for films **B** and **C** are summarized in **Table III.1**.

To further verify that polymerization did not occur, elliposometry measurements of the film thickness were obtained for films **B** and **C**. The film thickness measurements are very close to the theoretical values and the results are summarized in the table below.

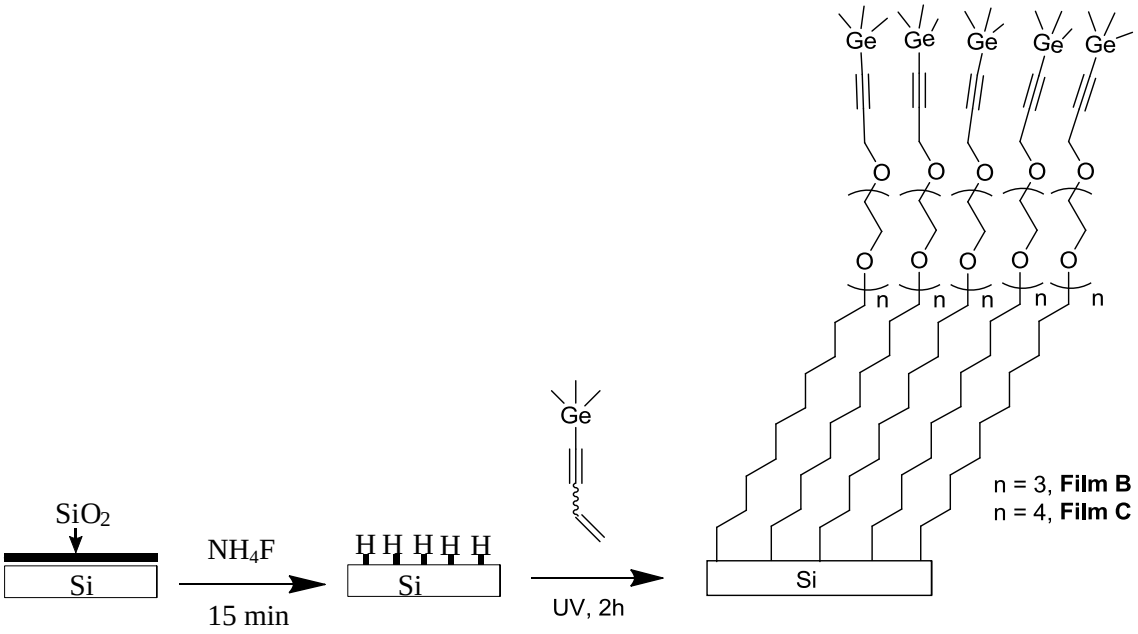

Scheme III.2. Preparation of the TMG-terminated Film **B** and **C** from Alkenyne **8** and **9,** respectively.

Table III.1. Atomic Composition for Films **B** and **C**.

Entry	Description	C-O/C-C ratio	C/O/Ge composition
1	film B experimental value	1.75	22.36/5.44/1
2	film B theoretical value	1.71	22/4/1
3	film C experimental value	1.40	21.64/5.36/1
4	film C theoretical value	1.39	24/5/1

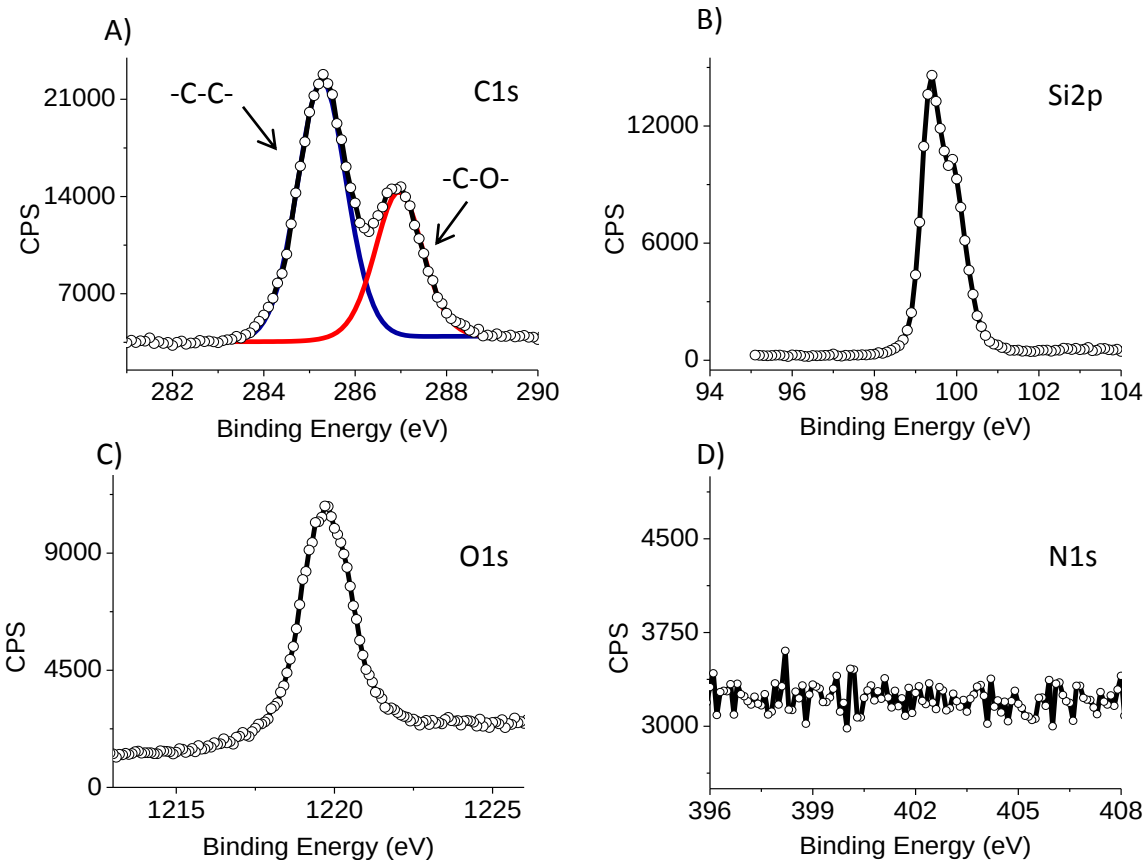

Figure III.5. High-resolution XPS spectra of film **B**. (A) Narrow scan of C1s region, the area ratio of C-C/C-O peaks is 1.40, which is close to theoretical value 1.39; (B) Narrow scan of the Si 2p region, showing absence of oxide growth during surface hydrosilylation; (C) Narrow scan of O1s region, which arises after surface hydrosilylation; (D) Narrow scan of N1s region, which shows absence of nitrogen signal due to physisorption.

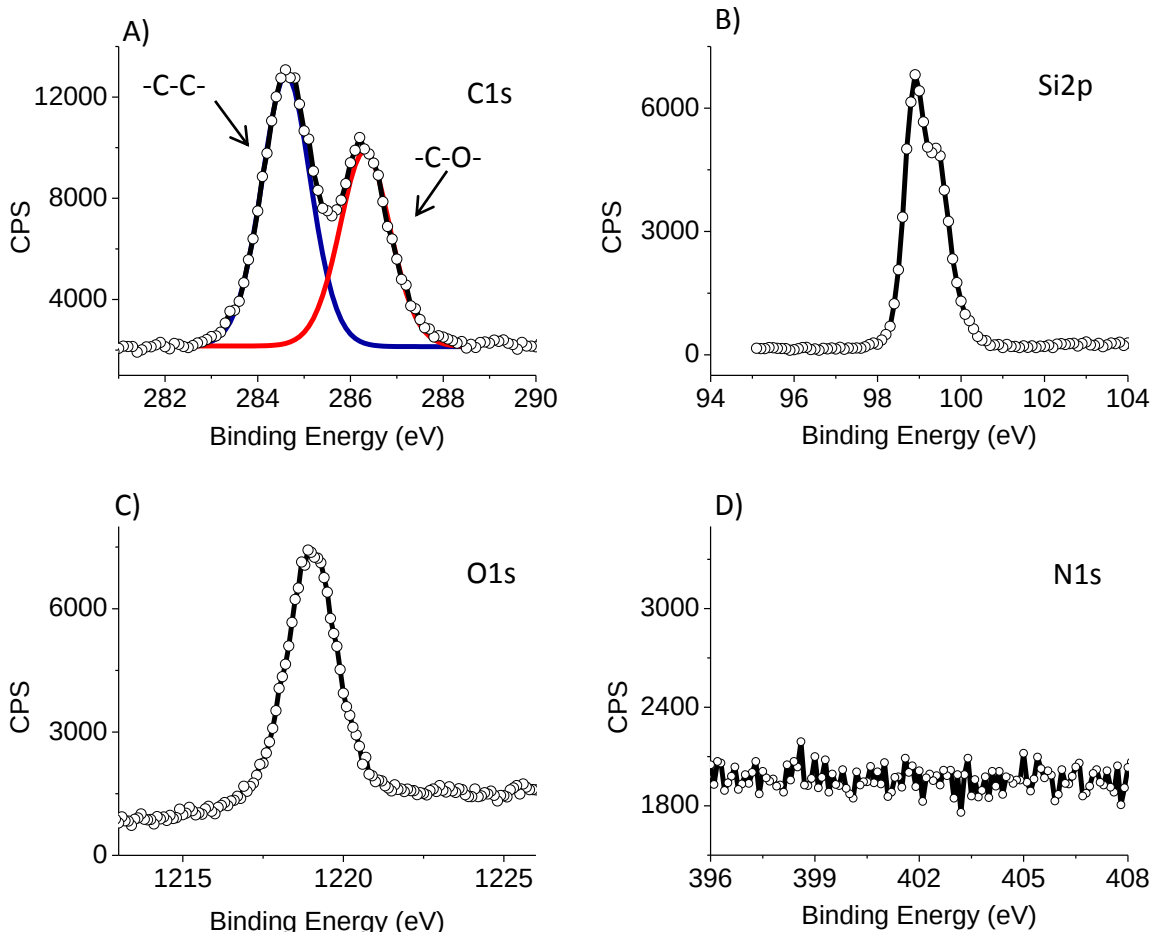

Figure III.6. High-resolution XPS spectra of film **C**. (A) Narrow scan of C1s region: the area ratio of C-C/C-O peaks is 1.75, which is close to theoretical value 1.71; (B) Narrow scan of the Si 2p region, showing absence of oxide growth during surface hydrosilylation; (C) Narrow scan of O1s region, which arises after surface hydrosilylation; (D) Narrow scan of N1s region, which shows absence of nitrogen signal due to physisorption.

Table III.2. Ellipsometry Measurements for Films **B** and **C**.

Entry		Film thickness (Å)
1	film B experimental value	28.40 ± 0.93
2	film B theoretical value	29.10
3	film C experimental value	33.99 ± 1.00
4	film C theoretical value	33.40

Since the degermanylation of films **B** and **C** is the pre-requisite for the subsequent “Click” coupling, in order to demonstrate the possibility of a one-pot deprotection and CuACC reaction, we tested the efficiency of the degermanylations using film **B** under the same CuACC catalytic system, consisting $CuSO_4$, ligand **11**, and sodium ascrobate in aqueous solution. After reacting for 1 h, the films were sonicated in EDTA (25 mM) for 10 sec. The extent of degermanylation was analyzed by the narrow scan of Ge2p region using high-resolution XPS.

Our results showed that a large amount of tri-methyl germanyl groups remained on the surface. This result is conflicting with the degermanylation efficiency of the film formed by the compound **1**, reported by former Group member Dr. Guoting Qin (95%). In solution degermanylation, however, produced ethynyl-terminated compound that is completely free of the tri-methyl germanyl protecting groups within 30 mins in the presence of $CuSO_4$, ligand **11**, and sodium ascrobate.

Table III.3. Optimization of Hydrosilylation Conditions for Efficient Degermanylation.

Entry	Film **B** UV exposure time (h)	% Ge remain	Film thickness before degermanylation (Å)	Film thickness after degermanylation (Å)
1	2	42	26.83	19.79
2	3	43	27.45	20.32
3	4	55	33.73	49.39
4	6	90	43.25	75.23

III.2.2. OEG monolayer derived from TMG protected ethynyl SAMs via CuACC

We have since confirmed that the degermanylation of both films **B** and **C** could occur in the presence of Cu(I) catalyst. Subsequently we performed Huisgen 1,3-dipolar cycloaddition on both films **B** and **C** in the presence of the ligand **11** (**Scheme III.3**).

The Huisgen 1,3-dipolar cycloaddition was performed inside an anaerobic chamber in the ultra-pure nitrogen environment. The films were immersed in a mixture of $CuSO_4$ (1.25 mM), ligand **11** (12.5 mM), and azide **12** (5 mM). Sodium ascorbate (25 mM) was introduced in the end to reduce $CuSO_4$ into reactive Cu(I) in situ in order to initiate the reaction.

Cu^+ ligand:

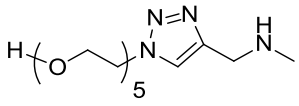

11

Azide:

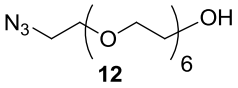

12

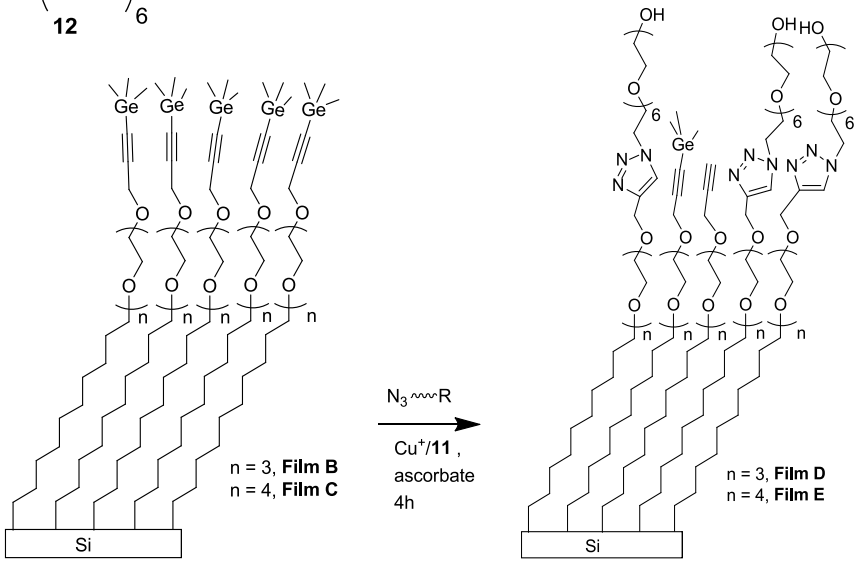

Scheme III.3. Direct CuACC Reactions of Films **B** and **C** with Azide **12** Promoted by Cu^+ and Ligand **11** to Form Films Presenting OEG (Film **D** and **E**).

Films **D** and **E** derived from **B** and **C** via CuACC reaction were characterized using both high-resolution XPS (**Figure III.7**) and elliposometer. The C1s spectrum was deconvoluted and fitted into two components at 285.1 eV and 286.7 eV after deconvolution to two peaks, corresponding to the alkyl (C-C) and the etheric (C-O) signals respectively.

The attachment of the azide **12** via the click chemistry was demonstrated by the rise of the N1s signal in the high-resolution XPS spectrum. After

the deconvolution, the N1s signal can be fitted into two speaks, corresponding to the doubly bonded nitrogen at 401.5 eV, and singly bonded nitrogen at 400.0 eV respectively. We calculated the ratio of peak areas to be 2:1, which is consistent with the structure of the newly formed trizole ring.

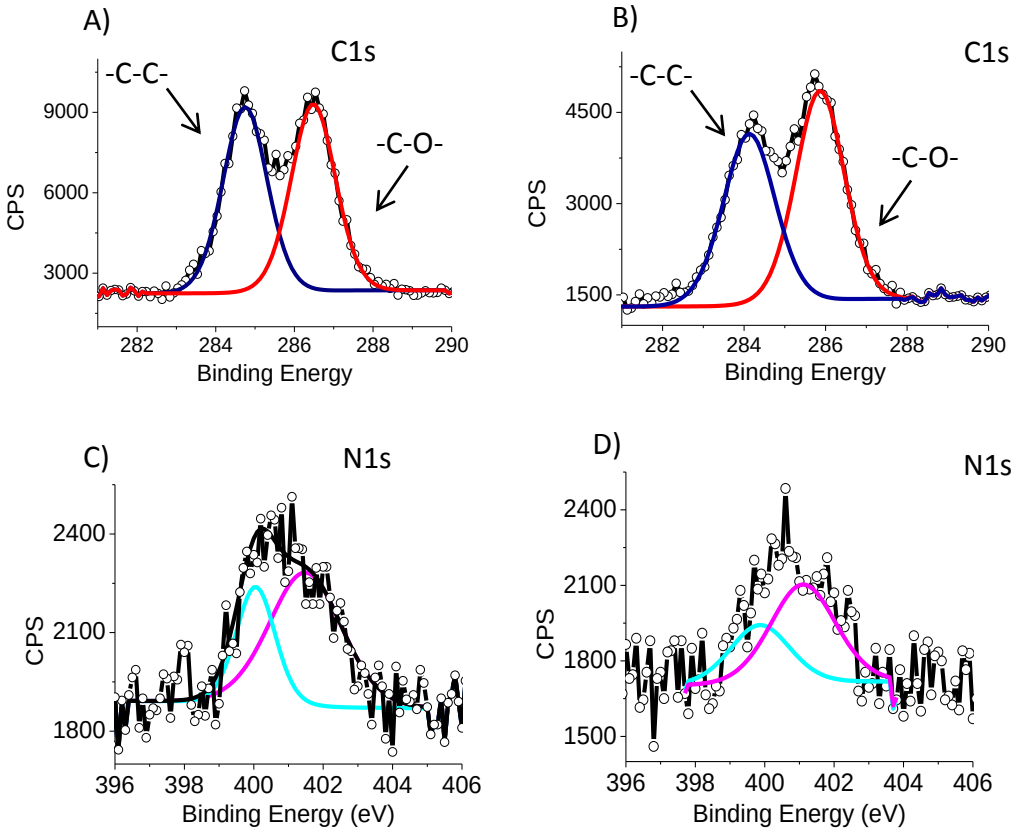

Figure III.7. High-resolution XPS spectra of films **D** and **E**. (A) Narrow scan of C1s region of film **D**: the area ratio of C-C/C-O peaks is 1.40, which is close to theoretical value 1.39; (B) Narrow scan of C1s region of film **E**, the area ratio of C-C/C-O peaks is 1.40, which is close to theoretical value 1.39; (C) Narrow scan of N1s region of film **D**, the area ratio of the two peaks is 1:2; D) Narrow scan of N1s region of film **E**, the area ratio of the two peaks is 1:2. The nitrogen

peak corresponds to the doubly bonded nitrogen (purple) and singly bonded nitrogen (cyan) respectively, validating the click formation.

A direct measurement of film density after CuACC reaction cannot be determined for films **D** and **E,** as the newly attached etheric carbons cannot be distinguished from the etheric carbons in the base SAMs; furthermore, the former terminal ethynyl carbons cannot be distinguished from sp^3 hybridized carbons in the alkyl chain. Therefore, we estimated the rough yield using the following formula:

$$\text{surface CuACC yield} = \frac{S_{ML}^{C\text{-}C} / S_{ML}^{C\text{-}O}}{S'_{ML}{}^{C\text{-}C} / S'_{ML}{}^{C\text{-}O}} \times 100\% \quad (1)$$

which $S_{ML}^{C\text{-}C}$ is the integration area of XPS C-C signal of the monolayer; and $S_{ML}^{C\text{-}C}$ is the integration area of C-O signal. $S'_{ML}{}^{C\text{-}C}$ and $S'_{ML}{}^{C\text{-}O}$ are theoretical integration areas of C-C signal and C-O signal respectively. This yields a very rough estimation of 60.2%, which tends to be underestimated due to the attenuation effect of C-O signal in the XPS. The AFM topographic characterization using the contact mode revealed that the homogeneity of films was retained after CuACC reaction, indicating that the yield is high.

The anti-biofouling property of OEG films **D** and **E** derived from CuACC were tested using the fibrinogen solution. In order to mimic the isotonic condition in human body, 1× *phosphate buffered saline* (PBS) was used to dissolve fibronogen (1 mg/mL). The anti-biofouling property of both films **E**, and **F** was tested by the complete immersion of these films in the fibrinogen (1 mg/mL)

solution for 1 h at 37 °C followed by washing with Milipore water for 30 sec. The amount of absorbed protein was evaluated from the N1s signal from XPS (**Figure III.8**).

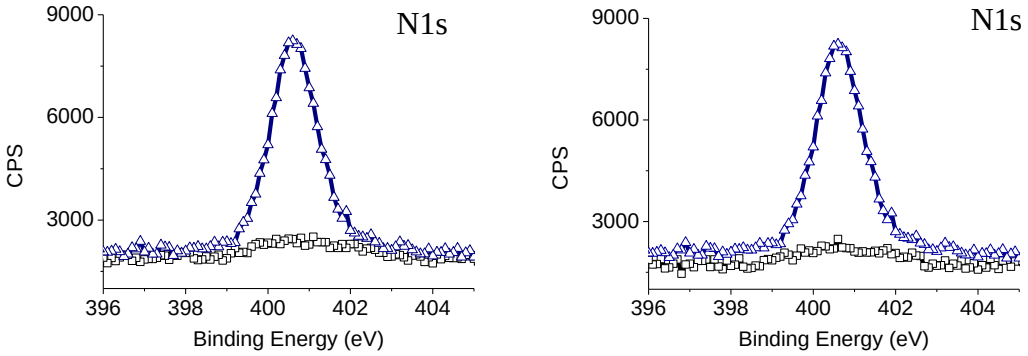

Figure III.8. High-resolution N1s spectra of films **E** (left) and **F** (right) after 1 h incubation in fibrinogen solution (1 mg/mL) in 0.01M PBS buffer at room temperature for hydrogen-terminated silicon (Δ), for clicked EG6 film (□).

To address the existing nitrogen signal from films E and F, we modified the equation used in previous chapter to calculate the percentage protein absorption to the following formula:

$$\text{Absprotein \%} = (S'^{N}_{ML} - S^{\circ N}_{ML})/S^{N}_{SiH} \times 100\% \quad (2)$$

which $S^{\circ N}_{ML}$ and S'^{N}_{ML} is the integration area of XPS N1s signal of the clicked film before and after incubation in the fibrinogen solution; and S^{N}_{SiH} is the integration area of the XPS N1s signal of the freshly prepared hydrogen-terminated silicon. The percentage protein absorption was calculated to be 3.12% and 3.15% for

film D and E respectively.

As film **D** and **E** form from **A** and **B** respectively, the surface becomes increasing hydrophilic and the contact angle decreases (**Table III.4**).

Table III.4. Contact Angle Measurements for Films **D** and **E**

Film description	Contact Angle (°)
Hydrogen-terminated Si (111)	77
Film **D**	87
Film **E**	88

III.2.3. Electrochemical functionalization of TMG protected ethynyl SAMs via CuACC

The electroactive ferrocene moiety was “Clicked” onto the acetylenyl film **B** by **Scheme III.4** in the aqueous solution with minimal copper contamination to the surface.

Azide:

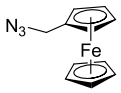

13

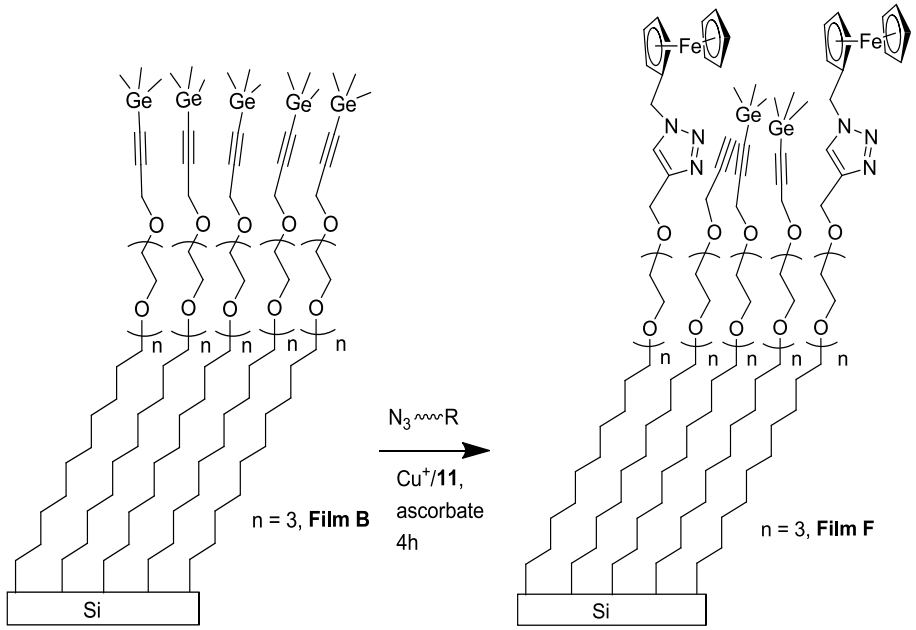

Scheme III.4. Preparation of Proposed Electroactive Film F from TMG-terminated Film **B**.

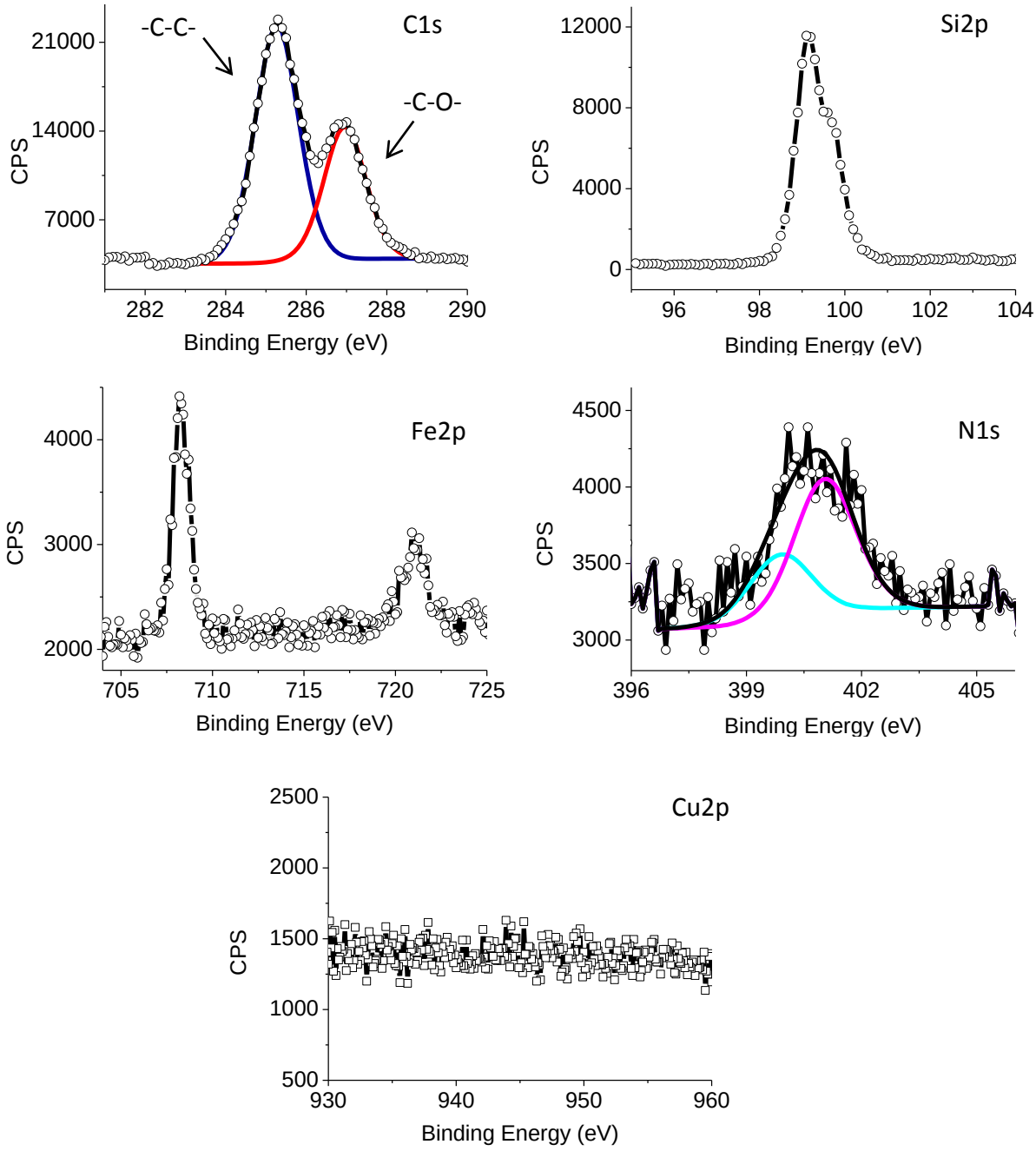

Figure III.9. High-resolution XPS spectra of ferrocene-derived Si(111) surface prepared using azide **7** via **Scheme III.4**.

Film **F** was characterized by the high-resolution XPS (**Figure III.9**). The

narrow scan of C1s region can be deconvoluted into two peaks at 285.2 and 286.9 eV. The former peak corresponds to the carbon-carbon and the carbon from the cyclopentadienyl rings, while the etheric carbon formed the major component of the later peak. The absence of oxide in the narrow scan of the Si2p region indicates a good quality of the modified film **F**. The high-resolution XPS scan showed two major peaks at 708.7 and 721.5 eV, corresponding to Fe $2p_{3/2}$ and Fe $2p_{1/2}$ respectively, which indicates Fe(II) species dominate the film surface.[56] Narrow scan of N1s region of film can be deconvuluted to two peaks. The area ratio of the two peaks is 1:2, which corresponds to the doubly bonded nitrogen (purple) and the singly bonded nitrogen (cyan) respectively, thus validating the click formation. We were able to estimate the surface click reaction yield to be approximately 66%.

Despite the surface click reaction yield to be comparable to literature report of azidomethylferrocene on Si(100),[57] Neither cathodic nor anodic peak can be observed from the cyclic voltammogram shown in **Figure III.10**.

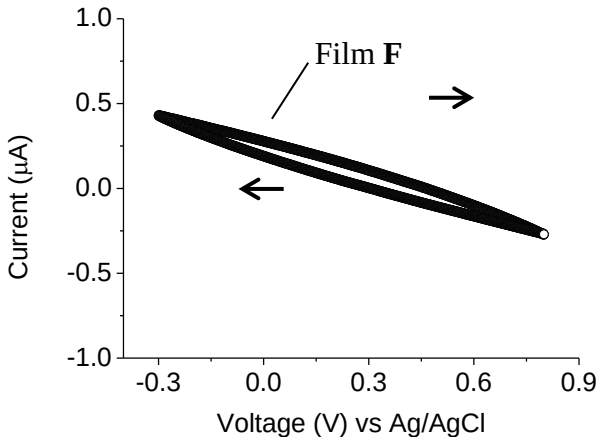

Figure III.10. Voltammograms of film **F** as electrode in CH_3CN containing $NaClO_4$ (0.1 M).

We believe that the inability of allowing electron transfer through Film **F** was contributed to the high dielectric constant of both ethylene glycol units and underneath alkyl chain. Furthermore, the relatively long chain length prevented tunneling to occur. We proposed an alternative “Click” strategy to achieve the addition of the electroactive ferrocene moiety with in-situ deprotection of the TMG protecting group (**Scheme III.5**).

Azide:

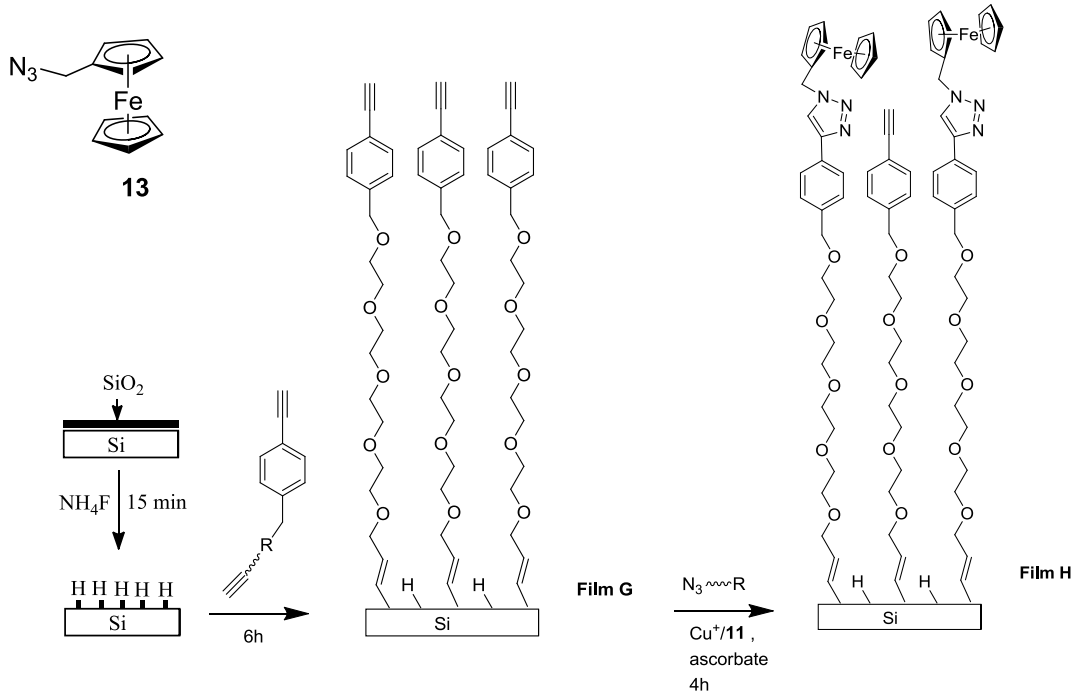

Scheme III.5. Preparation of Proposed Electroactive Film **H** from Acetylenyl Film **G**.

The resulting film was characterized by the high-resolution XPS, which supports the successful formation of Film **H** by a set of peaks ascribed to Fe2p, N1s, as well as C1s (**Figure III.11**). Narrow scan of the C1s region can be deconvoluted into two peaks at 284.8 and 286.4 eV; the former peak corresponds to phenyl carbons, benzoic carbons, and carbons from cyclopentadienyl rings, while the latter corresponds to the etheric carbons. The high-resolution XPS scan showed two major peaks at 708.7 and 721.5 eV, corresponding to Fe $2p_{3/2}$ and Fe $2p_{1/2}$ respectively. This indicates the absence of Fe(III) species.[56] The narrow scan of N1s region of the film can be

deconvoluted into two peaks with area ratio of 1:2, which corresponds to the doubly bonded nitrogen (purple) and the singly bonded nitrogen (cyan) respectively. The area ratio of nitrogen peaks validates the click formation. The surface click reaction yield was approximated by C1s signal to be 53%.

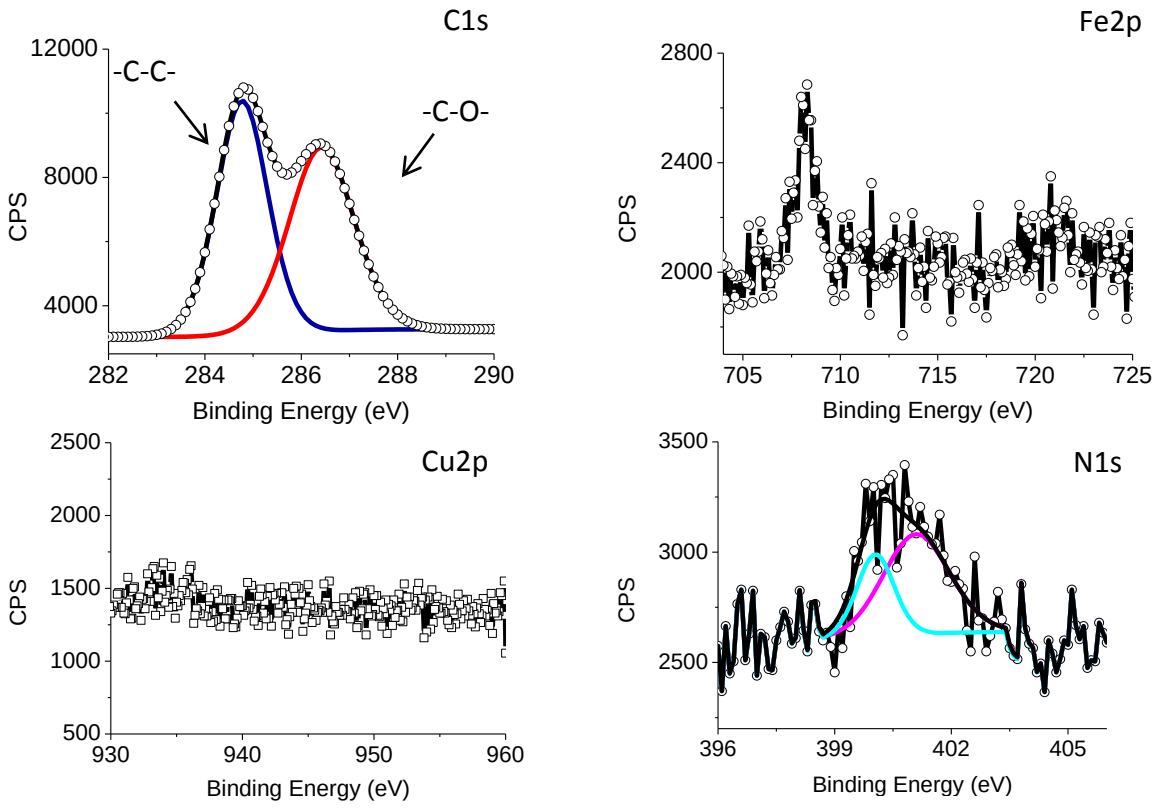

Figure III.11. High-resolution XPS spectra of ferrocene-derived Si(111) surface prepared using azide **7** via **Scheme III.5.**

Due to the elimination of alkyl chain component, which processes high dielectric constant, and the reduced thickness of the SAMs prepared from **Scheme III.5**, we were able to obtain the electrochemical data from the surfaces prepared using this method. The cyclic voltammogram was obtained for the ferrocene bearing Film **H** (**Figure III.12**). The formal redox potential E'

was 187 mV and shows deviation from 370 mV, which is recently reported by Tajimi and co-workers for densely packed vinylferrocene-based assemblies on Si(111),[58] this maybe contributed to the low yield of surface “Click” reaction.

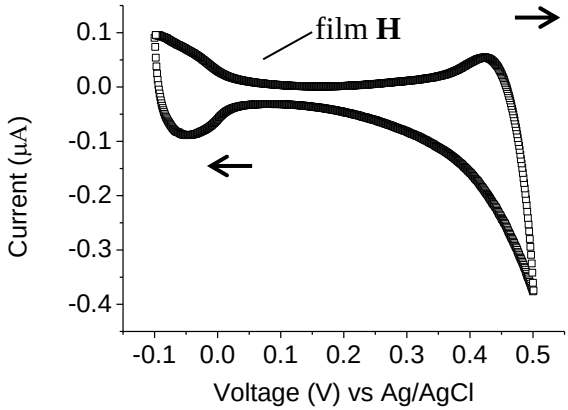

Figure III.12. Voltammograms of film **H** as electrode in CH_3CN containing $NaClO_4$ (0.1M).

III. 3. Conclusion

In the previous chapter, using a *pre-synthesized* strategy we have shown that the OEG chains directly grafted onto hydrogen-terminated silicon produces a monolayer that is highly resistant to the nonspecific adsorption of proteins tested up to 56 days. We are interested to facilitate a *step-wise* strategy to factionalize the Si(111) surface that allow more versatile functionalization with the different chemical groups. Therefore we have demonstrated that the acetylenylation of the Si(111) surface was achieved using the trimethylgermanyl (TMG) protecting group that allows one-pot deprotection and “Click” cycloaddition. Thus a vertatile

acetylenylated monolayer platform was established. We have shown that the OEG chains can be grafted onto this platform and the grafted film exhibits resistivity to the nonspecific adsorption of proteins. We screened different base monolayers with different ethylene glycol (EG) units; however, no particular effect has been found toward the anti-biofouling property of the OEG “clicked” films. To demonstrate the versatility of our acetylenylated monolayer platform film **E**, we grafted it with the electroactive ferrocene moiety, unfortunately neither cathodic nor anodic peak were observed from the cyclic voltammogram.

The absence of the redox potential can be contributed to the high dielectric constant of both ethylene glycol and alkyl components of the base monolayer, which inhibits the direct electron transfer between the redox-mediating molecule and the surface. The relatively high monolayer thickness can also be an obstacle to prevent electron tunneling to occur on the film. Based on our observation, we proposed a new acetylenylated monolayer platform film **H**. With shortened SAMs thickness and substituting the alkyl chain with the phenyl group, we were able to record the redox activity with the formal redox potential E’ of 187mV.

III.4. Experimental procedures

Material. 14-(4-((methylamino)methyl)-1H-1,2,3-triazol-1-yl)-3,6,9,12-tetraoxatetra-decan-1-ol (**5**) and 20-Azido-3,6,9,12,15,18-hexaoxaicosan-1-ole (**6**) were sunthesized by Dr. Amit Kumar, Azidomethylferrocene (**7**) was synthesized

by Dr. Jun Wang in our group. Air sensitive reactions were performed under the nitrogen environment using the Schlenk technique. All reagents were purchased from Sigma-Aldrich and Quanta Biodesign, and were used without further purification. Flash chromatography was carried out on silica gel using 230-400 mesh silica gel from SiliCycle. Thin layer chromatography was performed using TLC Aluminum foils precoated with silica gel purchased from Fluka. Solutions of 200 proof ethanol, $CuSO_4$, sodium ascorbate, H_2O_2, NH_4F (40%), and H_2SO_4 were purchased from Sigma-Alderch Co. and were used without further purification. Fibrinogen and 10 $\times$ PBS buffer were purchased from Invitrogen Co.

All 1H- and 13C-NMR spectrum were recorded on 400 MHz 1H and 500 MHz 1H spectrometers in deuterochloroform with chloroform as an internal reference unless otherwise stated. Chemical shifts are reported in ppm (δ). Coupling constants, J, are reported in Hz.

Surface hydrosilylation of alkene adsorbates under 10^{-8} torr vacuum. In order to remove residual gas and moisture effectively, we built a home-made ultra-high vacuum chamber capable of generating 1×10^{-8} torr vacuum and was able to passive 4” silicon wafer. The surface hydrosilylation procedure is described in the previous chapter. The same surface hydrosilylation procedure was used to prepare hydrosilylation on hydrogen-terminated silicon substrate using adsorbates **8, 9,** and **18**.

Preparation of 1 mg/mL fibrinogen in 0.08 M PBS buffer. Fibrinogen solution (1 mg/mL) in PBS solution (pH 6.7, ionic strength 0.08 M) was

prepared as follows. The fibrinogen stock solution was shaken at 80 rpm at room temperature and is completely dissolved in 15 min. To obtain working fibrinogen solution (1 mg/mL) in PBS solution at pH 6.7, the fibrinogen stock solution was diluted 2 times. Finally the fibrinogen working solution (1 mg/mL) was settled for 1 hour at room temperature before use.

Protein Resistance. Films **D, E,** and hydrogen-terminated silicon surface were freshly prepared, and XPS N1s signal intensity was measured. All above films were immersed in the fibronigen solution (1 mg/mL in 0.01 PBS buffer) at pH 7.4. The films were gently shaken by an orbital shaker and were incubated for 1 h. The films were washed with the mili-Q water thoroughly to wash away any non-binding fibrinogens, and dried under a steam of an ultra-high purity argon gas. After incubation, the elliposometer showed the hydrogen-terminated silicon surface had increased to 61 Å, which roughly corresponded to a monolayer of fibrinogen. All incubated films were measured for XPS N1s signal intensity again. The percentage of fibronogen absorbance of films **D** and **E** were calculated by dividing the increase of N1s signal by that of the hydrogen-terminated silicon surface.

X-ray photoelectron spectroscopy (XPS). XPS data was collected on a PHI 5700 X-ray photoelectron spectrometer, which is equipped with a monochromatic Al KR X-ray source (1486.7 eV), with takeoff angle (TOA) of 45° from the film surface. High- and low-resolution XPS spectra were recorded with window pass energies of 23.5 and 187.85 eV respectively. Electron

binding energies were calibrated using C1s line as reference at 286.4 eV (C-C). The atomic concentrations were calculated using the PHI Multipak 5.0 software (Physical Electronics).

Huisgen's 1,3-dipolar cycloaddition reaction of aqueous soluble azide on films with adsorbates 8 and 9. Air sensitive Huisgen's 1,3-dipolar cycloaddition reaction using Cu(I) catalyst was achieved inside an anaerobic chamber under a ultra-high purity nitrogen with 0 ppm oxygen. Both water-soluble ligand **11** and OEG azide **12** was prepared by former group member Dr. Amit Kumar. The TMG-protected alkyne-presenting films **B** and **C** were placed inside a petra dish. A solution of $CuSO_4$ (1.25 mM) in the mili-Q water, an azide solution **12** (5 mM) in the mili-Q water, and a copper ligand **11** solution (12.5 mM) in the mili-Q water were added into the petra dish so that the alkyne-presenting films were completely immersed. At the end, the ascorbic acid solution (25 mM) in the mili-Q was added to activate the Cu(I) catalyst. In order to reduce the water evaporation, the petra dish with films and reactants were covered and sealed inside an aluminum foil. An orbital shaker was used to ensure the homogeneity of the reaction mixture. After incubation for 4 h, the sample was taken out and sonicated in the 25 mM EDTA solution for 10 sec to remove the copper. The films were cleaned by washing with both milli-Q and ethanol, and finished by drying under a stream of ultra-high purity argon gas.

Huisgen's 1,3-dipolar cycloaddition reaction of non-aqueous soluble azide on films with adsorbates 8 and 18. Air sensitive Huisgen's 1,3-dipolar

cycloaddition reaction using Cu(I) catalyst was achieved inside an anaerobic chamber under a ultra-high purity nitrogen with 0 ppm oxygen. The water-soluble ligand **11** was prepared by Dr. Amit Kumar from our group. Azidomethylferrocene **13** was prepared by Dr. Yan Li from our group. TMG-protected alkyne-presenting films **B** and **G** were placed inside a petra dish. A solution of $CuSO_4$ (1.25 mM) in mili-Q water, an azidomethylferrocene **13** solution (5 mM) in dimethyl sulfoxide/propanol (3:1), and a copper ligand **11** solution (12.5 mM) in mili-Q water were added into the petra dish so that the alkyne-presenting films were completely immersed. At the end, the ascorbic acid solution (25 mM) in mili-Q was added to activate the Cu(I) catalyst. The petra dish with films and reactants were covered and sealed inside an aluminum foil, and an orbital shaker was used to ensure the homogeneity of the reaction mixture. Incubation and clean procedure were same as described above.

Electrochemical characterizations. All electrochemical measurements were performed using a DY2100 mini potentiostat. A home-made teflon three-electrode cell was used. Films **F** and **H** were used as the working electrodes. All films were fixed inside the home-made Teflon electrode cell with a Viton O-ring. Only 78.50 mm^2 of the film surface was exposed to the electrolyte. The backside of the films was rubbed rapidly with glass scriber to form a series of diamond marks in order to expose the bulk silicon. Ohmic contact was achieved by tapping the exposed bulk silicon with a copper wire using the carbon conductive tape. A platinum wire was used as the counter electrode, and a Sensorex S900C

BNC AgCl electrode was used as the reference electrode. 1.0 M perchloric acid dissolved in acetonitrile was used as the electrolyte and was degassed by the ultra-high purity argon gas before use. The 1.0 M perchloric acid was conveniently stirred using a small stream of the ultra-high purity nitrogen gas at the rate of one bubble per sec. All cyclic voltammograms were acquired in the degassed 1.0 M perchloric acid solution at the room temperature. All potentials were reported versus the reference electrode.

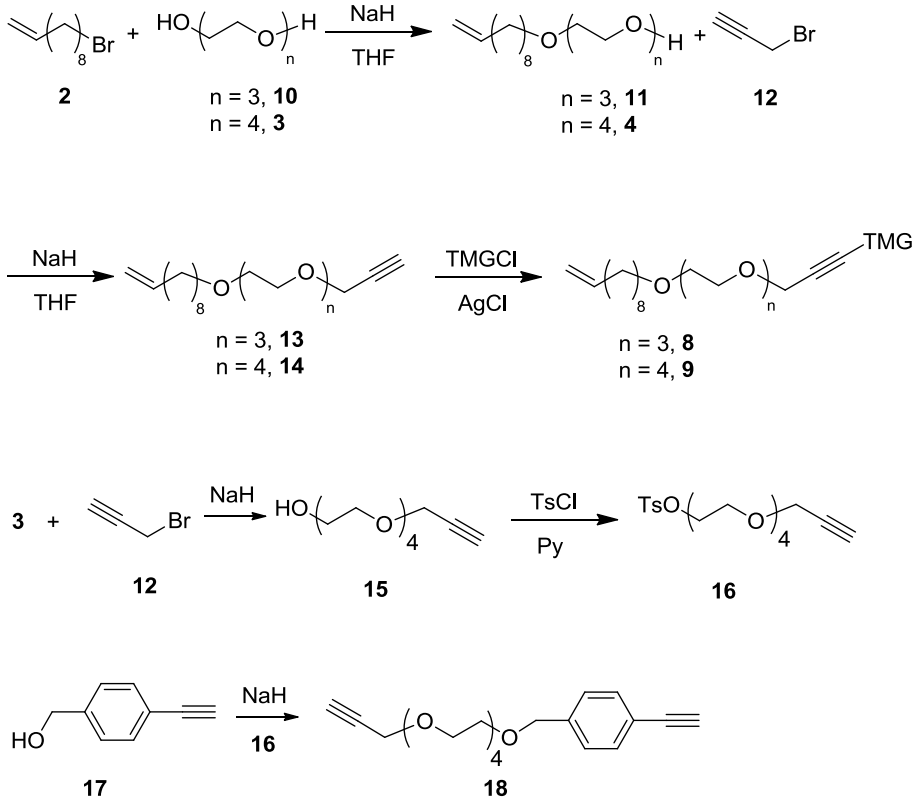

2-(2-(2-(dec-9-en-1-yloxy)ethoxy)ethoxy)ethanol (11)

The alcohol **10** (8.23 mL, 60.27 mmol) was dissolved in the anhydrous THF (80

mL). Sodium hydride (1.00 g, 60% in oil, 25 mmol) was added into the mixture at 0 °C under the nitrogen environment. After the reaction mixture was stirred for 2 h, the bromide **2** (3.14 mL, 15.07 mmol) was added into the mixture. The reaction mixture was stirred at the room temperature overnight. The mixture was diluted with water. The aqueous phase was extracted with dichloromethane, and the combined organic extracts were dried over Na_2SO_4, concentrated in vacuum, and purified by flash chromatography (ethylacetate) to give **11** (3.52g, 81% yield) as a colorless oil. ^{1}H NMR was consistent with previously reported values.[59]

^{1}H NMR (500 MHz, $CDCl_3$) δ 5.80 (m, 1H), 5.02 – 4.88 (m, 2H), 3.80 – 3.55 (m, 12H), 3.44 (t, *J* = 6.9 Hz, 2H), 2.07 – 1.98 (m, 2H), 1.58 (m, 4H), 1.29 (m, 8H).

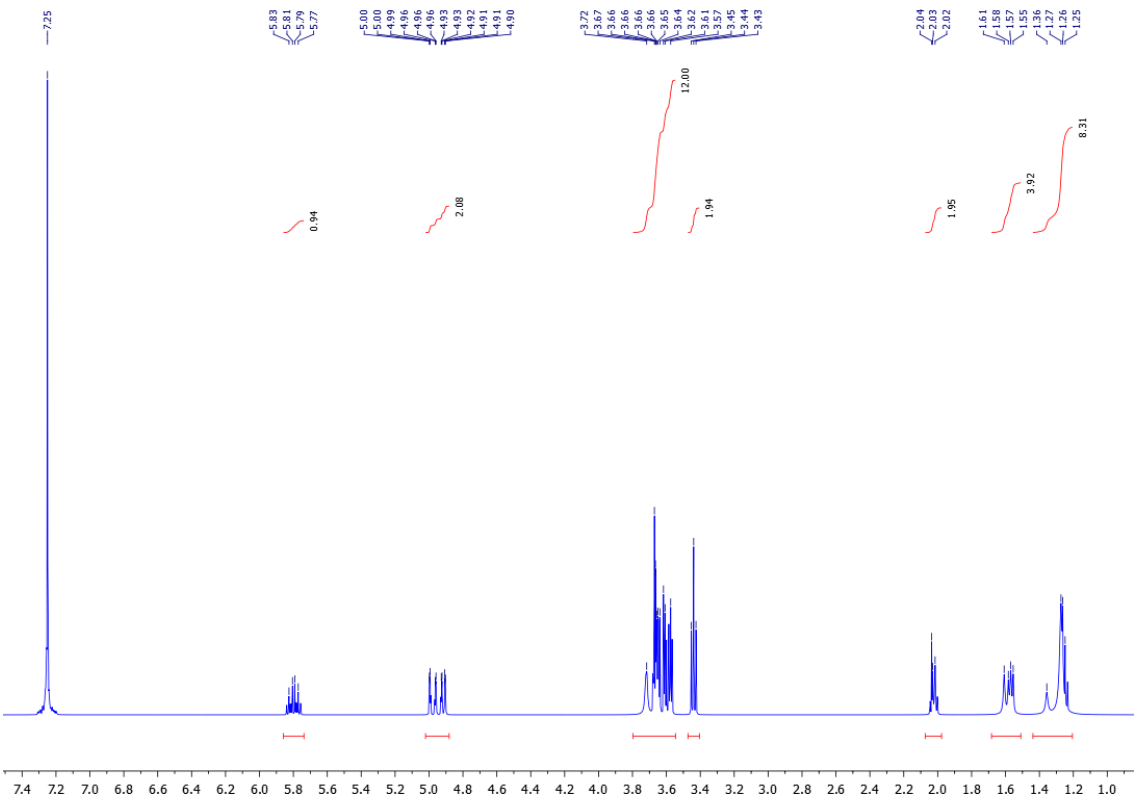

3,6,9,12-tetraoxadocos-21-en-1-ol (4)

To a solution of **3** (865.26 mg, 3.0 mmol) dissolved in the anhydrous THF (10 mL), the sodium hydride (120 mg, 60% in oil, 3.0 mmol,) was added into the mixture at 0 °C under the nitrogen environment. After the reaction mixture was stirred for 2 h, the bromide **2** (267 µL, 3.0 mmol) was added into the mixture, and stirred at the room temperature overnight. The reaction was quenched by water. The mixture was extracted by CH_2Cl_2 (3 × 30 mL). The organic layers were combined, washed with water (30 mL) and brine (30 mL), dried over Na_2SO_4, and filtered. The residue was purified by the flash chromatography (ethyl acetate) to give product **4** (720 mg, 73.5% yield) as light yellow oil. ^{1}H NMR was consistent with previously reported values.[33]

^{1}H NMR (500 MHz, $CDCl_3$) δ 5.80 (m, 1H), 5.03 – 4.88 (m, 2H), 4.20 (d, *J* = 2.5 Hz, 2H), 3.73 – 3.52 (m, 14H), 3.44 (t, *J* = 6.8 Hz, 2H), 2.42 (s, 1H), 2.03 (d, *J* = 7.7 Hz, 2H), 1.65 – 1.51 (m, 4H), 1.28 (s, 8H).

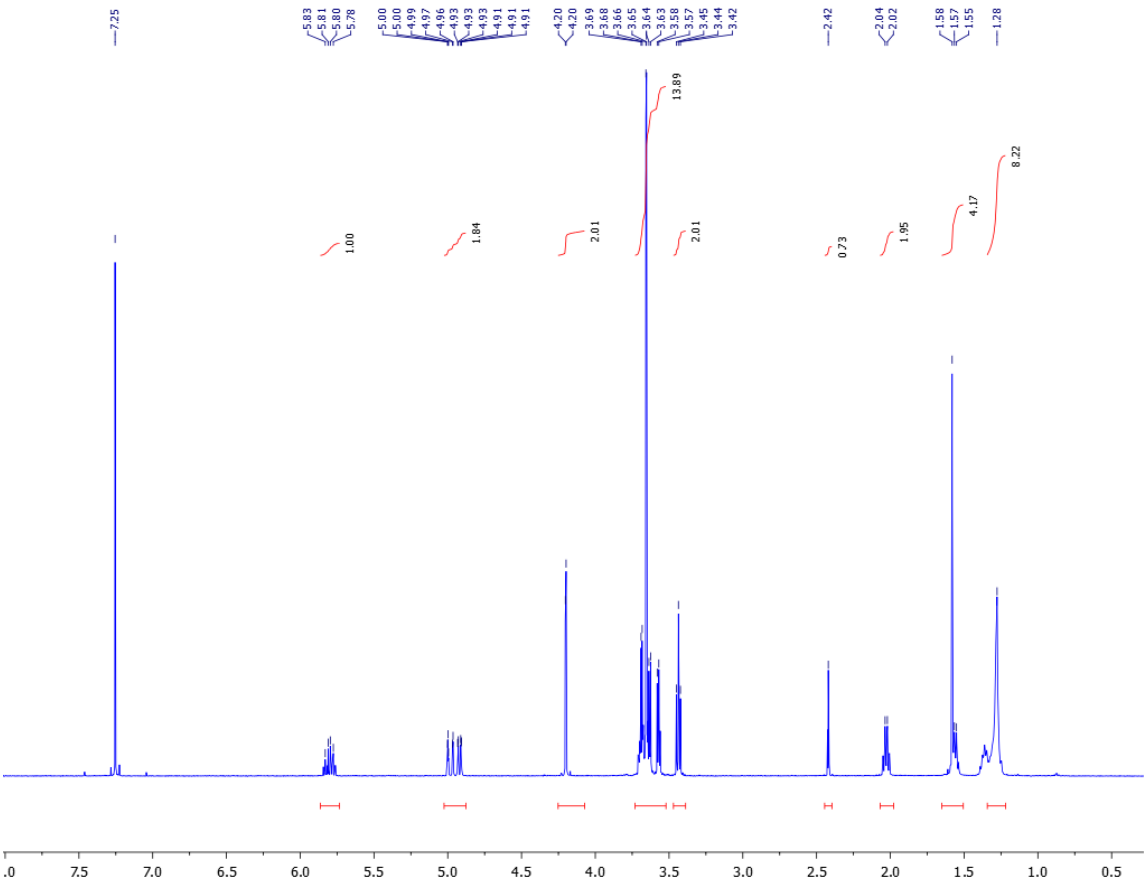

4,7,10,13,16,19,22-heptaoxadotriacont-31-en-1-yne (13)

To a solution of **11** (998.34 mg, 3.0 mmol) dissolved in anhydrous THF (10 mL), the sodium hydride (120 mg, 3.0 mmol, 60% in oil) was added into the mixture at 0 °C under the nitrogen environment. After the reaction mixture was stirred for 2 h, the bromide **12** (267 µL, 3.0 mmol) was added into the mixture, and stirred at the room temperature overnight. The reaction was quenched by water. The mixture was extracted by CH_2Cl_2 (3 × 30 mL). The organic layers were combined, washed with water (30 mL) and brine (30 mL), dried over Na_2SO_4, and filtered. The residue was purified by the flash chromatography (ethyl acetate) to give product **10** (977 mg, 71 % yield) as light yellow oil.

^{1}H NMR (500 MHz, $CDCl_3$) δ 5.85 – 5.73 (m, 1H), 4.94 (m, 2H), 4.19 (d, *J* = 2.6 Hz, 2H), 3.76 – 3.49 (m, 22H), 3.42 (t, *J* = 6.7 Hz, 2H), 2.41 (dd, *J* = 3.0, 1.6 Hz, 1H), 2.01 (dd, *J* = 14.5, 7.1 Hz, 2H), 1.62 – 1.46 (m, 2H), 1.43 – 1.12 (m, 8H).

^{13}C NMR (101 MHz, $CDCl_3$) δ 139.56, 114.45, 80.00, 74.86, 71.88-70.38 (m), 69.44, 34.15, 29.95, 29.77, 29.42, 29.25, 26.41.

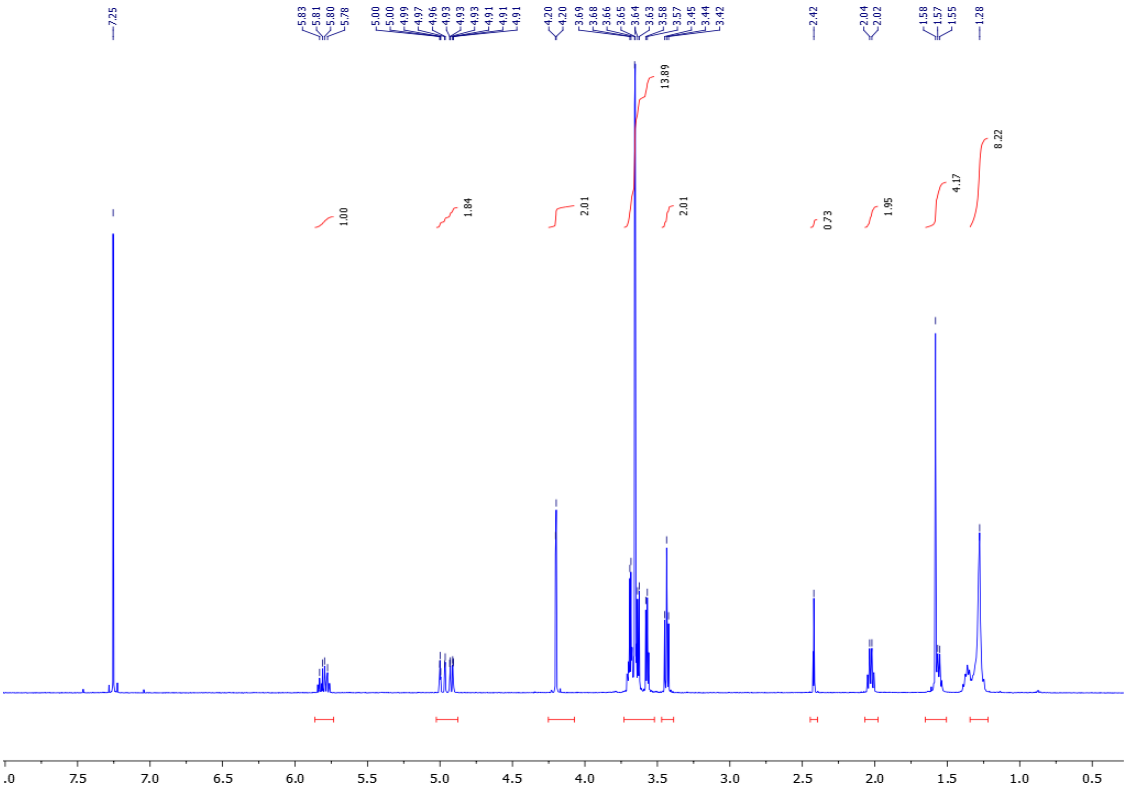

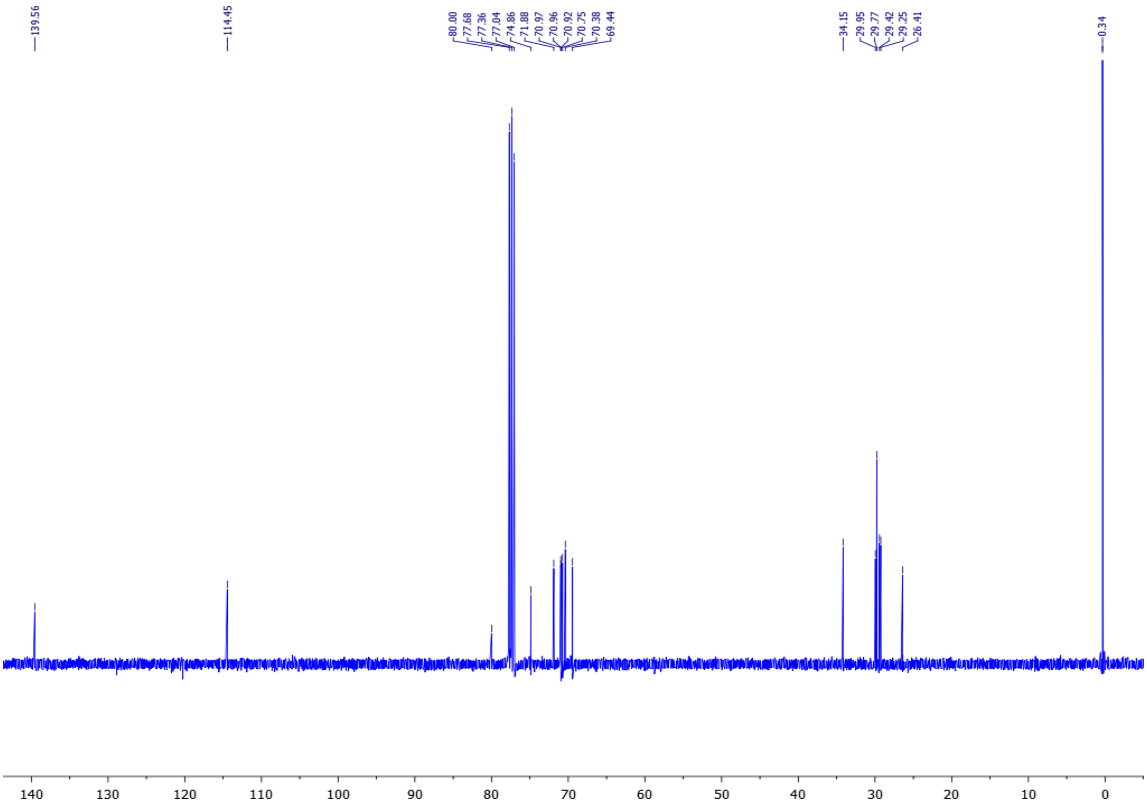

4,7,10,13,16-pentaoxahexacos-25-en-1-yne (14)

To a solution of **4** (998.34 mg, 3.0 mmol) dissolved in anhydrous THF (10 mL), the sodium hydride (120 mg, 3.0 mmol, 60% in oil) was added into the mixture at 0^{o}C under the nitrogen environment. After the reaction mixture was stirred for 2 h, the bromide **12** (267 µL, 3.0 mmol) was added into the mixture, and stirred at room temperature overnight. The reaction was quenched by water. The mixture was extracted by CH_2Cl_2 (3 × 30 mL). The organic layers were combined, washed with water (30 mL) and brine (30 mL), dried over Na_2SO_4, and filtered. The residue was purified by the flash chromatography (ethyl acetate) to give product **14** (977 mg, 71 % yield) as light yellow oil.

1H NMR (500 MHz, $CDCl_3$) δ 5.85 – 5.73 (m, 1H), 4.94 (m, 2H), 4.19 (d, *J* = 2.6 Hz, 2H), 3.76 – 3.49 (m, 16H), 3.42 (t, *J* = 6.7 Hz, 2H), 2.41 (dd, *J* = 3.0, 1.6 Hz, 1H), 2.01 (dd, *J* = 14.5, 7.1 Hz, 2H), 1.62 – 1.46 (m, 2H), 1.43 – 1.12 (m, 8H).

^{13}C NMR (126 MHz, $CDCl_3$) δ 139.25, 114.21, 79.72, 76.92, 74.64, 71.59-70.12 (m), 69.17, 58.46, 33.86, 29.69, 29.49, 29.13, 28.97, 26.14.

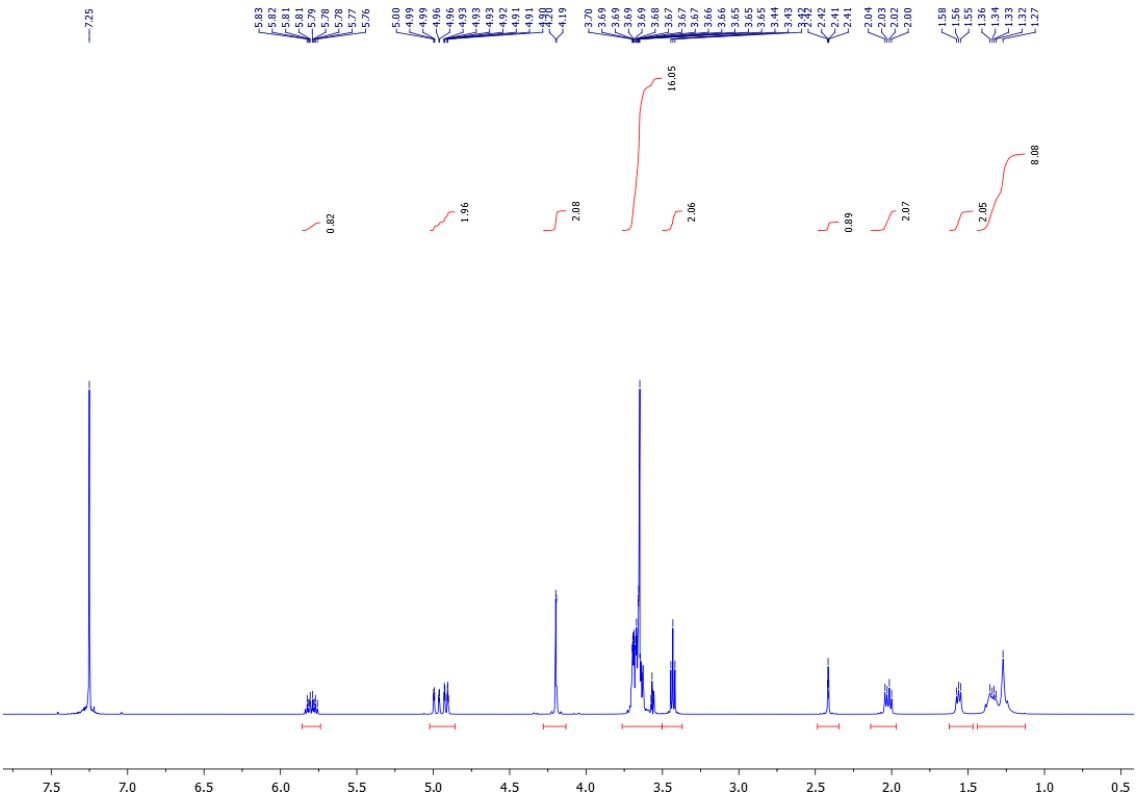

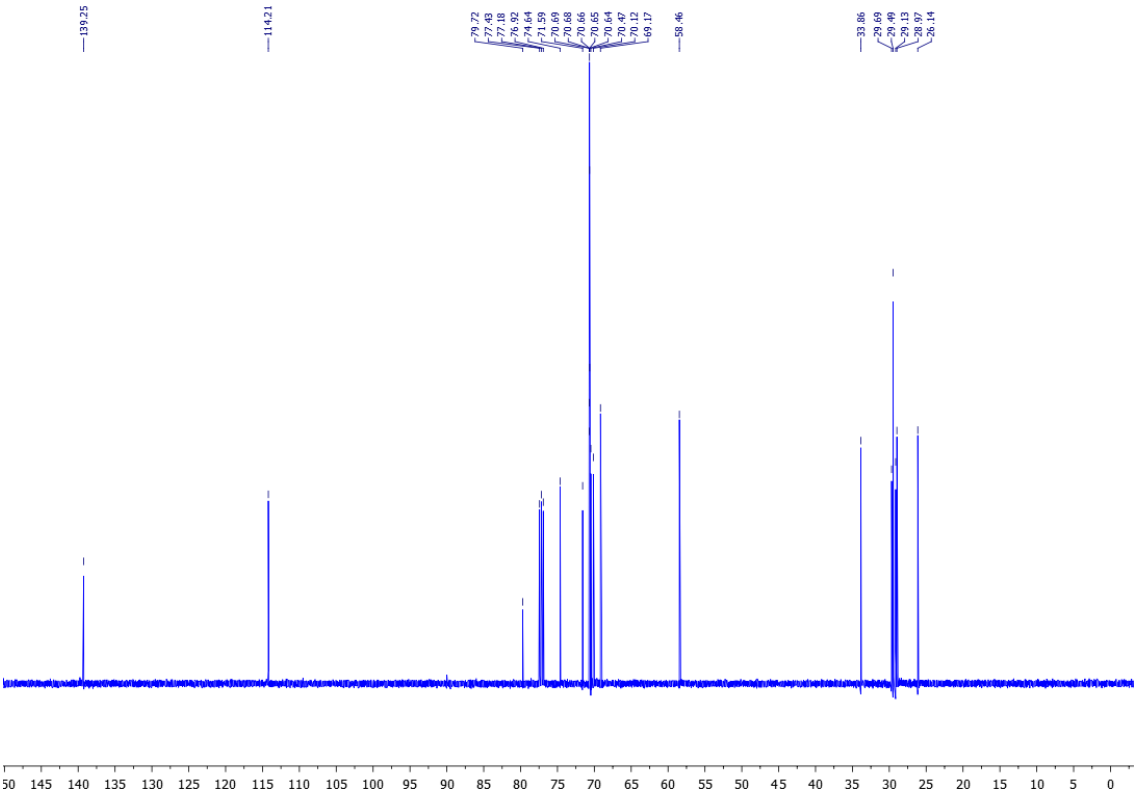

2,2-dimethyl-6,9,12,15-tetraoxa-2-germapentacos-24-en-3-yne (8)

13 (602 mg, 1.85 mmol) was dissolved in the anhydrous DCM (5 mL). Under the nitrogen environment, silver chloride (264 mg, 1.85 mmol) was added to the solution, followed by the addition of DBU (359 mg, 2.36 mmol). The reaction mixture was placed in the water bath and was heated to 40 °C. TMSCl (313.5 µL, 2.67 mmol) was added dropwise into the reaction mixture. After an overnight reaction, the reaction mixture was allowed to return to the room temperature and was quenched by adding *n*-hexane (200 mL). The organic layer was washed with $NaHCO_3$ (2 × 50 mL), followed by water (50 mL), dried over $MgSO_4$, and filtered. The organic layer was concentrated *in vacuo* and purified by the flash

chromatography (methanol/ethyl acetate = 1/99) to give product **8** (675 mg, 82.5% yield) as a colorless oil.

^{1}H NMR (500 MHz, $CDCl_3$) δ 5.80 (m, 1H), 5.04 – 4.87 (m, 2H), 4.19 (s, 2H), 3.74 – 3.60 (m, 10H), 3.57 (d, *J* = 5.3 Hz, 2H), 3.44 (t, *J* = 6.8 Hz, 2H), 2.10 – 1.95 (m, 2H), 1.60 – 1.51 (m, 2H), 1.43 – 1.20 (m, 10H), 0.34 (s, 9H).

^{13}C NMR (500 MHz, $CDCl_3$) δ 139.83, 114.72, 100.79, 92.13, 72.13, 71.24-71.04 (m), 70.65, 69.57, 59.84, 34.40, 30.22, 30.03, 29.67, 29.51, 26.67.

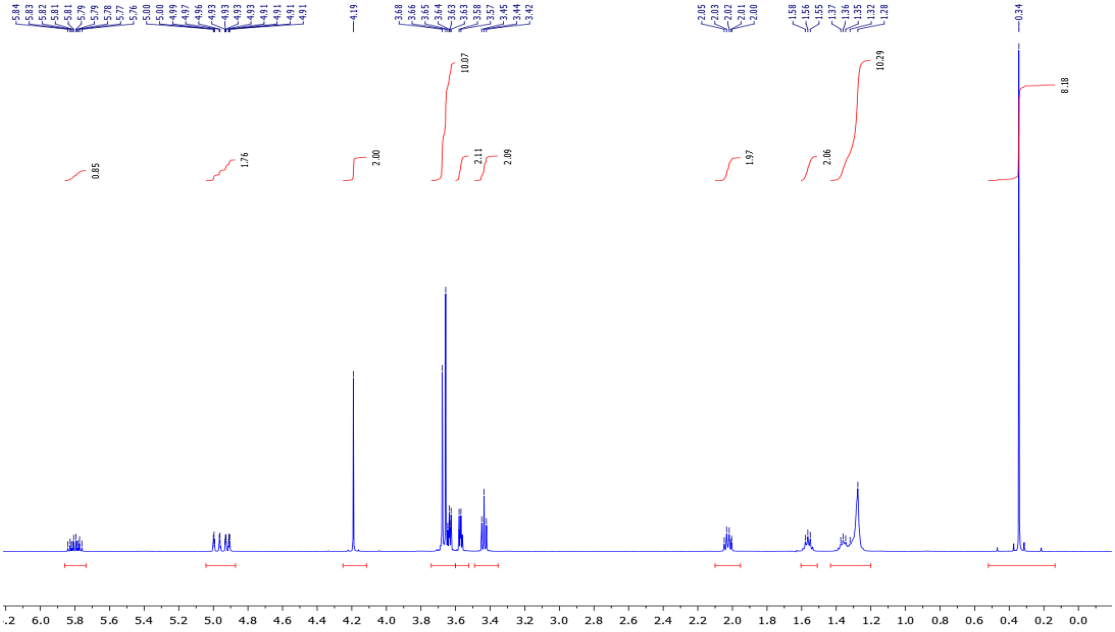

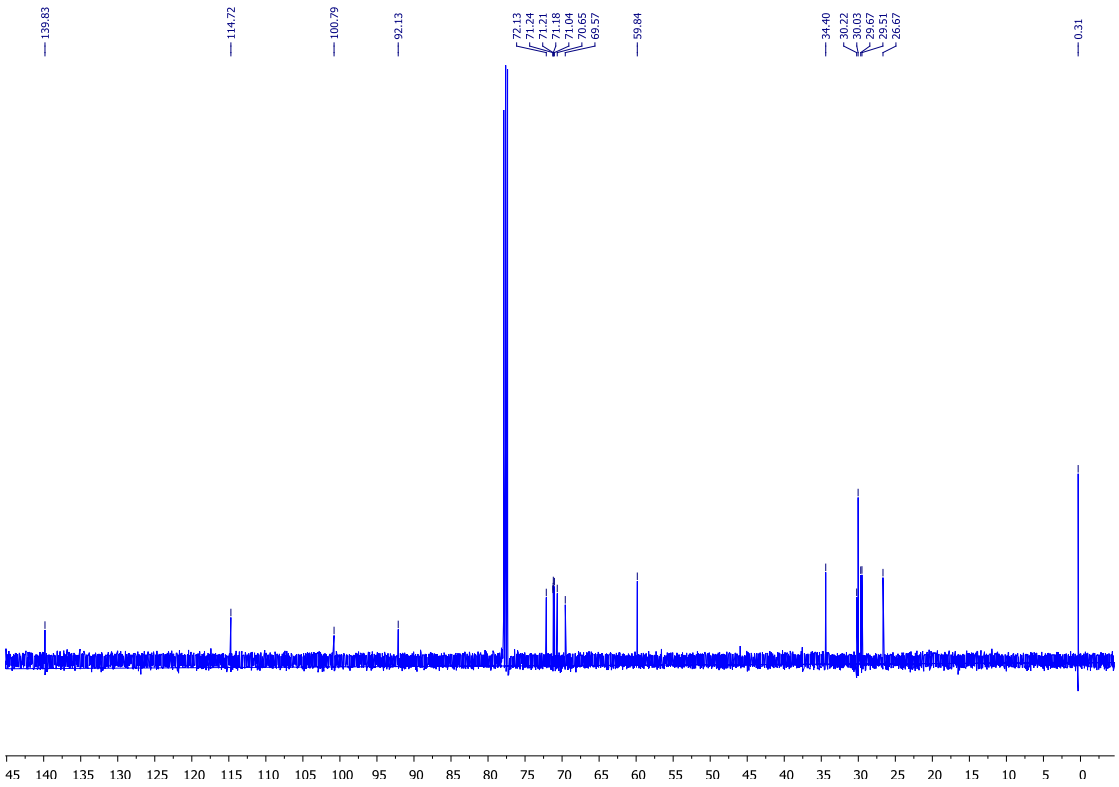

2,2-dimethyl-6,9,12,15,18-pentaoxa-2-germaoctacos-27-en-3-yne (9)

14 (495 mg, 1.34 mmol) was dissolved in the anhydrous DCM (3.75 mL). Under the nitrogen environment, silver chloride (191.36 mg, 1.34 mmol) was added to the solution, followed by the addition of DBU (260 mg, 1.71 mmol). The reaction mixture was placed in water bath and was heated to 40 °C. TMSCl (227 µL, 1.93 mmol) was added dropwise into the reaction mixture. After an overnight reaction, the reaction mixture was allowed to return to the room temperature and was quenched by adding *n*-hexane (200 mL). The organic layer was washed with $NaHCO_3$ (2 × 50 mL), followed by water (50 mL), dried over $MgSO_4$, and

filtered. The organic layer was concentrated *in vacuo* and purified by the flash chromatography (methanol/ethyl acetate = 1/99) to give product **9** (540 mg, 83.0% yield) as a colorless oil.

^{1}H NMR (500 MHz, $CDCl_3$) δ 5.80 (ddt, *J* = 16.8, 10.1, 6.6 Hz, 1H), 5.03 – 4.85 (m, 2H), 4.19 (s, 2H), 3.75 – 3.59 (m, 13H), 3.57 (d, *J* = 5.5 Hz, 2H), 3.43 (t, *J* = 6.8 Hz, 2H), 2.02 (dd, *J* = 14.4, 6.9 Hz, 2H), 1.58 – 1.48 (m, 2H), 1.37 – 1.25 (m, 8H), 0.34 (s, 9H).

^{13}C NMR (126 MHz, $CDCl_3$) δ 139.57, 114.46, 100.53, 91.87, 71.88, 70.99-70.40 (m), 69.32, 59.59, 34.15, 29.97, 29.77, 29.42, 29.25, 26.42, 0.06.

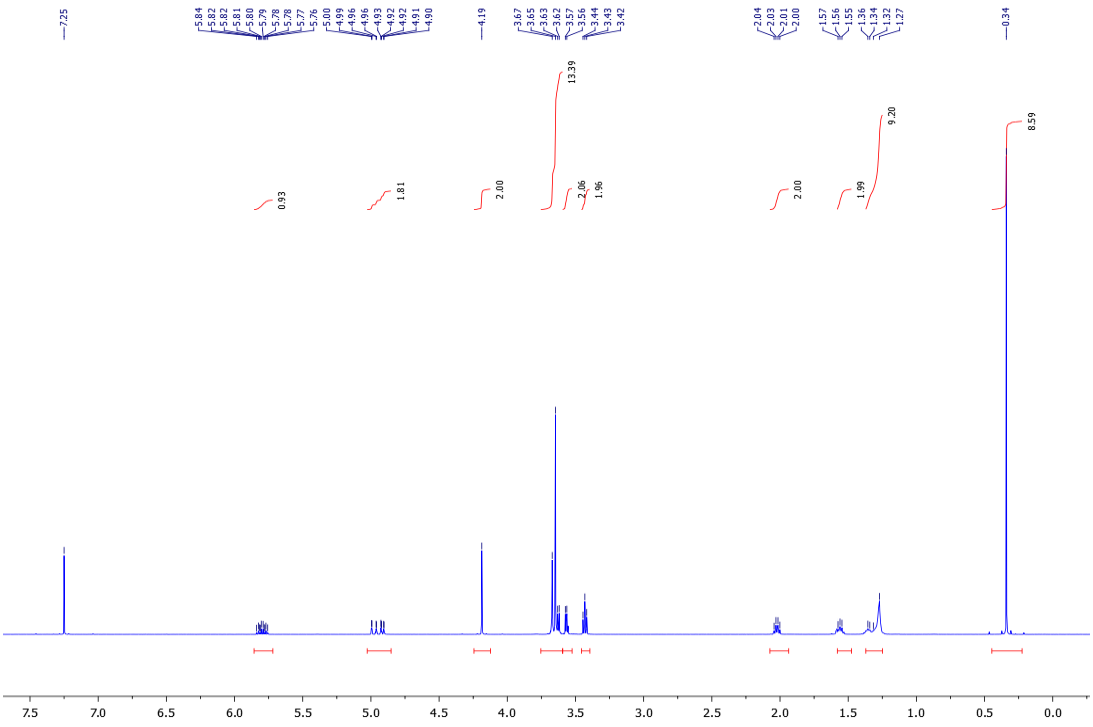

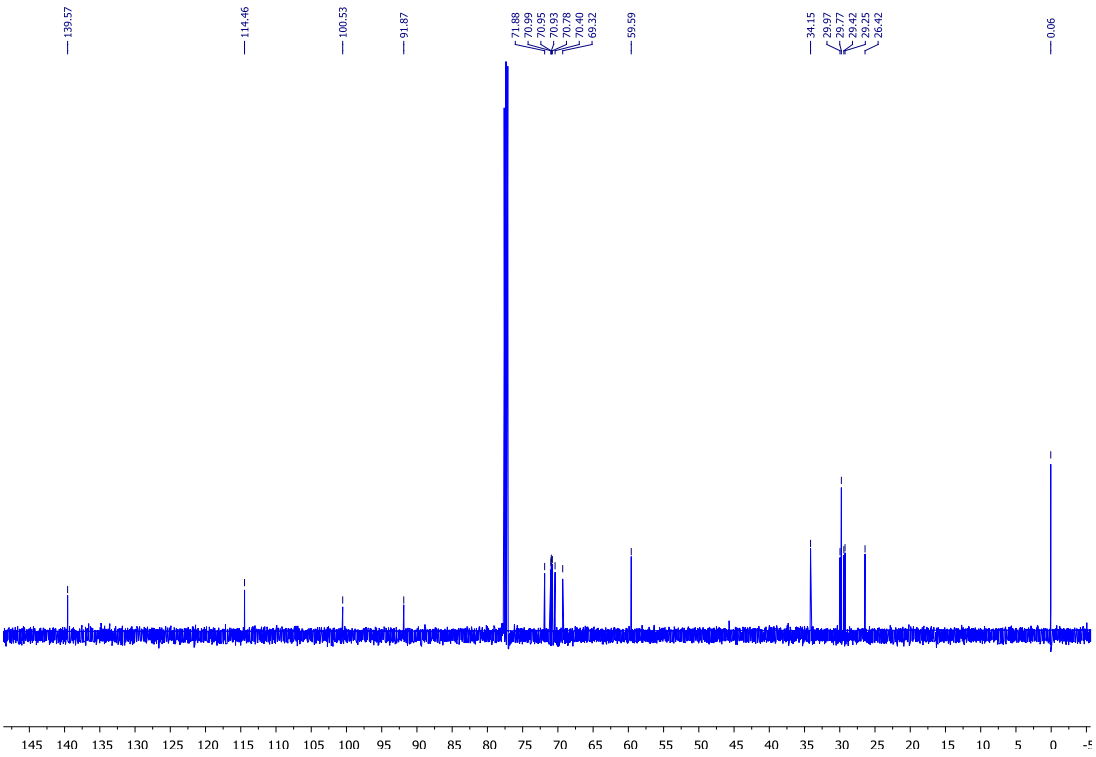

3,6,9,12-tetraoxapentadec-14-yn-1-ol (15)

To tetraethylene glycol (5.14 mL, 30 mmol) dissolved in the anhydrous THF (50 mL), slowly add sodium hydride (783 mg, 20 mmol) at 0 °C. The reaction mixture was stirred until no more gas was generated. After that, propargyl bromide (1.34 mL, 38 mmol) was added drop wise into the reaction mixture. The reaction mixture was stirred overnight at the room temperature before concentrated *in vacuo*. The residue was diluted in DCM (150 mL), washed with saturated $NaHCO_3$ (2 × 50 mL) and brine (50 mL). The organic layer was dried by $MgSO_4$ and filtered. The crude was concentrated *in vacuo* and was

purified by the column chromatography (hexane /ethyl acetate = 2/3) to give product 15 as a light yellow oil, 2.11 g (61%). ^{1}H NMR was consistent with previously reported values.[41]

^{1}H NMR (500 MHz, $CDCl_3$) δ 4.19 (d, *J* = 2.3 Hz, 2H), 3.73 – 3.61 (m, 10H), 3.59 (dd, *J* = 5.3, 3.9 Hz, 2H), 2.76 (s, 1H), 2.42 (t, *J* = 2.4 Hz, 1H).

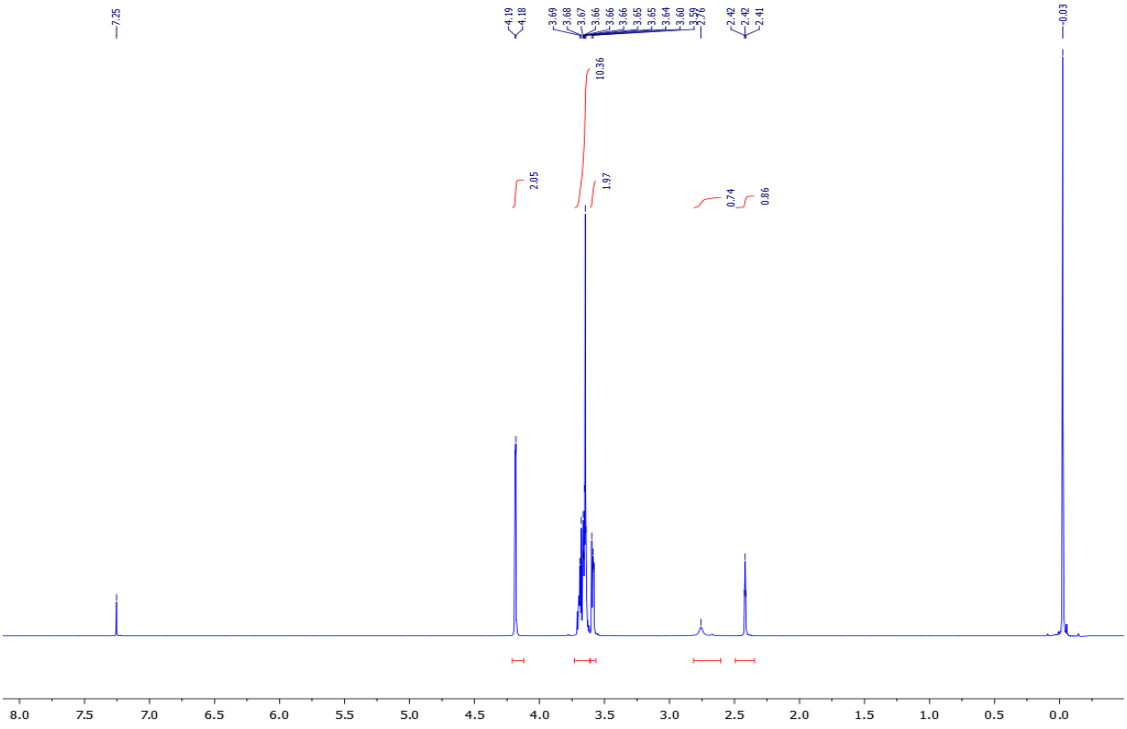

3,6,9,12-tetraoxapentadec-14-yn-1-yl 4-methylbenzenesulfonate (16)

To a solution of **15** (589 mg, 2.53 mmol) in anhydrous dichloromethane (4 mL), add the anhydrous pyridine (340 µL, 3.83 mmol) in the nitrogen environment. After p-toluenesulfonyl chloride (722 mg, 3.7 mmol) was added, the reaction mixture was stirred at the room temperature overnight. The reaction

mixture was concentrated *in vacuo* and purified by the flash chromatography (hexane/ethyl acetate=1/2) to give **16** as a colorless oil (981 mg, 85% yield), which is used in the next step without further purification.

1-(4-ethynylphenyl)-2,5,8,11,14-pentaoxaheptadec-16-yne (18)

To **17** (248 mg, 1.88 mmol) dissolved in the THF (6 mL) in the nitrogen environment, the sodium hydride (136 mg, 2.04 mmol, 60% in oil) was added into the mixture at 0^{o}C. The reaction mixture was stirred until no more gas is generated. **16** (789 mg, 2.04 mmol) was added into the reaction mixture. The reaction mixture was stirred at the room temperature overnight. After an overnight reaction, the reaction mixture was diluted by adding dichloromethane (200 mL). The organic layer was washed with $NaHCO_3$ (2 × 50 mL), followed by brine (50 mL), dried over $MgSO_4$, and filtered. The organic layer was concentrated *in vacuo* and purified by the flash chromatography (ethyl acetate) to give **18** as a light yellow oil (640 mg, 82% yield).

^{1}H NMR (500 MHz, $CDCl_3$) δ 7.46 (d, *J* = 8.2 Hz, 2H), 7.29 (d, *J* = 8.1 Hz, 2H), 4.56 (s, 2H), 4.19 (d, *J* = 2.0 Hz, 2H), 3.69 – 3.61 (m, 12H), 3.06 (s, 1H), 2.42 (s, 1H).

^{13}C NMR (126 MHz, $CDCl_3$) δ 139.25, 132.21, 127.57, 121.30, 83.62, 79.73, 77.28, 74.67, 72.79, 70.71, 70.68, 70.67, 70.65, 70.46, 69.69, 69.16, 58.47, 20.76.

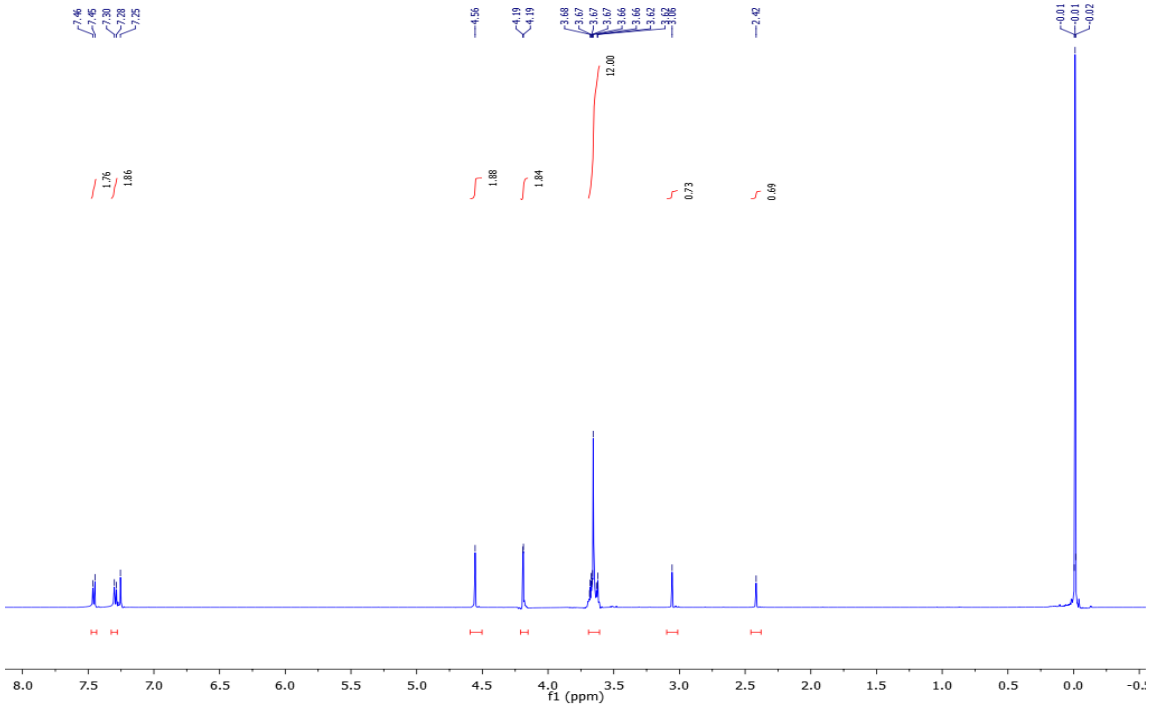
7.46
7.45
7.30
7.28
7.25
4.56
4.19
4.19
3.68
3.67
3.67
3.67
3.66
3.66
3.62
3.06
2.42
0.01
0.01
0.02
12.00
1.76
1.86
1.88
1.84
0.73
0.69
8.0
7.5
7.0
6.5
6.0
5.5
5.0
4.5
4.0
3.5
3.0
2.5
2.0
1.5
1.0
0.5
0.0
f1 (ppm)

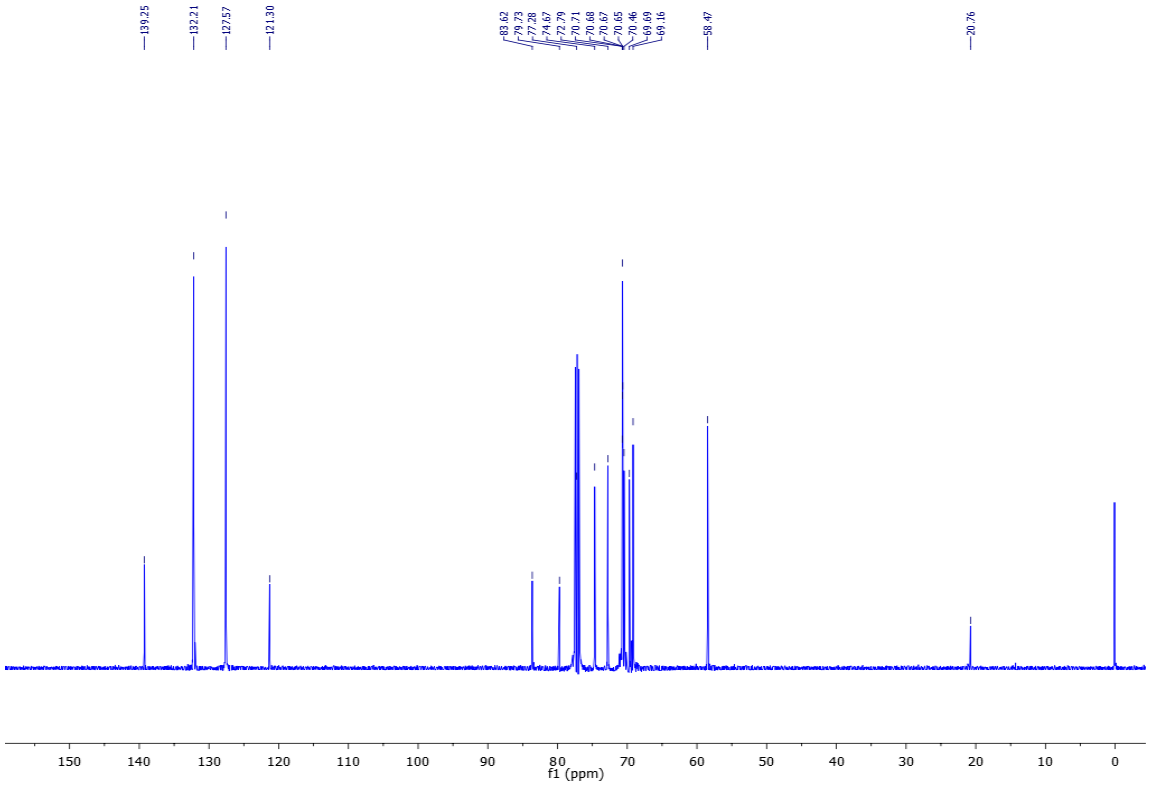
139.25
132.21
127.57
121.30
83.62
79.73
77.28
74.67
72.79
70.71
70.68
70.67
70.65
70.46
69.69
69.16
58.47
20.76
150
140
130
120
110
100
90
80
70
60
50
40
30
20
10
0
f1 (ppm)

III.5. References

(1) Basarkar, A.; Singh, J. *Int. J. Nanomed.* **2007**, *2*, 353.

(2) Can, O. D.; Ozturk, Y. *Turkiye Klinikleri Tip Bilimleri Dergisi* **2009**, *29*, 968.

(3) Clauw, D. J.; Chrousos, G. P. *Neuroimmunomodulation* **1997**, *4*, 134.

(4) Jensen, J. E.; Conn, R. R.; Hazelrigg, G.; Hewett, J. E. *Am. J. Sports Med.* **1985**, *13*, 27.

(5) HUXLEY, A. L. H. A. F. *Nature* **1939**.

(6) Spelman, F. A. *Audiol. Neurootol.* **2006**, *11*, 77.

(7) Allongue, P.; de Villeneuve, C. H.; Cherouvrier, G.; Cortes, R.; Bernard, M. C. *J. Electroanal. Chem.* **2003**, *550*, 161.

(8) Allongue, P.; de Villeneuve, C. H.; Pinson, J.; Ozanam, F.; Chazalviel, J. N.; Wallart, X. *Electrochim. Acta* **1998**, *43*, 2791.

(9) deVilleneuve, C. H.; Pinson, J.; Bernard, M. C.; Allongue, P. *J. Phys. Chem. B* **1997**, *101*, 2415.

(10) Faucheux, A.; Gouget-Laemmel, A. C.; de Villeneuve, C. H.; Boukherroub, R.; Ozanam, F.; Allongue, P.; Chazalviel, J. N. *Langmuir* **2006**, *22*, 153.

(11) Clark, I. T.; Aldinger, B. S.; Gupta, A.; Hines, M. A. *J. Phys. Chem. C* **2010**, *114*, 423.

(12) Hess, G.; Russell, M.; Gong, B.; Parkinson, P.; Ekerdt, J. G. *J. Vac. Sci. Technol. A* **1997**, *15*, 1129.

(13) Dittrich, T.; Angermann, H.; Fussel, W.; Flietner, H. *Phys. Status Solidi A* **1993**, *140*, 463.

(14) Fabre, B. *Acc. Chem. Res.* **2010**, *43*, 1509.

(15) Badjic, J. D.; Kostic, N. M. *J. Phys. Chem. B* **2000**, *104*, 11081.

(16) Scheres, L.; Giesbers, M.; Zuilhof, H. *Langmuir* **2010**, *26*, 10924.

(17) Kolb, H. C.; Finn, M. G.; Sharpless, K. B. *Angew. Chem.Int. Ed.* **2001**, *40*, 2004.

(18) Kolb, H. C.; Sharpless, K. B. *Drug Discovery Today* **2003**, *8*, 1128.

(19) Meldal, M. *Macromol. Rapid Commun.* **2008**, *29*, 1016.

(20) Stoeckmann, H.; Neves, A. A.; Stairs, S.; Brindle, K. M.; Leeper, F. J. *Org. Biomol. Chem.* **2011**, *9*, 7303.

(21) Jewett, J. C.; Sletten, E. M.; Bertozzi, C. R. *J. Am. Chem. Soc.* **2010**, *132*, 3688.

(22) Kurt Alder, G. S. a. H. F. *Justus Liebigs Ann. Chem.* **1931**, *485*.

(23) Huisgen, R.; Ooms, P. H. J.; Mingin, M.; Allinger, N. L. *J. Am. Chem. Soc.* **1980**, *102*, 3951.

(24) Hayden, A. E.; Houk, K. N. *J. Am. Chem. Soc.* **2009**, *131*, 4084.

(25) Schoenebeck, F.; Ess, D. H.; Jones, G. O.; Houk, K. N. *J. Am. Chem. Soc.* **2009**, *131*, 8121.

(26) Ess, D. H.; Jones, G. O.; Houk, K. N. *Organic Lett.* **2008**, *10*, 1633.

(27) Agard, N. J.; Baskin, J. M.; Prescher, J. A.; Lo, A.; Bertozzi, C. R. *Acs Chem. Biol.* **2006**, *1*, 644.

(28) Agard, N. J.; Prescher, J. A.; Bertozzi, C. R. *J. Am. Chem. Soc.* **2004**, *126*, 15046.

(29) Baskin, J. M.; Bertozzi, C. R. *Qsar Comb. Sci.* **2007**, *26*, 1211.

(30) Baskin, J. M.; Prescher, J. A.; Laughlin, S. T.; Agard, N. J.; Chang, P. V.; Miller, I. A.; Lo, A.; Codelli, J. A.; Bertozzi, C. R. *Proc. Nat. Acad. Sci. USA* **2007**, *104*, 16793.

(31) Beatty, K. E.; Fisk, J. D.; Smart, B. P.; Lu, Y. Y.; Szychowski, J.; Hangauer, M. J.; Baskin, J. M.; Bertozzi, C. R.; Tirrell, D. A. *Chembiochem* **2010**, *11*, 2092.

(32) Sletten, E. M.; Bertozzi, C. R. *Acc. of Chem. Res.* **2011**, *44*, 666.

(33) Qin, G.; Cai, C. *Science China-Chemistry* **2010**, *53*, 36.

(34) Lim, R. K. V.; Lin, Q. *Science China-Chemistry* **2010**, *53*, 61.

(35) Ciampi, S.; Boecking, T.; Kilian, K. A.; James, M.; Harper, J. B.; Gooding, J. J. *Langmuir* **2007**, *23*, 9320.

(36) Haensch, C.; Hoeppener, S.; Schubert, U. S. *Chem. Soc. Rev.* **2010**, *39*, 2323.

(37) Rohde, R. D.; Agnew, H. D.; Yeo, W.-S.; Bailey, R. C.; Heath, J. R. *J. Am. Chem. Soc.* **2006**, *128*, 9518.

(38) Collman, J. P.; Devaraj, N. K.; Chidsey, C. E. D. *Langmuir* **2004**, *20*, 1051.

(39) Lee, J. K.; Chi, Y. S.; Choi, I. S. *Langmuir* **2004**, *20*, 3844.

(40) Lummerstorfer, T.; Hoffmann, H. *J. Phys. Chem. B* **2004**, *108*, 3963.

(41) Sun, X. L.; Stabler, C. L.; Cazalis, C. S.; Chaikof, E. L. *Bioconjugate Chem.* **2006**, *17*, 52.

(42) Hurley, P. T.; Nemanick, E. J.; Brunschwig, B. S.; Lewis, N. S. *J. Am.*

Chem. Soc. **2006**, *128*, 9990.

(43) Ciampi, S.; Eggers, P. K.; Le Saux, G.; James, M.; Harper, J. B.; Gooding, J. J. *Langmuir* **2009**, *25*, 2530.

(44) Gallant, N. D.; Lavery, K. A.; Amis, E. J.; Becker, M. L. *Adv. Mater.* **2007**, *19*, 965.

(45) Ciampi, S.; Harper, J. B.; Gooding, J. J. *Chem. Soc. Rev.* **2010**, *39*, 2158.

(46) Kruse, P.; Johnson, E. R.; DiLabio, G. A.; Wolkow, R. A. *Nano Letters* **2002**, *2*, 807.

(47) Bateman, J. E.; Eagling, R. D.; Worrall, D. R.; Horrocks, B. R.; Houlton, A. *Angew. Chem. Int. Ed.* **1998**, *37*, 2683.

(48) Cossi, M.; Iozzi, M. F.; Marrani, A. G.; Lavecchia, T.; Galloni, P.; Zanoni, R.; Decker, F. *J. Phys. Chem. B* **2006**, *110*, 22961.

(49) Huang, K.; Duclairoir, F.; Pro, T.; Buckley, J.; Marchand, G.; Martinez, E.; Marchon, J.-C.; De Salvo, B.; Delapierre, G.; Vinet, F. *Chemphyschem* **2009**, *10*, 963.

(50) Riveros, G.; Gonzalez, G.; Chornik, B. *J. Braz. Chem Soc.* **2010**, *21*, 25.

(51) Fabre, B.; Hauquier, F. *J. Phys. Chem. B* **2006**, *110*, 6848.

(52) Kilian, K. A.; Boecking, T.; Gooding, J. J. *Chem. Commun.* **2009**, 630.

(53) Kilian, K. A.; Bocking, T.; Gaus, K.; Gal, M.; Gooding, J. J. *Biomaterials* **2007**, *28*, 3055.

(54) Ernst, A.; Gobbi, L.; Vasella, A. *Tetrahedron Lett.* **1996**, *37*, 7959.

(55) Cai, C. Z.; Vasella, A. *Hel. Chim. Acta* **1995**, *78*, 732.

(56) Zanoni, R.; Aurora, A.; Cattaruzza, F.; Coluzza, C.; Dalchiele, E. A.; Decker, F.; Di Santo, G.; Flamini, A.; Funari, L.; Marrani, A. G. *Mat. Sci. Eng. C-Bio. S.* **2006**, *26*, 840.

(57) Ciampi, S.; Le Saux, G.; Harper, J. B.; Gooding, J. J. *Electroanalysis* **2008**, *20*, 1513.

(58) Tajimi, N.; Sano, H.; Murase, K.; Lee, K. H.; Sugimura, H. *Langmuir* **2007**, *23*, 3193.

(59) Samanta, D.; Faure, N.; Rondelez, F.; Sarkar, A. *Chem. Commun.* **2003**, 1186.

CHAPTER IV. CONCLUSIONS AND RECOMMENDATIONS

Promoted by the rapid development of the neural prosthetic devices, one of our research group's long term objectives is to design a versatile platform that allows electrochemical interaction, and is capable of guiding differentiation of the neural progenitor targets. Previously Dr. Guoting Qing from our group has explored the feasibility of immobilizing oligo (ethylene glycol) (OEG) onto the Si/SiC substrate via the Huisgen 1,3-dipolar cycloaddition (Click) reaction. The scope of this dissertation is primary based on improving the design of the self-assembling molecules to form inert matrix, as well as exploring the versatility of the current platform by grafting with different functional groups, and characterizing the electrochemical properties of the platform.

In Chapter II, significant work was contributed to the improvements in the Si(111) passivation in the ultra-high vacuum (UHV) condition. We have grafted freshly prepared hydrogen-terminated silicon surface with EG7-OMe, the resulting film demonstrated extraordinary anti-biofouling ability in both 1 mg/mL fibrinogen solution as well as 10 % fetal bovine serum (FBS) solution. The film is stable enough to remain protein-resistant in 1 $\times$ PBS for at least 56 days, and the anti-biofouling ability was not compromised after exposures to 1mg/mL fibrinogen solutions. These results show that the UHV effectively eliminates reactive oxygen

and water radicals from the film, which allows surface hydrosilylation to proceed at near-ideal condition. Moreover, 4” silicon wafer can be passivated using our apparatus, which could be used to prepare OEG-presenting silicon wafer in large batch.

To further improve the film preparation, it could be beneficial to pre-cut the silicon wafer with the photoresist mask using the dry etching technique. Currently we rely on the glass scriber to tailor functionalized silicon wafer into the desired dimensions, the sharp silicon debris would scribble film surfaces during the cleaning step. As the result, both anti-biofouling and electrochemical properties could be compromised, and film degradation could be accelerated at the defect sites.

In Chapter III we focus on the optimization of the design of self-assembling monolayer which can be used to form a versatile ethynyl-presenting monolayer. We compared the effects of pre-assembled and stepwise approach to passivate films via two case studies. Based on the trimethylgermanyl protecting group strategy, which was previously developed by Dr. Guoting Qing, we have designed and synthesized multiple 1-alkene adsorbates with significant fewer amount of ethylene glycol units. We envisioned that the new adsorbates would increase the packing density of the monolayer by reducing the steric hindrance of self-assembling molecules; furthermore, the shorter chain length could benefit the electron transfer via tunneling effects. Our screening has shown

that varying EG units in the self-assembling molecules has no significant effects in terms of improving anti-biofouling property. Unfortunately, the cyclic voltammetry (CV) experiments were unable to record any detectable signals from the ethynyl films grafted with the electro-active ferrocene group, which significantly limits our platform's potential as a versatile 3D scaffold to communicate with neuron cells. To tackle this obstacle, we designed our second generation self-assembling molecules based on the 1-alkyne approach. Such novel approach allows passivation to be conducted at the ambient conditions, which prevents multi-layer build-up as well as pre-mature cleavage that are common to the UV-assisted surface hydrosilylation approach. The resulting film has shown success in the electro-chemical response as proven by the cyclic voltammetry experiments.

Although our second generation self-assembling monolayer have shown potential in the surface redox ability, we have shown that the conjugated phenyl self-assembling molecules have relatively low surface coverage comparing to the alkyl chains based ones, which is possibly due to the photo quenching effect of the conjugated phenyl group. Furthurmore, the degermination efficiency is far lesser than ideal, promoting us to further explore other viable alternatives to serve as the molecular skeleton of the biocompatible electro-active SAMs.